CP Violation in $\bar{B} \to \psi X$ and $\bar{B} \to D\bar{D}$:

A Small Step for a Penguin

Zur Erlangung des akademischen Grades eines

DOKTORS DER NATURWISSENSCHAFTEN

von der Fakultät für Physik

des Karlsruher Instituts für Technologie (KIT)

genehmigte

DISSERTATION

von

M.Sc. Philipp Ernst Frings

aus Wesel

Tag der mündlichen Prüfung:	18.12.2015
Referent:	Prof. Dr. Ulrich Nierste
Korreferent:	Prof. Dr. Kirill Melnikov

Contents

Introduction

The history of the Standard Model (SM) is a history of many theoretical and experimental successes and achievements. It has found its most recent success in the unambiguous discovery of the Higgs boson by the ATLAS and CMS collaborations [1, 2]. This discovery follows a range of impressive quantitative confirmations of SM predictions in many experiments.

There are thousands of confirmations of the SM and only very few deviations from SM predictions at particle physics experiments. Nevertheless, we know from cosmological observations that the SM is insufficient to describe cosmological aspects of particle physics. The SM does neither explain neutrino masses nor the baryon asymmetry nor dark matter. Furthermore, the SM is also unsatisfying from a theoretical point of view because its parameters range over large scales from $\mathcal{O}(1)$ for the top-quark Yukawa coupling to $\mathcal{O}(10^{-6})$ for the electron Yukawa coupling. Moreover, the overall pattern of the couplings remains to be understood. Therefore, it is most likely that the SM is not the final theory of particle physics in our universe and that, eventually, deviations from SM predictions will be measured.

One possibility to measure these new-physics effects is the direct discovery of new particles if they contribute via new decay channels or enhance differential decay rates. The complementary method is to measure the quantum corrections that are induced by new particles. Since the particles do not need to be produced on-shell, this indirect method is sensitive to particles that are much heavier than the particles that can be found with direct detection experiments.

In flavor physics, the measurement of charge-parity (CP) asymmetries is such an indirect method to search for new physics (NP), since the couplings of the new particles in general should violate the CP symmetry. Flavor physics deals with the transitions of flavored hadrons which are mediated by the weak interaction. In the SM these processes always involve entries of the Cabibbo-Kobayashi-Maskawa (CKM) matrix [3, 4]. Some of these CKM entries have a complex phase called weak phase. If two decay amplitudes

with two different weak phases contribute to the same process this leads to the breaking of the *CP* symmetry called *CP* violation. Roughly speaking this means that matter and antimatter behave differently. *CP* violation is quantified in terms of *CP* asymmetries, for the decay of a $\bar{B}$ meson to a final state f the *CP* asymmetry is defined as

$$A_{CP}(B \to f) \equiv \frac{\Gamma(\bar{B} \to \bar{f}) - \Gamma(B \to f)}{\Gamma(\bar{B} \to \bar{f}) + \Gamma(B \to f)}. \tag{1}$$

To identitify *CP*-violating new-physics contributions, it is important to have reliable predictions of *CP*-violating observables in the SM. We will determine *CP*-violating observables in exclusive decays that are dominated by the quark level process $b \to c\bar{c}q$, $q \in \{d, s\}$. The most famous representatives of these decays are $\bar{B}_d \to J/\psi K_S$, $\bar{B}_s \to J/\psi\phi$, and $\bar{B}_s \to D_s^+ D_s^-$ [5]. They are the prime candidates to measure the $\bar{B}_p - B_p$ mixing phases ϕ_p with $p \in \{d, s\}$ which can be directly linked to weak phases in the CKM matrix. Furthermore, measuring the $\bar{B}_p - B_p$ mixing phases is one of the best probes for indirect new physics because the $\bar{B}_p - B_p$ mixing amplitudes are sensitive to scales above 100 TeV.

We will refer to the exclusive decays that are dominated by the quark-level transition $b \to c\bar{c}q$ as $\bar{B} \to \psi X$ and $\bar{B} \to D\bar{D}$ decays. In these decays the framework of QCD factorization [6–10] that is very successful in describing most $\bar{B}$ decays is not applicable. The reason for this is that in calculations the hadronization effects of the final- and initial-state mesons cannot be systematically separated. Thus, there exist no first-principles predictions for decay amplitudes and direct *CP* asymmetries in $\bar{B} \to \psi X$ and $\bar{B} \to D\bar{D}$ decays. The aim of this thesis is to improve this situation.

We will exploit that there is a large momentum transfer q^2 from the initial to the final state to expand the decay amplitude in $\Lambda_{\rm QCD}/\sqrt{q^2}$. This corresponds to the formalization of the Bander-Silverman-Soni (BSS) mechanism [11] by an operator-product expansion (OPE) which leads to as simpler structure of the decay amplitude. This allows together with $1/N_C$ counting [12] to set first-principles bounds on *CP*-violating quantities in $\bar{B} \to \psi X$ and $\bar{B} \to D\bar{D}$ decays. In particular, we derive for the first time first-principles theoretical uncertainties of the determination of the mixing phases ϕ_d and ϕ_s.

Outline

In the first chapter, we introduce basic properties of $\bar{B}$ meson decays in the SM. We focus on the flavor-changing transitions that cause $\bar{B}$ decays and *CP* violation and motivate the necessity of this thesis in more detail. In the second chapter, we present the OPE that

we use to simplify the decay amplitudes in $\bar{B} \to \psi X$ and $\bar{B} \to D\bar{D}$ decays. This includes the factorization formula and some general properties. The third chapter is dedicated to the proof of the OPE, most notably we investigate in depth the infrared structure of the up-quark penguin and spectator scattering. We also generalize our results to $\bar{B} \to D\bar{D}$ decays. In the fourth chapter, we investigate the phenomenological consequences of our OPE and predict a plethora of *CP*-violating observables in $\bar{B} \to \psi X$ and $\bar{B} \to D\bar{D}$ decays.

In the fifth chapter we conclude. A list of abbreviations and variables is given in the appendix.

Chapter 1

$\bar{B}$ Physics in the Standard Model

In this chapter, we introduce notation and basic properties of $\bar{B}$ decays to which we will refer throughout this thesis. We discuss how *CP* violation is generated in the Standard Model (SM) and how the measurement of *CP* asymmetries in the aforementioned decay modes can be related to the *CP*-violating phases β and β_s. Subsequently, we identify the theoretical uncertainties of this determination and discuss their origin. In the next chapter, we will discuss how we aim at the improvement of these theoretical uncertainties by means of an operator product expansion.

1.1 *CP* violation in $\bar{B}$ meson decays

1.1.1 *CP* violation in the Standard Model

In the SM all quark flavor changing processes, such as $\bar{B}$ decays, are induced by charged weak currents. In the SM Lagrangian these are described by the coupling of $W^\pm$ bosons to left-handed quarks. The relevant part of the SM Lagrangian is given by [13–15]

$$\mathcal{L}_W = \frac{g_W}{\sqrt{2}} \sum_{j,k=1,2,3} \left[V_{jk}\, \overline{u}_{jL}\, \gamma^\mu d_{kL}\, W_\mu^+ + V_{jk}^*\, \overline{d}_{kL}\, \gamma^\mu u_{jL}\, W_\mu^- \right], \tag{1.1}$$

here g_W is the real-valued weak coupling constant and V_{jk} are entries of the unitary Cabibbo-Kobayashi-Maskawa (CKM) matrix [3, 4]

$$V_{\text{CKM}} = \begin{pmatrix} V_{ud} & V_{us} & V_{ub} \\ V_{cd} & V_{cs} & V_{cb} \\ V_{td} & V_{ts} & V_{tb} \end{pmatrix}. \tag{1.2}$$

Requiring that $\mathcal{L}_W$ is Hermitian implies that g_W is real. However, V_{CKM} is not real-valued, as a consequence $\mathcal{L}_W$ is not *CP* invariant because the weak quark transitions mediated by $V_{jk}\,\overline{u}_{jL}\,\gamma^\mu d_{kL}\,W_\mu^+$ and its *CP* conjugate process $V_{jk}^*\,\overline{d}_{kL}\,\gamma^\mu u_{jL}\,W_\mu^-$ have complex-conjugated phases. This leads to *CP* violation if two weak transitions with two different phases contribute to the same process.

The sum in Eqn. (1.1) runs over the quark flavors with $(u_1, u_2, u_3) = (u, c, t)$ and $(d_1, d_2, d_3) = (d, s, b)$. Quarks only appear in bound states because they are colored objects, this confinement into hadrons is induced by quantum chromodynamics (QCD). Therefore, in weak flavor transitions there is always an intricate interplay of the weak interaction and QCD. The QCD Lagrangian is given by [16]

$$\mathcal{L}_{\mathrm{QCD}} = -\frac{1}{4} G^a_{\mu\nu} G^{a,\mu\nu} + \sum_p \bar{p}(\mathrm{i}\not{D} - m_p)p, \tag{1.3}$$

where p runs over the quark flavors u, d, s, c, b, t. $D_\mu = \partial_\mu + \mathrm{i}g_S A^a_\mu T^a$ denotes the covariant derivative and $G^a_{\mu\nu} = \partial_\mu A^a_\nu - \partial_\nu A^a_\mu - g_S f^{abc} A^b_\mu A^c_\nu$ the field strength tensor. The field A^a_μ is the gauge field of the strong interaction and associated to the gluon, the gauge boson of the strong interaction. Hence, the non-abelian term in $-\frac{1}{4} G^a_{\mu\nu} G^{a,\mu\nu}$ also leads to gluon-gluon interactions. Requiring $\mathcal{L}_{\mathrm{QCD}} = \mathcal{L}^\dagger_{\mathrm{QCD}}$ implies a real coupling constant g_S. Thus, it seems that the QCD Lagrangian does not lead to *CP* violation but this is only true because we did not include the term $\epsilon^{\mu\nu\rho\sigma} G^a_{\mu\nu} G^a_{\rho\sigma}$ into the Lagrangian [17, 18]. This term is gauge invariant but violates P, T and *CP*. However, it has not been observed experimentally so far which means that it must have a very small coefficient [19]. The absence/smallness of this term is referred to as the strong *CP* problem and will not be further considered.

We conclude that the CKM matrix is the only source of *CP* violation in the SM.[1] Since we want to use *CP* violation as a tool to find new physics we are interested in the properties and the structure of the CKM matrix to which we draw our attention in what follows. In particular, we are interested in the CKM-element combination

$$\lambda_{pq} \equiv V^*_{pq} V_{pb} \tag{1.4}$$

because it appears in $\bar{B} \to \psi X$ and $\bar{B} \to D\bar{D}$ decays that are governed by the quark-level process $b \to \bar{p}pq$ with $p \in \{u, c, t\}$ and $q \in \{d, s\}$.

[1] In the SM neutrinos are assumed to be massless. In reality they have very small but nonzero masses. Depending on whether these are Dirac or Majorana masses this may lead to up to three additional *CP*-violating phases but these are irrelevant for our considerations.

1.1.2 CKM metrology

In the SM, all weak flavor changing transitions are proportional to entries of the CKM matrix. The CKM matrix is an unitary 3×3 matrix. A generic $U(3)$ matrix can be parametrized by three real Euler angles and six phases. In the CKM matrix, however, only one phase is physical. Indeed, by redefining the phases of the quark fields u_i and d_i in Eqn. (1.1), one can remove five phases. The remaining complex phase induces all *CP* violation the SM. Thus, the CKM matrix can be parametrized by three real and one phase. How the phase is chosen is convention dependent; the standard parametrization is due to Wolfenstein [20, 21]

$$V_{\mathrm{CKM}} = \begin{pmatrix} 1-\lambda^2/2 & \lambda & A\lambda^3(\bar{\rho}-i\bar{\eta}) \\ -\lambda & 1-\lambda^2/2 & A\lambda^2 \\ A\lambda^3(1-\bar{\rho}-i\bar{\eta}) & -A\lambda^2 & 1 \end{pmatrix} + \mathcal{O}\left(\lambda^4\right). \tag{1.5}$$

Conveniently, the Wolfenstein parametrization makes the experimentally observed size pattern of the matrix elements explicit with an expansion in $\lambda = 0.225$ [22]. Since V_{CKM} is unitary, $V_{\mathrm{CKM}} V_{\mathrm{CKM}}^{\dagger} = \mathbf{1}$ leads to a plethora of testable relations that are phase-convention independent. Of these, the six vanishing relations can be represented as triangles in the complex plane. In particular

$$V_{ud}V_{ub}^{*} + V_{cd}V_{cb}^{*} + V_{td}V_{tb}^{*} = 0 \tag{1.6}$$

is most advantageous because all three terms are $\mathcal{O}(\lambda^3)$. Furthermore, these CKM entries contribute to $b \to \bar{p}pd$ quark transitions with $p \in \{u, c, t\}$, this means we obtained a sum rule

$$\lambda_{ud}^{*} + \lambda_{cd}^{*} + \lambda_{td}^{*} = 0 \tag{1.7}$$

for the λ_{pq} defined in Eqn. (1.4). The angles of this triangle are

$$\alpha \equiv \arg\left(-\frac{V_{td}V_{tb}^{*}}{V_{ud}V_{ub}^{*}}\right), \tag{1.8}$$

$$\beta \equiv \arg\left(-\frac{V_{cd}V_{cb}^{*}}{V_{td}V_{tb}^{*}}\right), \tag{1.9}$$

$$\gamma \equiv \arg\left(-\frac{V_{ud}V_{ub}^{*}}{V_{cd}V_{cb}^{*}}\right), \tag{1.10}$$

they are physical quantities and have the advantage that their size is of several ten degrees. An illustration of these angles within the unitarity triangle (UT) can be found in Fig. 1.1.

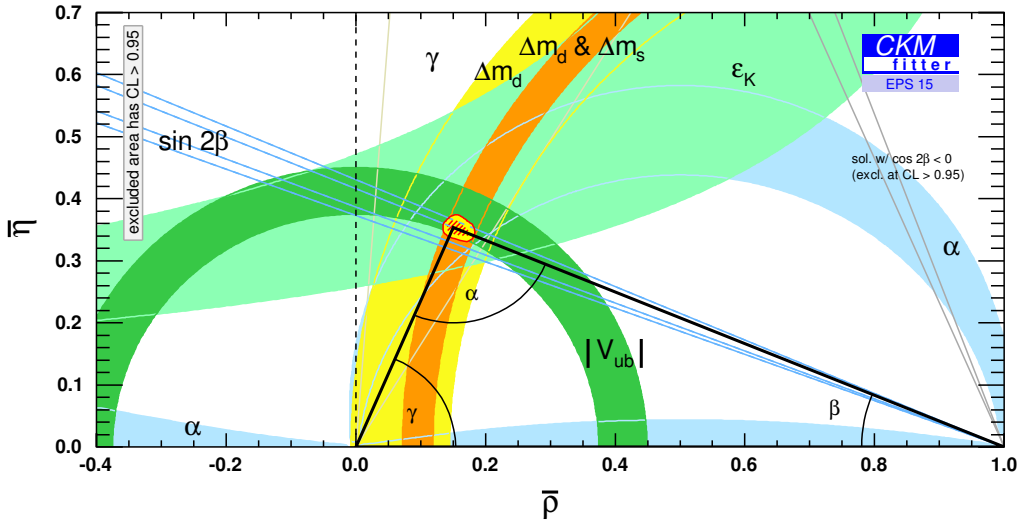

Figure 1.1: The $B_d - \bar{B}_d$ unitarity triangle in the $\bar{\rho} - \bar{\eta}$ plane [22]. Several measurements (colored bands) constrain the sides and angles (the base is normalized to one). The apex is overconstrained: if an experimental constraint deviates from the SM prediction, the different constraints will not overlap pointing to new physics.

It also displays several colored bands that represent the current experimental constraints on the angles and sides. The aim is to overconstrain the triangle as much as possible and to find tensions between the different measurements. If there are significant tensions this implies that the CKM matrix is insufficient to describe all flavor changing transitions and points to NP contributions.

The triangle relevant for $b \to \bar{p}ps$ transitions

$$V_{us}V_{ub}^* + V_{cs}V_{cb}^* + V_{ts}V_{tb}^* = 0 \tag{1.11}$$

$$\lambda_{us}^* + \lambda_{cs}^* + \lambda_{ts}^* = 0 \tag{1.12}$$

is quite squashed. The first term is $\mathcal{O}(\lambda^4)$ and the two latter terms are $\mathcal{O}(\lambda^2)$. Hence, it is almost an isosceles triangle and has one very small angle

$$\beta_s \equiv \arg\left(-\frac{V_{ts}V_{tb}^*}{V_{cs}V_{cb}^*}\right). \tag{1.13}$$

The value $\beta_s = 0.0188 \pm 0.0004$ is very precisely known from global fits [22, 23].

In general the length of the triangle sides are accessible in branching ratio measurements and the angles are observable in CP asymmetries. How the angle β and β_s can be accessed in measurements will be discussed in the following.

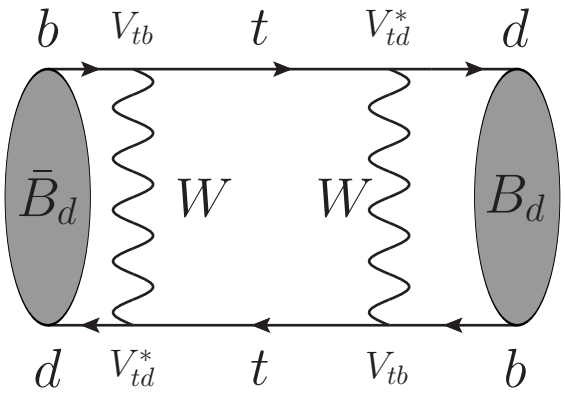

Figure 1.2: Due to the weak interaction neutral mesons can oscillate into their antiparticles. $\bar{B}_d - B_d$ oscillations are dominated by the top quark.

1.1.3 Neutral particles and *CP* violation

Before we discuss *CP*-violating observables in detail we must first discuss neutral-meson oscillations that enrich the neutral meson phenomenology considerably. At fourth order in g_W the Lagrangian $\mathcal{L}_W$ leads to neutral-meson oscillations. This means, the neutral mesons K^0, D^0, B_d and B_s can transform into their antiparticle. We are interested in the oscillations of $\bar{B}_d$ and $\bar{B}_s$ mesons. In the following we discuss $\bar{B}_d$ mesons, for $\bar{B}_s$ mesons every d must be replaced by an s. The quark-level diagram of $\bar{B}_d$ oscillations is shown in Fig. 1.2. Even though all up-type quarks contribute at the intermediate level, this process is dominated by the top quark, the dominant contribution is [24]

$$\langle B_d|\mathcal{H}_{\text{eff}}^{\Delta B=2}|\bar{B}_d\rangle \approx M_{12} \sim (V_{tb}V_{td}^*)^2\, m_t^2/M_W^4 \tag{1.14}$$

where $\mathcal{H}_{\text{eff}}^{\Delta B=2}$ is an effective Hamiltonian that can be derived from Eqn. (1.1), for details and the derivation of this formula we refer to references [24, 25]. A consequence of neutral-meson oscillation is that the flavor eigenstates are no mass eigenstates. However, we may define the mass eigenstates as

$$|B_L\rangle \equiv p\,|B_d\rangle + q\,\left|\bar{B}_d\right\rangle \tag{1.15}$$

$$|B_H\rangle \equiv p\,|B_d\rangle - q\,\left|\bar{B}_d\right\rangle. \tag{1.16}$$

with q and p being coefficients that obey $|q|^2 + |p|^2 = 1$. The flavor eigenstates that are produced at colliders propagate as linear combinations of the mass eigenstates. Hence, the flavor eigenstates evolve in time and a $\bar{B}_d$ may oscillate into a B_d. These oscillations

are characterized by the ratio q/p. The evaluation of the diagram in Fig. 1.2 leads to [26]

$$\left.\frac{q}{p}\right|_{B_d} \approx -\sqrt{\frac{M_{12}^*}{M_{12}}} = -\frac{V_{tb}^* V_{td}}{V_{tb} V_{td}^*} + \text{ small corrections.} \tag{1.17}$$

This means that $|q/p| = 1$ is a good approximation for $\bar{B}_d$ mesons (and $\bar{B}_s$ mesons).

On the other hand $\arg(q/p)$ gives us access to the phases of the CKM parameters in the standard phase convention, more precisely[2]

$$\begin{aligned} \phi_d &\equiv -\arg(-q/p)|_{\bar{B}_d} = 2\beta + \mathcal{O}\left(\lambda^4\right), \\ \phi_s &\equiv -\arg(-q/p)|_{\bar{B}_s} = -2\beta_s + \mathcal{O}\left(\lambda^6\right). \end{aligned} \tag{1.18}$$

Hence, measuring the $\bar{B}_d - B_d$ ($\bar{B}_s - B_s$) *mixing phase* ϕ_d (ϕ_s) allows us to determine the CKM angle β (β_s). It remains to be shown how the mixing phase can be accessed via an observable. These observables are *CP* asymmetries which we discuss now.

1.1.4 *CP*-violating observables for a general $\bar{B}$ decay

CP violation is, roughly speaking, the difference in the behavior of particles and antiparticles, since the *CP* symmetry relates particles with their antiparticles. It can be observed by considering rate differences of *CP*-conjugated decays

$$A_{CP}(B \to f) \equiv \frac{\Gamma(\bar{B} \to \bar{f}) - \Gamma(B \to f)}{\Gamma(\bar{B} \to \bar{f}) + \Gamma(B \to f)}. \tag{1.19}$$

There are three kinds of *CP* violation, direct *CP* violation, *CP* violation in mixing and mixing-induced *CP* violation. They are explained in detail in references [24, 25]. We focus on mixing-induced *CP* violation which appears in the interference of decay with and without mixing. It is possible if a neutral meson, e.g. $\bar{B}_p$ with $p \in \{d, s\}$, decays into a *CP* eigenstate f with $(CP)\,|f\rangle = \eta_f\,|f\rangle$. This means the interference of the processes

$$\bar{B}_p \to f \quad \text{and} \quad B_p \to \bar{B}_p \to f \tag{1.20}$$

[2]The phase of q/p is in fact dependent on the choice of the *CP* phase ξ in $(CP)\,|B_d\rangle = e^{i2\xi}\,|\bar{B}_d\rangle$ and is in principle an unphysical quantity. However, it is correct to say that once we have chosen $\xi = \xi_0$ we can relate $\arg(q/p)$ to a physical quantity.

leads to *CP* violation. In this case the *CP* asymmetry is time-dependent and can be written as [27, 28]

$$A_{CP}(B_p \to f)(t) \equiv \frac{\Gamma(\bar{B}_p(t) \to f) - \Gamma(B_p(t) \to f)}{\Gamma(\bar{B}_p(t) \to f) + \Gamma(B_p(t) \to f)} \tag{1.21}$$

$$= \frac{S_f \sin(\Delta m_p t) - C_f \cos(\Delta m_p t)}{\cosh(\Delta\Gamma_p t/2) + A_{\Delta\Gamma_p} t/2 \sinh(\Delta\Gamma_p t/2)}. \tag{1.22}$$

where Δm_p and $\Delta\Gamma_p$ are the mass and width difference of the mass eigenstates B_H and B_L in the $\bar{B}_p - B_p$ system defined in Eqn. (1.16). The *CP*-violating coefficients are given by

$$C_f \equiv \frac{1 - |\lambda_f|^2}{1 + |\lambda_f|^2}, \qquad S_f \equiv \frac{2\mathrm{Im}\lambda_f}{1 + |\lambda_f|^2}, \qquad A_{\Delta\Gamma_p} \equiv -\frac{2\mathrm{Re}\lambda_f}{1 + |\lambda_f|^2}. \tag{1.23}$$

All information on *CP* violation is encoded in

$$\lambda_f \equiv \frac{q}{p}\frac{\bar{A}_f}{A_f}. \tag{1.24}$$

The decay amplitudes A_f and $A_{\bar{f}}$ have the general form[3]

$$A_f = A(B_p \to f) = \lambda^*_{cq} t_f + \lambda^*_{uq} p_f, \tag{1.25}$$

$$\bar{A}_f = A(\bar{B}_p \to f) = -\eta_f(\lambda_{cq} t_f + \lambda_{uq} p_f), \tag{1.26}$$

which exploits the unitarity of the CKM matrix. The CKM combinations λ_{cq} and λ_{uq} have been defined in Eqn. (1.4). In $b \to c\bar{c}q$ decays, the dominant contribution to t_f is tree-level, and to p_f only loop-suppressed (penguin) diagrams can contribute. For a $\bar{B}_d$ decay the denominator in Eqn. (1.22) can be set to one since $\Delta\Gamma_d$ is very small and $\Delta\Gamma_d = 0$ is a very good approximation.

With $\epsilon_q \equiv \lambda_{uq}/\lambda_{cq}$, $a_f \equiv p_f/t_f$ and the mixing phases defined in Eqn. (1.18) we rewrite λ_f as

$$\lambda_f = \eta_f e^{-i\phi_p} \frac{1 + \epsilon_q a_f}{1 + \epsilon^*_q a_f}. \tag{1.27}$$

and expect $|a_f| < 1$.

For the measurement of $\phi_d = 2\beta$ and $\phi_s = -2\beta_s$ reference [5] suggested the de-

[3]Some inconsistency appears here in the notation, while the LHS is only a function of f the RHS also shows dependence on the quark flavors p and q. When we give generic expressions they will always only carry an index f. We keep the f as a gentle reminder that the decay amplitude is dependent on the final state f **and** the quark flavors p and q. In a specific decay we fix the quark flavors p and q and the final state f according to the decay mode.

cays $\bar{B}_d \to J/\psi K_S$ and $\bar{B}_s \to J/\psi\phi$, respectively. The authors realized that in these decay modes the term $\mathcal{O}(|\epsilon_s a_f|)$ in Eqn. (1.27) is small because the amplitude p_f is loop-suppressed and the CKM-element combination $|\epsilon_s| = 0.02$ is small. With terms $\mathcal{O}(|\epsilon_s a_f|)$ neglected the *CP*-violating observables simplify to

$$C_f = 0, \qquad S_f = -\eta_f \sin(\phi_p), \qquad A_{\Delta\Gamma_p} = -\eta_f \cos(\phi_p). \tag{1.28}$$

Thus, the time-dependent rate asymmetries allow for the measurement of β and β_s under the condition $|\epsilon_s a_f| \ll 1$.

The decays $\bar{B}_d \to J/\psi K_S$ and $\bar{B}_s \to J/\psi\phi$ have also the experimental advantages that the J/ψ is reconstructed via $J/\psi \to \mu^+\mu^-$ which has a not too small ($\approx 6\%$) branching ratio and a clear signature. Similarly, the K_S is reconstructed via $K_S \to \pi^+\pi^-$ (69%) and the ϕ is reconstructed via $\phi \to K^+K^-$ (49%).

When β finally had been measured by the B factories *BABAR* and Belle, this was the ultimate confirmation the of the KM model [4] and led to the award of the 2008 Nobel Prize in Physics to Kobayashi and Maskawa. The current world averages [29] are

$$S_{J/\psi K_S} = \sin(\phi_d) = 0.691 \pm 0.017, \quad S_{J/\psi\phi} = \sin(\phi_s) = -0.034 \pm 0.033. \tag{1.29}$$

The measurement of $S_{J/\psi K_S}$ represents the most precise direct determination of β and makes β the best-determined CKM angle. The measurement of $S_{J/\psi\phi}$ is not yet significant because the expected value $-\sin(2\beta_s)$ is tiny due to $\beta_s = 0.0188 \pm 0.0004$ [22, 23].

From the picture drawn above it becomes clear that measuring the *CP* violation in $\bar{B}_d \to J/\psi K_S$ and $\bar{B}_s \to J/\psi\phi$ gives access to the $\bar{B}_p - B_p$ mixing phases. However, this was made under the assumption that $|\epsilon_s a_f| \ll 1$. The assumption $|a_f| < 1$ is based on the fact that p_f in $a_f = p_f/t_f$ is loop-suppressed. However, p_f cannot be exactly calculated and could also be enhanced by some nonperturbative dynamics. Furthermore, depending on the value of $|a_f| \lesssim 1$ the experimental uncertainties $\sim 0.02 - 0.03$ in Eqn. (1.29) are similar to $|\epsilon_s| = 0.02$ which is the size of the theoretical uncertainty. Therefore, it is of utmost importance to get control over the *penguin pollution* $a_f = p_f/t_f$ in Eqn. (1.27), in particular in view of the increasing experimental precision. So far the only serious estimates of this penguin in $B_d \to J/\psi K_S$ have been achieved by the use of flavor symmetries [30–34]. This approach is based on an approximate $SU(3)_F$ symmetry which rotates the light quarks into each other (The $SU(2)$ subgroup rotating only d and s is called *U-Spin*), but these flavor symmetry approaches have considerable disadvantages (unknown size of $SU(3)_F$ breaking and low statistics in $b \to \bar{c}cd$ 'control channels'). The

use of flavor symmetries entirely fails in $B_s \to J/\psi\phi$ because the ϕ does not belong to a single representation of the $SU(3)_F$ symmetry but is an admixture of singlet and octet.

It is desirable to have a constraint on a_f from first principles, which will be the subject of this thesis. The formalism that will be presented in the next chapters will not only be applied to these two famous decays but to all $\bar{B} \to \psi X$ and $\bar{B} \to D\bar{D}$ decays. Before we come to this we will discuss the standard approaches to calculate exclusive $\bar{B}$ decay amplitudes and why they fail in $\bar{B} \to \psi X$ and $\bar{B} \to D\bar{D}$.

1.2 $\bar{B}$ meson decay amplitudes

In the preceding section it became clear that we need to understand the structure of $\bar{B}$ decay amplitudes to get a handle on the penguin pollution a_f. Therefore, we will now discuss the low-energy effective Hamiltonian that is used to derive $\bar{B}$ decay amplitudes. Furthermore, we discuss naive factorization, QCD factorization and $1/N_C$ counting, since with these approaches some $\bar{B}$ meson decay matrix elements can be evaluated. We also discuss why these approaches do not work (sufficiently) in $\bar{B} \to \psi X$ and $\bar{B} \to D\bar{D}$ decays.

1.2.1 The low-energy effective Hamiltonian

The decays $\bar{B} \to \psi X$ and $\bar{B} \to D\bar{D}$ are mediated by the quark-level process $b \to \bar{c}cq$ with $q \in \{d, s\}$. The energy release is of the order of the mass of the decaying meson $m_B \approx 5.3$ GeV. This scale is considerably smaller than the mass of the weak gauge boson $M_W = 80.4$ GeV that mediates these decays. Therefore, it is favorable to integrate out the heavy degrees of freedom instead of using the full SM Lagrangian in Eqns. (1.1) and (1.3). The contributions of Z and W bosons and of the top quark are then described by an effective Hamiltonian. Consequently, we describe the $b \to \bar{c}cq$ processes by the *low-energy effective Hamiltonian* [35]

$$\mathcal{H}^{\Delta B=1} = \frac{G_F}{\sqrt{2}} \sum_{p' \in \{u,c\}} \lambda_{p'q} \left[\left(C_1 Q_1^{p'} + C_2 Q_2^{p'} \right) + \sum_{i=3}^{6,8G} C_i Q_i \right]. \tag{1.30}$$

Here, G_F is Fermi's coupling constant and $\lambda_{p'q} = V_{p'q}^* V_{p'b}$ the typical combinations of CKM elements that contribute. The Wilson coefficients C_i with $i \in \{1, 2, 3, 4, 5, 6, 8G\}$ represent the effective couplings of the effective operators Q_i. These are the *current-*

current operators, defined by

$$Q_1^{p'} \equiv (\bar{p}'_\alpha b_\beta)_{V-A}(\bar{q}_\beta p'_\alpha)_{V-A} \tag{1.31}$$

$$Q_2^{p'} \equiv (\bar{p}' b)_{V-A}(\bar{q} p')_{V-A}, \tag{1.32}$$

and the *penguin operators*, defined by

$$Q_3 \equiv (\bar{q}b)_{V-A} \sum_p (\bar{p}p)_{V-A}, \tag{1.33}$$

$$Q_4 \equiv (\bar{q}_\alpha b_\beta)_{V-A} \sum_p (\bar{p}_\beta p_\alpha)_{V-A}, \tag{1.34}$$

$$Q_5 \equiv (\bar{q}b)_{V-A} \sum_p (\bar{p}p)_{V+A}, \tag{1.35}$$

$$Q_6 \equiv (\bar{q}_\alpha b_\beta)_{V-A} \sum_p (\bar{p}_\beta p_\alpha)_{V+A}, \tag{1.36}$$

$$Q_{8G} \equiv \frac{g_S}{8\pi^2} m_b \bar{q}\sigma^{\mu\nu}(1+\gamma^5)T^a G^a_{\mu\nu} b. \tag{1.37}$$

The sum over p runs over the active quark flavors u, d, s, c and b. The indices α and β are color indices with summation of repeated indices implied. The subscripts $(V \pm A)$ indicate the Lorentz structure of the operator, e.g. $(\bar{q}b)_{(V-A)}(\bar{p}p)_{(V\pm A)} \equiv (\bar{q}\gamma_\mu(1-\gamma_5)b)(\bar{p}\gamma^\mu(1 \pm \gamma_5)p)$. Furthermore, the QCD Lagrangian in Eqn. (1.3) describes the effects of the strong interaction of energies below the renormalization scale $\mu \sim m_b$. Thus, the sum in $\mathcal{L}_{\text{QCD}}$ does not run over t anymore.

The current-current operators derive from QCD-improved W exchange. The penguin operators derive from a (full Standard Model) one-loop penguin diagram involving the top quark and the W boson. For this reason we refer to them as the *top penguins* in contrast to the penguin diagrams in the effective theory that arise from insertions of the up and the charm quark current-current operators, see Fig. 1.3c. Note that we neglect electromagnetic effects in the whole thesis since they are negligible w.r.t. the leading QCD contributions.

From the effective Hamiltonian we derive the structure of the decay amplitudes of a $\bar{B}$ meson to a generic final state f

$$\mathcal{A}(\bar{B} \to f) = \lambda_{cq} t_f + \lambda_{uq} p_f \tag{1.38}$$

with

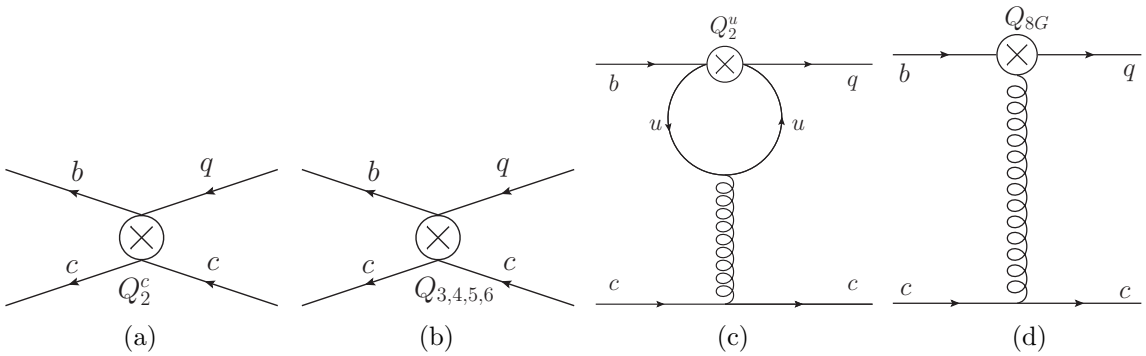

Figure 1.3: LO terms of a $\bar{B} \to f$ decay that is governed by the process $b \to c\bar{c}q$. Depending on how the quarks hadronize these diagrams contribute to $\bar{B} \to \psi X$ or $\bar{B} \to D\bar{D}$ and possibly involve further soft gluons. At tree-level only the $\bar{c}c$ component of the top penguins contribute. (a) Current-current operator insertion. (b) Top-penguin operator insertion. (c) Current-current operator insertion Q_2^u into the penguin diagram. (d) Insertion of the chromomagnetic dipole operator.

$$t_f = -\mathrm{i}\frac{G_F}{\sqrt{2}}\langle f|C_1Q_1^c + C_2Q_2^c + \sum_{i=3}^{6,8G} C_iQ_i|\bar{B}\rangle, \tag{1.39}$$

$$p_f = -\mathrm{i}\frac{G_F}{\sqrt{2}}\langle f|C_1Q_1^u + C_2Q_2^u + \sum_{i=3}^{6,8G} C_iQ_i|\bar{B}\rangle. \tag{1.40}$$

In Fig. 1.3 we show the corresponding LO Feynman diagrams on the quark level.

The Wilson coefficients $C_1 - C_6$ are calculated via a matching to the full SM and are known to next-to-leading order (NLO)[35] in the modified minimal subtraction scheme ($\overline{MS}$) [36] of naive dimensional regularization (NDR) we γ_5 take to be anti-commuting. The matrix elements $\langle Q_i\rangle$ are the fundamental difficulty in the evaluation of the $\bar{B}$ decay amplitude. Their calculation from first principles is impossible with current methods, since they cannot be evaluated in perturbation theory.

1.2.2 Evaluation of the matrix elements

Even though the calculation of the four quark matrix elements is not possible from first principles, there is a long history of approximate methods that had reasonable success in the description of the four-quark matrix elements. Most notable are naive factorization [37–39] and QCD factorization (QCDF) [6–8], whose applicability, however, has a limited scope. To explain these two concepts in order to relate them to our work let us discuss

the decay $\bar{B}_d \to D^+\pi^-$ in naive factorization and QCDF.

The assumption of naive factorization (a very concise discussion may be found in reference [40]) is that one of the final state particles (the π^-) separates itself very fast from the point-like effective vertex in an exclusive, nonleptonic, two-body decay. The hadronization of the decay products happens on much longer time scales than the decay. Hence, the two quarks, which ultimately form the pion, separate themselves from the $(\bar{B}D)$ system before they hadronize. Since they must be in a color singlet to form the pion, they are very insensitive to soft interactions because of color transparency [41]. In our example, the four-quark interaction is then split up into two separate currents

$$\langle D^+(p')\pi^-(q)|(\bar{c}b)_{V-A}(\bar{d}u)_{V-A}|\bar{B}_d(p)\rangle\big|_{fact} = \langle \pi^-(q)|\bar{d}\gamma_\mu\gamma_5 u|0\rangle\langle D^+(p')|\bar{c}\gamma^\mu b|\bar{B}_d(p)\rangle. \tag{1.41}$$

Let us define the form factors $F_0^{BD}(q^2)$ and $F_1^{BD}(q^2)$ of the $B \to D$ transition

$$\begin{aligned}\langle D(p')|\,\bar{q}\gamma_\mu b\,|B(p)\rangle \;\equiv\; & F_1^{BD}(q^2)\left((p+p')_\mu - \frac{m_B^2-m_D^2}{q^2}q_\mu\right) \\ & + F_0^{BD}(q^2)\frac{m_B^2-m_D^2}{q^2}q_\mu\end{aligned} \tag{1.42}$$

with $q = p - p'$. Furthermore, we define the pion decay constant f_π

$$\left\langle \pi^-(q)\right|\bar{d}\gamma_\mu\gamma_5 u\,|0\rangle \equiv \mathrm{i}f_\pi q_\mu. \tag{1.43}$$

Form factors and decay constants can be be determined in (semi-) leptonic decays. They are general properties of the involved particles and not decay-specific. We use them to rewrite the factorized matrix element as

$$\langle D^+(p')\pi^-(q)|(\bar{c}b)_{V-A}(\bar{d}u)_{V-A}|\bar{B}_d(p)\rangle\big|_{fact} = \mathrm{i}F^{BD}(m_{\pi^-}^2)f_{\pi^-}(m_{\bar{B}_d}^2 - m_{D^0}^2). \tag{1.44}$$

Thus, the unknown four-quark matrix element has been expressed by simpler and general hadronic quantities.

Clearly, this phenomenological approach does not include all QCD contributions since it neglects all interactions between the two hadronic currents. However, given the motivation above they should represent the dominant part of the full four-quark matrix element. We refer to terms that are neglected in naive factorization as 'nonfactorizable' terms. Naive factorization has reasonable success in many decay modes. Today, this success has been understood because naive factorization represents the (or a) zeroth order term of the amplitude in QCDF.

QCDF exploits that the energy release in $\bar{B}$ meson decays, $\mathcal{O}(m_b)$, represents a hard scale in the four-quark matrix elements. This allows an expansion of the matrix elements in $\frac{\Lambda_{\rm QCD}}{m_b}$ and leads to a similar decomposition as in Eqn. (1.41). The difference to naive factorization is that in QCDF dominant 'nonfactorizable' effects can be calculated systematically. A short introduction to QCDF can be found in reference [42].
In references [6, 7] it was realized that the 'nonfactorizable' hard-gluon exchange between the two hadronic currents can be calculated perturbatively. It can be described by a *hard-scattering kernel*, denoted by $T^I_{ij}(u)$. The 'nonfactorizable' soft-gluon exchange between the two currents is suppressed by $\frac{\Lambda_{\rm QCD}}{m_b}$. If M_1 is a heavy meson and M_2 is a light meson the four-quark matrix element can then be written as [42]

$$\langle M_1 M_2|Q_i|\bar{B}\rangle = \sum_j F_j^{BM_1}(m^2_{M_2}) \int_0^1 {\rm d}u T^I_{ij}(u)\Phi_{M_2}(u) + \mathcal{O}\left(\frac{\Lambda_{\rm QCD}}{m_b}\right). \tag{1.45}$$

In our example, $M_1 = D^+$ and $M_2 = \pi^-$, the form factor $F_j^{BM_1}(m^2_{M_2})$ that describes the $\bar{B} \to M_1$ transition is same as in Eqn. (1.42). The hard-gluon exchange of this transition with M_2 is described by a convolution of the hard-scattering kernel $T^I_{ij}(u)$ with $\Phi_{M_2}(u)$ which is the light-cone distribution amplitude (LCDA) of M_2. The $\Phi_{M_2}(u)$ describes the hadronization probability of an energetic quark carrying the light-like hard momentum fraction u and of an antiquark with momentum fraction $1-u$.

QCD factorization can be used to compute four quark matrix elements in the decays of a $\bar{B}$ meson to two light pseudoscalar or vector mesons or to a heavy-light final state, if the heavy meson (D meson) picks up the spectator quark. In contrast, QCDF is not applicable to light-heavy decays where the light meson picks up the spectator quark and to decays into heavy-heavy final states such as $\bar{B} \to D\bar{D}$. QCD factorization formally applies to $\bar{B}$ decays to charmonia but, actually, is not applicable because the formal suppression factor of soft contributions $\frac{\Lambda_{\rm QCD}}{\alpha_S(m_b)m_c} \sim 1$ is not small. For example, the branching ratio $\mathcal{B}(\bar{B}_d \to J/\psi K_S)$ has been calculated in QCDF in reference [9, 10] but fails to describe the experimental data by a factor of eight. QCDF fails if the emission particle M_2 separates itself too slowly from the $B \to M_1$ transition because the final-state particles begin to hadronize when they are still close. Thus, the hadronization of the final state particles cannot be separated and is dependent on decay-specific conditions.

Another interpretation of naive factorization is that it represents the lowest-order term in the large N_C limit [12, 40, 43, 44]. $N_C = 3$ is the number of colors. The $N_C \to \infty$ limit while keeping $N_C g_S^2 = $ const. allows to order four-quark matrix elements in terms of N_C. The naively-factorizable terms are leading while soft or hard gluon exchange lead to

terms suppressed by $1/N_C$.

Estimating matrix elements in the large N_C limit is a nonperturbative method independent of the perturbative expansion in α_S and also applicable to low-energy matrix elements such as matrix elements in $\bar{B} \to D\bar{D}$ or $\bar{B} \to \psi X$ decays. The disadvantages of N_C counting are that correction terms cannot be computed rigorously and that in view of $N_C = 3$ correction terms could be larger than expected.

The above discussion makes it clear that it is rather difficult to make reliable predictions about amplitudes in $b \to c\bar{c}q$ transitions with the current theoretical means. Nevertheless, this calculation seems rather desirable in view of the fact that they are the limiting theoretical uncertainty in the prediction of *CP* asymmetries and in the extraction of CKM parameters from observables.

This failure is due to our inability to compute four-quark matrix elements from first principles. The problem of calculating matrix elements can be divided into two subproblems.

First, there are the matrix elements of the four-quark operators that produce directly a $\bar{c}c$ pair such as $Q_2^c = (\bar{c}b)_{V-A}(\bar{q}c)_{V-A}$. The matrix elements of these operators largely determine the tree amplitude t_f and, therefore, are important for the prediction of branching ratios. It is possible to control these matrix elements with N_C counting.

Second, there are effective operators that do not directly produce a $\bar{c}c$ pair, they lead to nonlocal, multiscale matrix elements, such as $\langle Q_i^u \rangle$. They represent the dominant uncertainty in the penguin-to-tree ratio a_f which determines the *CP*-violation observables.

It is our aim to clarify the significance of these matrix elements. Their treatment will be the subject of the next two chapters. In Chapter 2, we will suggest an operator product expansion (OPE) to describe the arising nonlocal processes via local operators. In Chapter 3, we will prove that this OPE is viable. In the subsequent chapters, we focus on the phenomenology of $\bar{B} \to \psi X$ and $\bar{B} \to D\bar{D}$ decays.

Chapter 2

Operator Product Expansion

We have identified the four-quark matrix elements as the dominating uncertainty in the determination of *CP* violation observables. In particular, the operators that lead to nonlocal matrix elements, such as $\langle Q_i^u \rangle$, are problematic.

The diagrams that lead to nonlocal matrix elements are given in Fig. 2.1. We observe that there is a large momentum transfer $q^2 \sim m_\psi^2 \sim 10\ \text{GeV}^2$ to the $\bar{c}c$ line running through the loop and through the gluon. There has been the general conjecture of Bander, Silverman, and Soni (BSS) [11] that a loop process, if a large momentum runs through it, can be computed perturbatively. This conjecture is not proven for $b \to c\bar{c}q$ decays but the momentum running through the up quark loop q^2 certainly represents a large momentum in the sense that $q^2 \gg \Lambda^2_{\text{QCD}}$. The formal interpretation of the BSS conjecture is to describe the loop within an operator product expansion (OPE) that exploits $q^2 \gg \Lambda^2_{\text{QCD}}$. Our aim is to prove that it is possible to describe the nonlocal matrix elements in $b \to c\bar{c}q$ transitions with an OPE.

Unlike in the derivation of the low-energy effective Hamiltonian, no particles but merely a scale is integrated out in this OPE. Light quarks or gluons with an off-shellness of q^2 cannot contribute anymore. The consequence is that the diagrams in Fig. 2.1 are effectively a point-like process and can be represented by an effective interaction. The coupling strength of this interaction is then encoded in a perturbative Wilson coefficient.

In the literature we find already some OPEs that formalize the BSS conjecture. In particular QCDF includes the BSS idea but is a lot more sophisticated. Another OPE in the spirit of BSS has successfully been applied in $B \to K^{(*)} l^+ l^-$ decays [45–47]. Here, the momentum transfer q^2 to the $l^+ l^-$ pair is used to expand in $\Lambda^2_{\text{QCD}}/q^2$.

We will prove and apply an OPE to describe the nonlocal matrix elements in $b \to c\bar{c}q$ transitions. This resolves the problem of nonlocal matrix elements and reduces them to

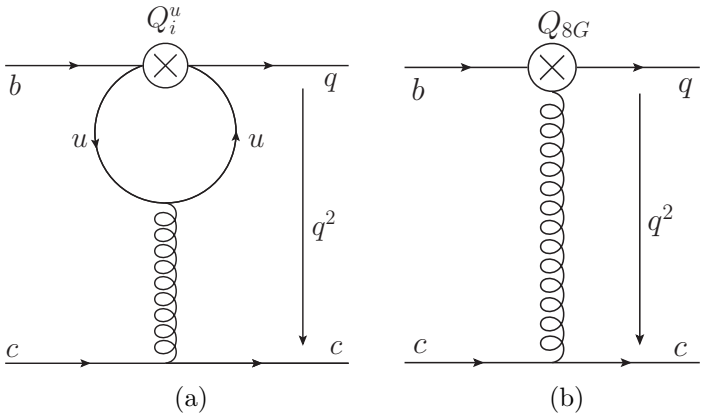

Figure 2.1: LO terms of the full theory that lead to nonlocal, multiscale matrix elements and which we describe with the OPE. (a) Insertion of a local four-quark operator into the penguin diagram. (b) Insertion of the chromomagnetic dipole operator.

matrix elements of local operators. The operator basis of these local operators consists of dimension-six and dimension-seven operators. We choose the following basis for the six-dimensional operators

$$\begin{aligned} Q_{0V} &\equiv \bar{q}\gamma_\mu(1-\gamma_5)b\,\bar{c}\gamma^\mu c, \\ Q_{0A} &\equiv \bar{q}\gamma_\mu(1-\gamma_5)b\,\bar{c}\gamma^\mu\gamma_5 c, \\ Q_{8V} &\equiv \bar{q}\gamma_\mu(1-\gamma_5)T^a b\,\bar{c}\gamma^\mu T^a c, \\ Q_{8A} &\equiv \bar{q}\gamma_\mu(1-\gamma_5)T^a b\,\bar{c}\gamma^\mu\gamma_5 T^a c. \end{aligned} \tag{2.1}$$

This basis can easily be related to Q_1^c and Q_2^c but has the advantage that it is color orthogonal and allows a transparent color counting later on.

Except for chiral and color structure there are only two genuine dimension-seven operators possible in the SM, all other operators can be reduced to dimension-six operators times a mass. We use as a basis for the dimension-seven operators

$$\begin{aligned} Q_{0T} &\equiv \frac{1}{m_b}\partial^\nu(\bar{q}\sigma_{\mu\nu}(1+\gamma_5)b)\,\bar{c}\gamma^\mu c, \\ Q_{8T} &\equiv \frac{1}{m_b}\partial^\nu(\bar{q}\sigma_{\mu\nu}(1+\gamma_5)T^a b)\,\bar{c}\gamma^\mu T^a c, \\ Q_{0\tilde{T}} &\equiv \frac{1}{m_b}\bar{q}\gamma_\mu(1-\gamma_5)b\,\partial_\nu(\bar{c}\sigma^{\mu\nu}c), \\ Q_{8\tilde{T}} &\equiv \frac{1}{m_b}\bar{q}\gamma_\mu(1-\gamma_5)T^a b\,\partial_\nu(\bar{c}\sigma^{\mu\nu}T^a c). \end{aligned} \tag{2.2}$$

These operators can be derived from the operators H^q, $\tilde{H}^q$, $\mathcal{H}^q$, and $\tilde{\mathcal{H}}^q$ in reference [48] where all dimension-seven operators in $b \to s$ transitions have been identified. The above basis implies that there is no dimension-seven four-quark-one-gluon effective interaction possible in the SM. The basis derived in reference [48] conceals this fact.

Let us now identify the terms that cannot directly be described by the basis in Eqn. (2.1) and Eqn. (2.2) and need to be treated in the OPE. For this we consider

$$\mathcal{A}(\bar{B} \to f) = \lambda_{cq} t_f + \lambda_{uq} p_f, \tag{2.3}$$

with

$$t_f = \frac{G_F}{\sqrt{2}} \langle f | C_1 Q_1^c + C_2 Q_2^c + \sum_{i=3}^{6,8G} C_i Q_i | \bar{B} \rangle, \tag{2.4}$$

$$p_f = \frac{G_F}{\sqrt{2}} \langle f | C_1 Q_1^u + C_2 Q_2^u + \sum_{i=3}^{6,8G} C_i Q_i | \bar{B} \rangle \tag{2.5}$$

in more detail. We decompose the penguin operators into a charm and a non-charm component, e.g.,

$$Q_3 = (\bar{q}b)_{V-A} \sum_{p \in \{u,d,s,c,b\}} (\bar{p}p)_{V-A} = Q_3^c + Q_3^{\text{nc}} \tag{2.6}$$

with $Q_3^c \equiv (\bar{q}b)_{V-A}(\bar{c}c)_{V-A}$ and $Q_3^{\text{nc}} \equiv (\bar{q}b)_{V-A} \sum_{p \in \{u,d,s,b\}} (\bar{p}p)_{V-A}$ and analogous definitions for Q_4, Q_5 and Q_6. The matrix elements of Q_1^c, Q_2^c and the charm component of the penguin operators Q_i^c with $i \in \{3,4,5,6\}$ emit the $\bar{c}c$ quark pair necessary for the final state. These matrix elements can simply be expressed with the operator basis in Eqn. (2.1). In contrast, the matrix elements of Q_1^u, Q_2^u, Q_{8G} and Q_i^{nc} with $i \in \{3,4,5,6\}$ must be nonlocal because the valence quark content of the operators does not match the final state. For example, the up quark pair of Q_2^u annihilates into a gluon that subsequently produces a $\bar{c}c$ pair as it is shown in Fig. 2.1a. Similarly, in the matrix element of the chromomagnetic dipole operator, depicted in Fig. 2.1b, the gluon annihilates into a $\bar{c}c$ pair. In the mentioned diagrams the charm quark pair is in a color octet state because the diagrams represent only the hard process, the correct color charges are arranged by soft gluons.

With the α_S-counting $C_1, C_2 \sim \mathcal{O}(1)$ and $C_3, C_4, C_5, C_6 \sim \mathcal{O}(\alpha_S)$ for the Wilson coefficients, the insertions of Q_i^{nc} with $i \in \{3,4,5,6\}$ into the penguin diagrams are $\mathcal{O}(\alpha_S^2)$. This is why we will neglect them for now, the inclusion of the Q_i^{nc} insertions is a straight-forward generalization of the Q_i^u insertions and will be done in section 4.1.1 after

the validity of the OPE has been shown. Hence, we only have to consider the insertions of Q_1^u, Q_2^u and Q_{8G} into the penguins for the OPE. It is then our aim to show that these insertions can systematically be expanded in the basis 2.1 and 2.2,

$$\boxed{\langle f|Q_j^{(u)}|\bar{B}\rangle = \sum_k \widetilde{C}_{j,k}\langle f|Q_k|\bar{B}\rangle + \mathcal{O}\left(\frac{\Lambda_{\rm QCD}}{M}\right),} \tag{2.7}$$

for $j \in \{1, 2, 8G\}$ and k running over $k = 0V, 0A, 8V, 8A, 0T, 8T, 0\tilde{T}, 8\tilde{T}$. The validity of the OPE is expected to be true up to $\mathcal{O}(\Lambda_{\rm QCD}/M)$ with $M \equiv \sqrt{q^2}$.

The coefficients $\widetilde{C}_{j,k} = \widetilde{C}_{j,k}^{(0)} + \frac{\alpha_S(\mu)}{4\pi}\widetilde{C}_{j,k}^{(1)} + \ldots$ can be calculated perturbatively, we find

$$\widetilde{C}_{2,8V}^{(0)} = P(q^2) \quad \text{and} \quad \widetilde{C}_{8G,8T}^{(0)} = -\frac{m_b^2}{q^2}\frac{\alpha_s(\mu)}{\pi}. \tag{2.8}$$

with the *penguin function* defined as

$$P(q^2) \equiv \frac{2}{3}\frac{\alpha_s(\mu)}{4\pi}\left[\ln\left(\frac{q^2}{\mu^2}\right) - \mathrm{i}\pi - \frac{2}{3}\right]. \tag{2.9}$$

All other coefficients vanish. The coefficients depend on the renormalization scale μ and on the momentum transfer q^2.

Before we dwell on to the proof of the relation in Eqn. (2.7), let us comment on some features.

- Since the OPE requires a certain kinematical configuration (q^2 must be transferred from the $b-s$ line to the $\bar{c}c$ pair), the OPE does not represent a full effective theory and cannot be represented by an effective Hamiltonian. Nevertheless, we will refer to the processes after the OPE as the *effective theory* and to the low-energy effective Hamiltonian in Eqn. (1.30) as the *full theory* because we will not refer to the full SM Lagrangian anymore.

- We only integrate out the hard penguin diagrams and cannot resolve the problem that the wave functions of the final-state particles have a large overlap and cannot be separated. This is why the OPE results into four-quark matrix elements.

- The dimension-seven operators must be counted as a dimension-six operator in our OPE because the derivative ∂^ν is replaced by $iq^\nu \sim M$ in the matrix element. Of the operators in Eqn. (2.2) only Q_{8T} arises in the OPE at LO and derives from the Q_{8G} penguin. It can be reduced to a proper dimension-six operator plus a dimension

seven operator which introduces a coupling to a gluon

$$\frac{1}{m_b}\partial^\nu(\bar{q}\sigma_{\mu\nu}(1+\gamma_5)T^a b)\,\bar{c}\gamma^\mu T^a c = Q_{8V} + \frac{2}{m_b}\bar{q}i\overleftarrow{D}_\mu(1+\gamma_5)T^a b\,\bar{c}\gamma^\mu T^a c \quad (2.10)$$

$$= Q_{8V} + \mathcal{O}\left(\frac{E_q}{m_b}\right) \quad (2.11)$$

Here, we used that $\partial_\nu = \overleftarrow{D}_\nu + \overrightarrow{D}_\nu$ and $\mathrm{i}\not{\overrightarrow{D}}b = m_b b$. A term $\bar{q}_i \mathrm{i}\overleftarrow{D}_\mu \equiv \mathrm{i}\partial_\mu\bar{q}_i - g\bar{q}_j A^a_\mu T^a_{ji}$ arises. This term is suppressed by E_q/m_b, where E_q is the energy of the light quark q in the $\bar{B}$ meson rest frame.

- The OPE still results into "unknown" matrix elements but the structure of the decay amplitude is greatly simplified in our approach. In particular, it becomes clear that the matrix element that controls the penguin pollution is already present in the branching ratio and consequently under control. Thus, our method is mostly suitable to make predictions for *CP*-violating observables and less suited to predict branching ratios but, of course, the simplified decay amplitude structure leads also to testable relations of decay amplitudes and, therefore, to testable relations of branching ratios.

- The OPE implies to good approximation that

$$p_f \propto (2C_2\widetilde{C}_{2,8V} + 2C_4 + 2C_6 + C_{8G}\widetilde{C}_{8G,8T})\,\langle Q_{8V}\rangle\,. \quad (2.12)$$

Since $\frac{2C_2\widetilde{C}_{2,8V}+C_{8G}\widetilde{C}_{8G,8T}}{2C_4+2C_6} \approx \frac{i}{2}$ at the scale $\mu = m_b$, this implies that the the up-quark and chromomagnetic penguin only add a small correction to the penguin pollution. The dominant contribution to the penguin pollution arises from the top-quark penguins.

It is the goal of this thesis to prove the validity of the OPE in Eqn. (2.7) and to apply it to decays that are governed by the quark-level process $b \to c\bar{c}q$. In the next chapter we will perform the proof. The reader interested in the phenomenological application may continue with reading Chapter 4.

Chapter 3

Factorization

In this chapter, we will first discuss the conditions and assumptions of the OPE and then prove the validity of the OPE to one-loop order.[1] Here, we use the term factorization unrelated to naive factorization or QCDF in the sense of 'factorization of scales'. It means that we can systematically separate long and short-distance effects in a particular process. Consequently, factorization implies that we can apply an OPE. This corresponds to integrating out high energy scales and to describe their effects by a Wilson coefficient. The low energy effects can be encapsulated into the matrix elements of effective operators or are power-suppressed. Proving factorization involves to show:

1. the factorization of hard and soft scales in $b \to c\bar{c}q$, i.e. on the quark level.
2. the suppression of soft and hard-collinear spectator scattering.
3. the suppression of soft penguins.
4. the suppression of additional soft or hard partons.

We will elaborate on these topics in the second section, they represent the main findings of this chapter.

In this thesis we consider the two decay classes $\bar{B} \to \psi X$ and $\bar{B} \to D\bar{D}$ which both derive from the quark-level transition $b \to c\bar{c}q$. The difference between both decay modes is that the final valence quarks hadronize in different configurations. Whereas in $\bar{B} \to \psi X$ decays the charm quarks hadronize into a charmonium, in $\bar{B} \to D\bar{D}$ decays the charm quarks hadronize into different final mesons. This leads to a different kinematic situation and a different treatment of the spectator quark. Therefore, we will first discuss

[1] One additional loop to the up-quark or chromomagnetic penguin

the proof for $\bar{B} \to \psi X$ modes to be more explicit, and discuss the necessary modifications for $\bar{B} \to D\bar{D}$ decays in section 3.8.

Furthermore, we will first only discuss the $\bar{B}$ decay as a b quark decay and ignore the spectator quark. The aspects due to the inclusion of the spectator quark are discussed in sections 3.3, 3.6 and 3.7.

3.1 Conditions and assumptions

We begin by spelling out the kinematical situation and then introduce our power counting. The assumptions will be discussed in the second subsection.

3.1.1 Kinematics

We will chose the $\bar{B}$ rest frame as the reference frame to describe the $\bar{B} \to \psi X$ decay. Even though the subsequent discussion does not depend on this choice, it simplifies our analysis. The momenta of the mesons are all fixed by four-momentum conservation (see Fig. 3.1a)

$$p_B = \begin{pmatrix} m_B \\ 0 \\ 0 \\ 0 \end{pmatrix}, \quad p_X = \begin{pmatrix} p_{\text{cm}} \\ 0 \\ 0 \\ -p_{\text{cm}} \end{pmatrix} = p_{\text{cm}} n_-, \quad \text{and} \quad p_\psi = \begin{pmatrix} E_\psi \\ 0 \\ 0 \\ p_{\text{cm}} \end{pmatrix} \tag{3.1}$$

with $E_\psi = \sqrt{m_\psi^2 + p_{\text{cm}}^2}$ and where X is considered massless. Consequently, p_X is on the light cone, this has been parametrized with the light-cone vector $n_\pm = (1, 0, 0, \pm 1)^\perp$. The center-of-mass momentum is

$$p_{\text{cm}} \equiv \frac{m_B^2 - m_\psi^2}{2m_B} \tag{3.2}$$

and a typical value is $p_{\text{cm}} = 1.7$ GeV. We consider the $\bar{B}$ meson in the heavy quark limit in its rest frame. In this case the b quark is at rest and the momentum $p_b \simeq m_b/2(n_+ + n_-)$. Since the b quark is confined in a $\bar{B}$ meson, this is only true up to corrections $\mathcal{O}(\Lambda_{\text{QCD}})$. Therefore, we use the "$\simeq$" which we use "as equal up to higher orders", here in Λ_{QCD}. The momentum that runs through the hard gluon that creates the ψ must have momentum $q \simeq p_\psi$. Since a ψ cannot be created by a single gluon, there are soft gluons that correctly arrange the quantum numbers but these are not drawn, since we only draw hard lines. $p' \simeq p_{\text{cm}} n_-$ is the momentum of the light quark q that stems from the effective vertex,

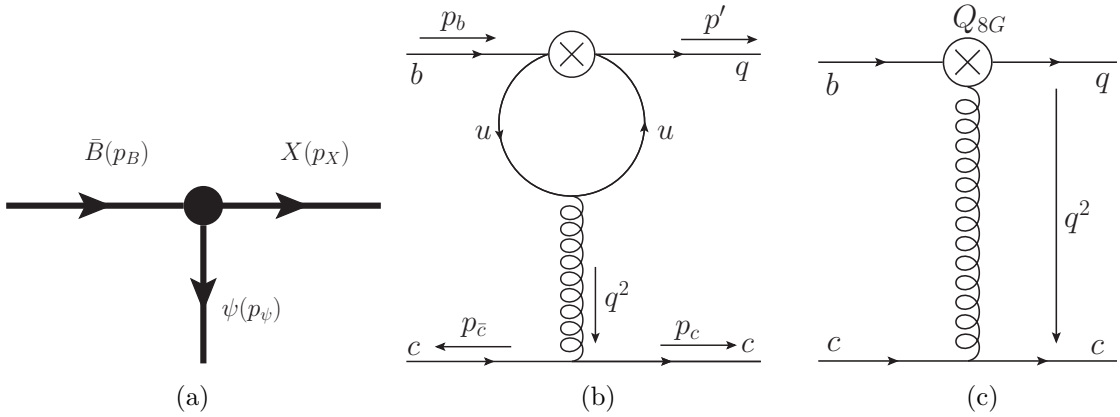

Figure 3.1: Naming conventions. (a) Naming convention for the external momenta mesons. (b) Naming convention for the external momenta quarks. (c) Q_{8G} penguin.

see Fig. 3.1b. Note, that we use the symbol q for the light quark created at the effective vertex and for the momentum transfer to the ψ, however, this should not lead to confusion since it should be clear from the context whether we refer to the momentum transfer or to the light quark.

Power counting: In the following we will rely on the heavy-mass limit with $m_b \to \infty$ and m_c/m_b fixed. The center-of-mass momentum $p_{\rm cm}$ is treated as a separate scale with

$$m_b \gg p_{\rm cm} \gg \Lambda_{\rm QCD}. \tag{3.3}$$

This is done because in reality $p_{\rm cm}$ is an intermediate scale between m_b and $\Lambda_{\rm QCD}$, even though the heavy-mass limit implies $p_{\rm cm} \sim \frac{m_b}{2}\left(1-\frac{4m_c^2}{m_b^2}\right) \sim m_b \to \infty$. Furthermore, instead of distinguishing m_b and $\sqrt{q^2}$ we will generally employ

$$m_b \sim \sqrt{q^2} \sim M \to \infty. \tag{3.4}$$

3.1.2 Assumptions

The factorization is subject to the assumption that there is no coherent configuration of soft gluons that transfers a hard momentum.

The result for $\widetilde{C}_{2,8V}^{(0)}$ in Eqn. (2.8) has an imaginary part, this reflects that the intermediate up quarks can go on shell. One may argue that this leads to resonances that cannot be described in perturbation theory. Indeed, the perturbative calculation as a function of q^2 does not necessarily describe the process correctly point-by-point. Nevertheless, if

q^2 is far away from the resonant region the penguins are correctly described. Such that at $q^2 \sim (2m_\pi)^2$ the OPE fails but since the virtuality $q^2 \sim m_\psi^2$ is far above the $\bar{u}u$ resonances the perturbative description is expected to be correct. This assumption is similarly made in the OPE in $B \to K^{(*)} l^+ l^-$ decays [45–47] and in QCDF [49]. Furthermore, it corresponds to the smearing method in the calculation of inclusive cross sections [50].

3.2 Factorization of hard and soft scales

We want to evaluate the contributions of the up-quark and chromomagnetic penguin in Figs. 3.1b and 3.1c. Since there is the large momentum transfer $q^2 = M^2$ in these processes, we want to extract the perturbative part of these penguins with an OPE. This is only possible if the perturbative part can systematically be separated from the nonperturbative contributions. In particular this means that by integrating out the scales of $\mathcal{O}(M)$, we should obtain Wilson coefficients that are infrared (IR) finite. To understand the IR structure of the penguins we will first give a short general introduction on IR divergences in QCD and then search for solutions of the Landau equations which are a necessary criterion for an IR divergence. To examine the solutions of the Landau equations we will subsequently employ a power counting to evaluate which of the solutions eventually leads to an IR divergence. We do not aim at an all order statement but will only consider the two-loop NLO penguin diagrams to get an understanding of our process. Furthermore, we do not need to consider diagrams in which the second gluon only connects external legs, since these factorize into the matrix elements. We will limit the discussion of the IR structure on the Q_i^u penguin insertions and comment shortly on the IR structure of the Q_{8G} penguins at the end of this section.

3.2.1 Notions on infrared divergences

In the context of flavor physics, infrared divergences only rarely turn up, for this reason we first discuss several general aspects of IR divergences before we consider them in our special case. Here, we follow references [16, 51].

Many quantum theories use perturbative methods to describe transition amplitudes, in perturbation theory usually Feynman integrals are necessary to make higher-order computations. Feynman integrals are functions of external momenta and masses. The singularities of Feynman integrals are called *Landau singularities* and depend on external momenta and internal masses. The singularities that are independent of the orientation of the external momenta and, consequently, only depend on external and internal masses are

called mass singularities and are a special class of Landau singularities. They are due to vanishing or finite loop momenta and are therefore called infrared (IR) singularities. More specifically we distinguish soft and collinear IR divergences. Soft divergences arise when a loop momentum goes to zero (becomes soft) and are related to massless gauge bosons, collinear divergences appear if massless matter fields interact with gauge bosons and both carry collinear momenta. In QCD, IR divergences arise if the long-distance structure is not correctly described by perturbation theory and are usually due to hadronization effects.

Ultraviolet (UV) singularities of Feynman integrals are due to infinite loop momentum, they are a short distance phenomenon and can be treated by renormalization, therefore, we will not consider them here.

If we are confronted with the exercise to investigate a given diagram on IR divergences, we can compute the integral in naive dimensional regularization, the IR singularities will then turn up as $\frac{1}{\epsilon}$ poles after proper renormalization of the UV poles. Nevertheless, computing loop diagrams which involve different mass scales can be a tedious exercise, furthermore the $\frac{1}{\epsilon}$ pole disguises the origin of the IR divergence. Fortunately, it is also possible to investigate the IR structure of a diagram without actually computing it with the help of the Landau equations [52] which enable us to find the possible IR singularities of a Feynman diagram. Unfortunately, the Landau equations are only a necessary and no sufficient criterion for an IR divergence. Thus, after having found possible IR divergences we will use a power counting to see whether a given diagram is actually IR divergent.

A pedagogical introduction to the Landau equations is given in the book of Böhm, Denner and Joos [51]. We follow their explanation here to introduce shortly the Landau equations. Consider a general Feynman diagram G with E external legs carrying the momenta p_j. Furthermore, it has L loops with loop momentum k_l and there are I internal lines with masses m_i and momenta q_i. The q_i must be linear combinations of some of the k_l and p_j. We then write a general Feynman integral as

$$F_G(p_j, m_n) = \int \left(\prod_{l=1}^{L} \mathrm{d}^4 k_l \right) N(p_j, k_l, m_n) \prod_{i=1}^{I} \frac{\mathrm{i}}{q_i^2 - m_i^2 + \mathrm{i}\epsilon}. \tag{3.5}$$

Here, $N(p_j, k_l, m_n)$ is the numerator of the Feynman integral and a regular function of its arguments. This integral can be IR divergent if the two Landau equations [52] are fulfilled

$$\lambda_i (q_i^2 - m_i^2) = 0 \quad \text{for all } i = 1, \ldots, I \tag{3.6}$$

and

$$\sum_{i=1}^{I} \lambda_i q_i \frac{\partial q_i}{\partial k_l} = 0 \quad \text{for all } l = 1, \ldots, L, \tag{3.7}$$

for a set of nonvanishing λ_i. The numerator $N(p_j, k_l, m_n)$ is immaterial to the Landau equations. The first equation requires that the respective denominator is actually zero. This means that the momentum is on the mass shell, yet, owing to the $+i\epsilon$ prescription this does not necessarily lead to a divergence. Most often the integration contour can still be deformed into the complex plane such that this vanishing denominator leads to a branch point. However, if also the second equation is satisfied for nonvanishing λ_i, the integration path cannot be deformed anymore in the complex plane in such a way that it would avoid the singularity. In other words this second Landau equation requires that the integration path is pinched between two or several singularities, such that the integration contour cannot be deformed anymore and necessarily goes through the singular point. For physical processes the λ_i must be real and positive. For a geometrical explanation of the Landau equations we refer to reference [53].

If all the equations are satisfied with all λ_i nonzero, the corresponding singularity is called the leading singularity. If, however, some λ_i need to be zero to satisfy all the equations, we consider only the set of Landau equations with nonvanishing λ_i. This corresponds to a reduced diagram, in which all propagators with $\lambda_i = 0$ are left out of consideration (contracted to a point). An important property of the Landau equations is that it is sufficient to find one nonvanishing Landau parameter to produce a potential singularity. If all other λ_i are zero it is still possible that some denominators $q_j^2 - m_j^2 = 0$ vanish by themselves, the degree of divergence is then enhanced by these vanishing propagators. There are two generic solutions of the Landau equations, that have been identified by Kinoshita [51, 54]. These are soft divergences (one $\lambda_i \neq 0$ and collinear divergences (two $\lambda_i \neq 0$), both divergences are always related to external legs. For one loop diagrams these are the only mass divergences that can arise.

3.2.2 Two-loop diagrams

With the Landau equations we obtained a necessary criterion to find IR divergences in any Feynman integral, we will apply this now to the NLO up quark penguin diagrams in Fig. 3.2, where we do not draw self-energy diagrams. Self-energy diagrams of external legs factorize they have a counterpart on the effective side of the OPE. The self-energy of the gluon cannot be IR divergent because the gluon is off-shell. The self-energies of the internal up quarks are regularized by the loop momentum that runs through them.

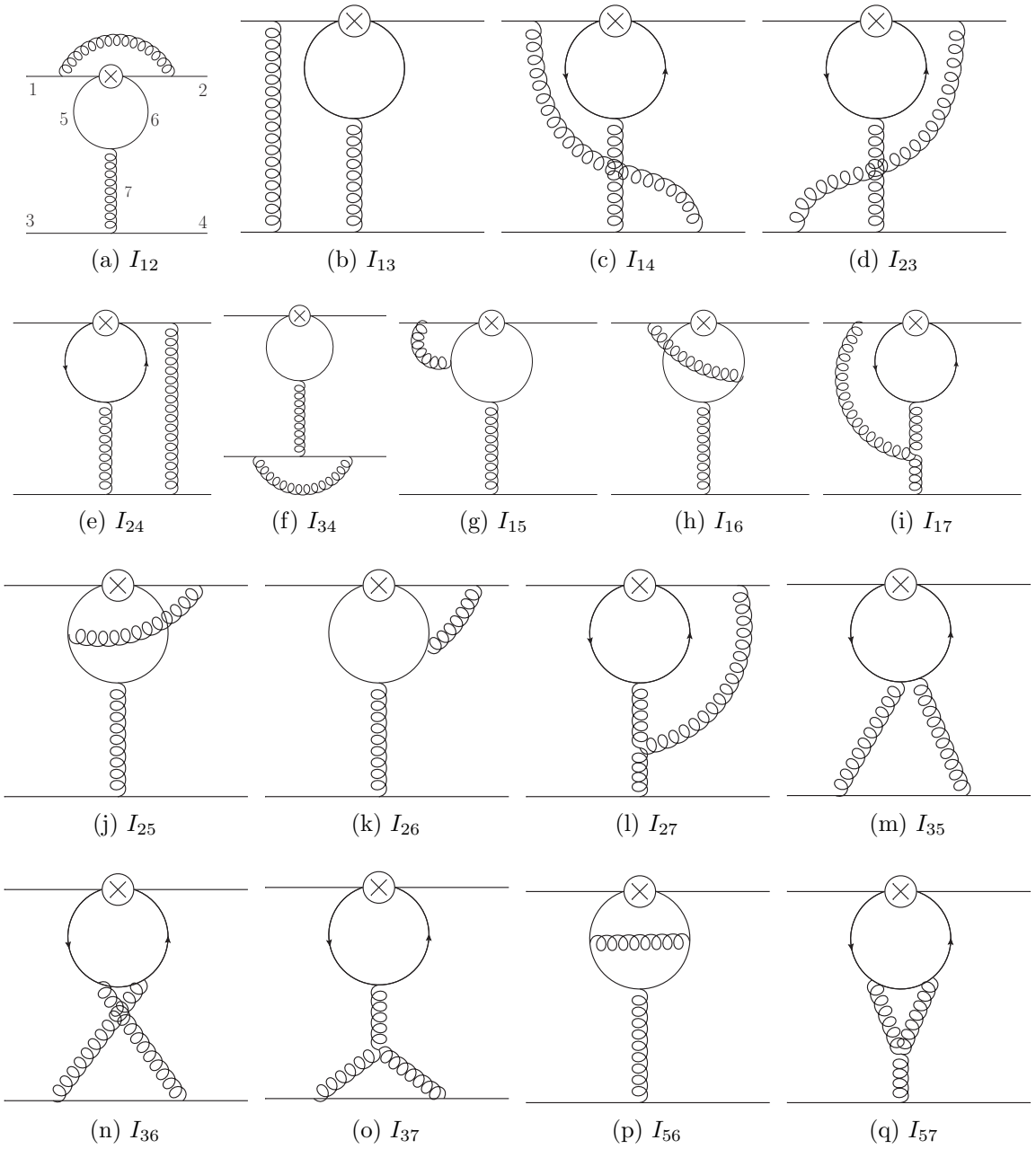

(a) I_{12} (b) I_{13} (c) I_{14} (d) I_{23}

(e) I_{24} (f) I_{34} (g) I_{15} (h) I_{16} (i) I_{17}

(j) I_{25} (k) I_{26} (l) I_{27} (m) I_{35}

(n) I_{36} (o) I_{37} (p) I_{56} (q) I_{57}

Figure 3.2: One-loop (NLO) corrections to the up quark penguins. We do not plot self-energies.

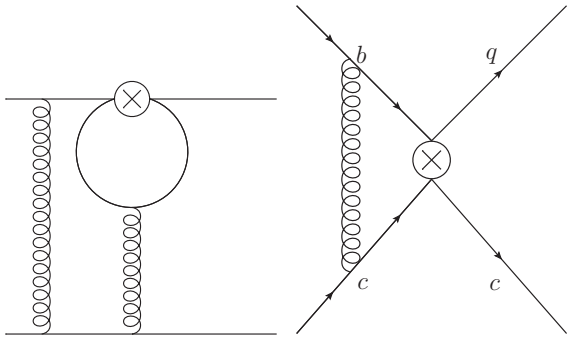

(a) I_{13} (b) I_{13e}

Figure 3.3: Diagrams in which the NLO gluon only connects external legs factorize in the OPE

To name the integrals we numbered the lines $(b, q, \bar{c}, c, \bar{u}, u, g) \to (1, 2, 3, 4, 5, 6, 7)$ as can be seen in Fig. 3.2(a), we then label the diagrams by the numbers of the two lines that are connected by the second gluon (the gluon not present in the LO penguin). The smaller index number comes first. If this prescription is ambiguous, we choose the configuration in which the first index is smaller.
The NLO diagrams in which the additional gluon only connects external legs – none of the indices is equal to 5, 6 or 7 – have an equivalent on the effective side of the OPE, a graphical example for I_{13} is given in Fig. 3.3. In contrast, the diagrams I_{ij} with at least one index equal to 5, 6, or 7 have no equivalent on the effective side of the OPE because the second gluon couples to an internal line, these NLO processes should be described by the perturbative OPE coefficient $\widetilde{C}^{(1)}_{j,k}$, consequently they have to be free of IR divergences.

Hence, we will apply the Landau equations to I_{15}, I_{16}, I_{17}, I_{25}, I_{26}, I_{27}, I_{35}, I_{36}, I_{37}, I_{56}, and I_{57} to investigate their IR structure. From the diagrams we derive the integral expressions given in the appendix, the integrals that we discuss in detail are

$$I_{15} = -\frac{g_s^4}{(2\pi)^8}\frac{\mathcal{C}_{15}}{q^2}\int \mathrm{d}^d k\, \mathrm{d}^d l \Gamma_1 \frac{\not{k}-\not{q}}{(k-q)^2}\gamma_\mu \frac{\not{k}}{k^2}\gamma_\nu \frac{\not{k}+\not{l}}{(k+l)^2}\Gamma_2 \frac{\not{l}+\not{p}_b+m_b}{(l+p_b)^2-m_b^2}\gamma^\nu \frac{1}{l^2}\otimes\gamma^\mu, \quad (3.8)$$

$$I_{25} = -\frac{g_s^4}{(2\pi)^8}\frac{\mathcal{C}_{25}}{q^2}\int \mathrm{d}^d k\, \mathrm{d}^d l \gamma_\nu \frac{\not{l}-\not{p}'}{(l-p')^2}\Gamma_1 \frac{\not{k}-\not{q}}{(k-q)^2}\gamma_\mu \frac{\not{k}}{k^2}\gamma^\nu \frac{\not{k}+\not{l}}{(k+l)^2}\Gamma_2 \frac{1}{l^2}\otimes\gamma^\mu, \quad (3.9)$$

Some notation has been introduced, we stripped the integral expressions from the spinors and separated the two quark currents with a "$\otimes$" instead. The first current is sandwiched between $\bar{u}_q(p')$ and $u_b(p_b)$, the second current is sandwiched between $\bar{u}_c(p_c)$ and $v_c(p_{\bar{c}})$. Furthermore we used the insertion of a generic operator $Q = \Gamma_1 V_1 \otimes \Gamma_2 V_2$ instead of

	Number of nonzero Landau parameters λ_i		
	One	Two	Three
Diagram			
I_{15}, I_{16}	(0,-), (-,0), $(k_0,-k_0)$, (q,-)	$(q,0)$, $(q,-q)$	$(0,0)$
I_{17}	$(-,0)$, $(k_0,-k_0)$, (q,-), $(-,-q)$	$(q,0)$	$(q,-q)$
I_{25}, I_{26}	(0,-), $(k_0,-k_0)$, (q,-)	$(q,-q)$	
I_{27}	$(k_0,-k_0)$, $(-q,-)$, $(-,q)$		$(-q,q)$
I_{35}, I_{36}, I_{56}, I_{57}	(0,-), $(-,0)$, $(k_0,-k_0)$, $(-q,-)$, $(-,q)$	$(0,q)$, $(-q,0)$	$(0,0)$, $(-q,q)$
I_{37}	(0,-), $(-,0)$, $(-q,-)$, $(-,q)$	$(0,0)$, $(-q,q)$, $(0,q)$, $(-q,0)$	

Table 3.1: Point-like solutions of the Landau Eqns. (3.6) and (3.7) given as tuples for the loop momenta (k_0, l_0) for all NLO up-quark penguin diagrams that do not have an equivalent after the OPE. A "-" means that the value is unconstrained e.g., in $(-,0)$ the loop momentum k is not constrained by the Landau equations. The solution $(k_0,-k_0)$ implies that $k=-l$ is also a solution this derives from the denominator $(k+l)^2$. The solutions of the Landau equations are unique, but how we parametrize the solution depends on how the loop momenta are routed through the diagram. These solutions correspond to the integral expressions given in the Appendix A.1.

	Number of nonzero Landau parameters λ_i		
	Two	Three	Four
Diagram			
I_{25}, I_{26}	$(-,\gamma p')$,		$(-\delta p', \gamma p')$
I_{27}	$(-,-\gamma p')$	$(\gamma p', -\gamma p')$	

Table 3.2: Solutions to Landau equations 3.6 and 3.7 that lie on a linear manifold parametrized by $0 \leq \delta \leq \gamma \leq 1$ and with the basis vector p'. For more explanations see the caption of Tab. 3.1.

specific Dirac (Γ_i) and color structure (V_i). We also factored out the color structures

$$\mathcal{C}_{15} = V_1 T^a T^b V_2 T^b \otimes T^a, \qquad \mathcal{C}_{25} = T^b V_1 T^a T^b V_2 \otimes T^a. \tag{3.10}$$

The application of the Landau equations is not difficult but a bit laborious, therefore, we simply present the solutions of the Landau equations in Tabs. 3.1 and 3.2 without deriving them.

Two generic solutions of the Landau equations arise: points such as $(k_0, l_0) = (0,0)$ or $(k_0, l_0) = (-q, q)$, and the solutions in which l_0 is collinear to p' and k_0 is arbitrary indicated by a "-" or also collinear. The point-like solutions can lead to soft IR divergences and are the only solutions for the integrals I_{15}, I_{16}, I_{56}, I_{35}, I_{36}, I_{17}, I_{57}, and I_{37} (all diagrams that do not have an index 2). In diagrams I_{25}, I_{26}, and I_{27}, in which the second

gluon couples to the light quark q, the possibility of a collinear singularity exists.

3.2.3 Power counting

We established in Tabs. 3.1 and 3.2 the solutions of the Landau equations which are the location of the possible IR singularities, we now have to investigate whether the integrals are actually IR divergent. For this we must understand whether in the specific integral the numerator or denominator goes faster to zero when we approach the singularity. If the solution is at a point such as $(k_0, l_0) = (0, 0)$ we can use naive power counting. For the solutions on a linear manifold such as $l = \gamma p'$ with $0 \leq \gamma \leq 1$ we must use a different power counting. We will not discuss every diagram individually here but simply show for every generic solution how the power counting is employed to investigate the properties of a certain integral.

Naive power counting For singular points we can use naive power counting. This means that, since we are considering a single point in the four (eight) dimensional loop-momentum space, we can redefine the loop momentum (momenta) such that the origin is at the singular point. We can then determine the degree of divergence of the integral when we send all momentum components to zero. Let us consider the example

$$I_{15} = -\frac{g_s^4}{(2\pi)^8}\frac{\mathcal{C}_{15}}{q^2}\int \mathrm{d}^d k\,\mathrm{d}^d l \quad \Gamma_1 \frac{\not{k} - \not{q}}{(k-q)^2}\gamma_\mu \frac{\not{k}}{k^2}\gamma_\nu \frac{\not{k} + \not{l}}{(k+l)^2}\Gamma_2 \frac{\not{l} + \not{p}_b + m_b}{l^2 + 2l.p_b}\gamma^\nu \frac{1}{l^2} \otimes \gamma^\mu. \quad (3.11)$$

We discuss the different solutions of the Landau equations. For $(k_0, l_0) = (0,\text{-})$ we use the power counting

$$k \sim \lambda, \quad k^2 \sim \lambda^2 \quad \mathrm{d}^4 k \sim \mathrm{d}\lambda\lambda^3 \quad (3.12)$$

and all other momenta being $\mathcal{O}(1)$. We set $d = 4$ because we are only interested in the IR structure. Since the value of l_0 is arbitrary we only introduced the power counting for k. We ignore the precise structure of the numerator, and assume that there are no extra cancellations between the different terms, inserting the power counting, we find

$$I_{15} \sim \int \mathrm{d}\lambda\lambda^3 \frac{\lambda}{\lambda^2} \to 0. \quad (3.13)$$

The same power counting as in Eqn. (3.12) can also be used for the singular point $(q,\text{-})$ and $(k_0, -k_0)$ after the coordinate shift $k \to k - q$ and $k \to k - l$, respectively, has been

performed in both cases we find the scaling

$$I_{15} \sim \int \mathrm{d}\lambda\lambda^3 \frac{\lambda}{\lambda^2} \to 0. \tag{3.14}$$

If we consider $(k_0, l_0) = (\text{-}, 0)$ instead, the counting is

$$l \sim \lambda, \quad l^2 \sim \lambda^2, \quad l^2 + 2l.p_b \sim \lambda, \quad \mathrm{d}^4 l \sim \mathrm{d}\lambda\lambda^3. \tag{3.15}$$

in this case the denominator $\frac{1}{l^2+2l.p_b}$ enhances the divergence of the denominator l^2 which pinches the integration path to run along $l = 0$. However, altogether there is still no divergence because there are only three powers of λ in the denominator

$$I_{15} \sim \int \mathrm{d}\lambda\lambda^3 \frac{1}{\lambda}\frac{1}{\lambda^2} \to 0. \tag{3.16}$$

For the points $(q, 0)$ and $(q, -q)$ where two Landau parameters are nonzero we first perform the loop momentum shifts $k \to k - q$, $l \to l$ and $k \to k - q$, $l \to l + q$, respectively, such that the singular point is in both cases at $(0, 0)$ of the new loop-momentum coordinates. We then investigate the degree of divergence of the diagram using the power counting

$$k \sim \lambda, \quad l \sim \lambda, \quad k^2 \sim \lambda^2, \quad l^2 \sim \lambda^2, \quad (k+l)^2 \sim \lambda^2, \quad \mathrm{d}^4 k\, \mathrm{d}^4 l \sim \mathrm{d}\lambda\lambda^7. \tag{3.17}$$

Since we consider a point in an eight-dimensional (loop-momentum) space the measure refers to eight-dimensional spherical coordinates. At the point $(q, 0)$ we find

$$I_{15} \sim \int \mathrm{d}\lambda\lambda^7 \frac{\lambda}{\lambda^2}\frac{1}{\lambda}\frac{1}{\lambda^2} \to 0, \tag{3.18}$$

at the point $(q, -q)$, we find

$$I_{15} \sim \int \mathrm{d}\lambda\lambda^7 \frac{\lambda}{\lambda^2}\frac{1}{\lambda^2} \to 0. \tag{3.19}$$

At last let us discuss the point $(0, 0)$ where three Landau parameters are nonzero, the power counting is as in Eqn. (3.17)

$$I_{15} \sim \int \mathrm{d}\lambda\lambda^2 \to 0. \tag{3.20}$$

We conclude that the integral I_{15} has no soft divergences and is IR finite. Every possible

singularity indicated by the Landau equations for I_{15} eventually turned out to be finite. This way we can treat all singular *points* in Tab. 3.1 and find that there are no soft divergences in these integrals. However, the integrals I_{12}, I_{13}, I_{14}, I_{23}, I_{24}, and I_{34} have soft divergences when the NLO gluon becomes soft. E.g the integral I_{13} has a soft divergence at (-, 0) with the power counting in Eqn. (3.15) we find

$$\begin{aligned} I_{13} &= -\frac{g_s^4}{(2\pi)^8}\mathcal{C}_{13}\int \mathrm{d}^d k\,\mathrm{d}^d l s\Gamma_1 \frac{\not{k}-\not{q}}{(k-q)^2}\gamma_\mu \frac{\not{k}+\not{l}}{(k+l)^2}\Gamma_2 \frac{\not{l}+\not{p}_b+m_b}{(l+p_b)^2-m_b^2}\gamma_\nu \\ &\qquad \otimes \frac{1}{l^2}\frac{1}{(l+q)^2}\gamma^\mu \frac{-\not{p}_{\bar{c}}-\not{l}+m_c}{(p_c+l)^2-m_c^2}\gamma^\nu \qquad (3.21) \\ &\sim \int \frac{\mathrm{d}\lambda\lambda^3}{\lambda^4} \qquad (3.22) \end{aligned}$$

This is a logarithmic (soft) IR divergence. The soft divergences of this kind are connected to the NLO gluon becoming soft and the external lines going on-shell. These processes can be factorized into the matrix elements as can be seen in Fig. 3.3.

We have now treated all integrals except for I_{25}, I_{26}, and I_{27} and found that the only soft divergences that arise factorize in the OPE. In the next paragraph, we describe how the solutions on the linear manifolds can be treated in power counting

Power counting for collinear divergent diagrams

Hard-collinear We still need to deal with the solutions of the Landau equations for the integrals I_{25}, I_{26}, and I_{27} described by e.g. $k_0 \neq 0$ arbitrary and $l_0 = \gamma p'$ with $0 \leq \gamma \leq 1$. Since all momenta are in general nonzero we count them as $\mathcal{O}(1)$, then for example, the IR behavior of I_{25} can be simplified to

$$I_{25} \sim \int \mathrm{d}^d l \frac{1}{(l-p')^2}\frac{1}{l^2}. \qquad (3.23)$$

We cannot use the naive power counting method because the possible divergence is on a linear manifold in the l space. Therefore, we have to use a power counting first proposed by Sterman [55]. We decompose the coordinate space into two subspaces, one subspace includes the points of the possible singularity, since $p' = p_{\mathrm{cm}} n_-$ the basis vector of this subspace is given by n_-. The other subspace is parametrized by coordinates that are Euclidean-orthogonal to n_-. Hence, it is useful to employ the Sudakov decomposition [56]

$$l = l_+ n_+ + l_- n_- + l_\perp \qquad (3.24)$$

with $n_\pm$ being light-cone vectors defined after Eqn. (3.1) that obey $n_+^2 = n_-^2 = 0$. Furthermore, the following relations hold

$$l_\perp = (0, l^1, l^2, 0), \quad n_+.n_- = 2, \quad n_+.l_\perp = n_-.l_\perp = 0, \quad l_\perp^2 = -\mathbf{l}_\perp^2, \quad \text{and} \quad l^2 = 2l_+l_- - \mathbf{l}_\perp^2. \tag{3.25}$$

On the manifold $l_0 = \gamma p'$ we have $l^2 = 0$. Therefore, in a neighborhood of this manifold l^2 must be small with $l^2 \sim \lambda^2$. This implies for nonzero l_- that $l_+ \sim \mathbf{l}_\perp^2 \sim \lambda^2$ and leads to the scaling [7]

$$(l_+, l_-, l_\perp) \sim (\lambda^2, 1, \lambda). \tag{3.26}$$

Furthermore, the scaling of the measure is

$$\int \mathrm{d}^4 l \sim \int \mathrm{d}l_+ \, \mathrm{d}l_- \, \mathrm{d}^2 l_\perp \sim \int \mathrm{d}\lambda \lambda^3 \tag{3.27}$$

in $d = 4$ dimensions. Let us apply this scaling to I_{25} we find

$$I_{25} \sim \int \mathrm{d}^4 l \frac{1}{(l-p')^2} \frac{1}{l^2} \sim \int \mathrm{d}l_+ \, \mathrm{d}l_- \, \mathrm{d}^2 l_\perp \frac{1}{2l_+.(l_- - p') - \mathbf{l}_\perp^2} \frac{1}{2l_+l_- - \mathbf{l}_\perp^2} \sim \int \mathrm{d}\lambda \frac{\lambda^3}{\lambda^4} \tag{3.28}$$

This means I_{25} has a logarithmic collinear IR divergence. Similarly, we find that I_{26} and I_{27} are collinearly divergent on the manifold $(\text{-}, \gamma p')$, since all three integrals have the same structure

$$I_{2j} = \int \mathrm{d}^d l \quad \bar{u}_q(p') \gamma^\mu \frac{\not{l} - \not{p}'}{(l-p')^2} \frac{g_{\mu\nu}}{l^2} \widetilde{\Gamma}_{2j}^\nu(l). \tag{3.29}$$

where we implicitly defined the remainder $\widetilde{\Gamma}_{2j}^\nu(l, q)$ and $\bar{u}_q(p')$ is the spinor of the outgoing light quark q.

Collinear-collinear Let us now investigate the collinear-collinear solutions in Tab. 3.2, these are $(-\delta p', \gamma p')$ with $0 \leq \delta \leq \gamma \leq 1$ for I_{25} and I_{26} and $(\gamma p', -\gamma p')$ for I_{27}. In this situation we obtain the power counting

$$(l-p')^2 \sim \lambda^2, \quad (k-q)^2 \sim 1, \quad k^2 \sim \lambda^2, \quad (k+l)^2 \sim \lambda^2, \quad l^2 \sim \lambda^2. \tag{3.30}$$

whereas the measure scales as

$$\mathrm{d}^4 k \, \mathrm{d}^4 l \sim \mathrm{d}\lambda \lambda^7. \tag{3.31}$$

Counting powers in I_{25} and neglecting the numerator once again, the integral seems IR divergent in this region of loop-momentum space.

$$\tilde{I}_{25} = \int \mathrm{d}^d k\, \mathrm{d}^d l \frac{1}{(l-p')^2} \frac{1}{(k+l)^2} \frac{1}{l^2} \frac{1}{k^2} \frac{1}{(k-q)^2} \sim \int \mathrm{d}\lambda \lambda^7 \frac{1}{\lambda^2} \frac{1}{\lambda^2} \frac{1}{\lambda^2} \frac{1}{\lambda^2} \frac{1}{1} \sim \int \frac{\mathrm{d}\lambda}{\lambda} \tag{3.32}$$

However, if we do not neglect the numerator and use $\not{k}\gamma^\nu = -\gamma^\nu \not{k} + 2k^\nu$ we arrive at

$$\begin{aligned} I_{25} &\sim \int \mathrm{d}^d k\, \mathrm{d}^d l \gamma_\nu \frac{\not{l} - \not{p}'}{(l-p')^2} \Gamma_1 \frac{\not{k} - \not{q}}{(k-q)^2} \gamma_\mu \frac{-\gamma^\nu \not{k} + 2k^\nu}{k^2} \frac{\not{k} + \not{l}}{(k+l)^2} \Gamma_2 \frac{1}{l^2} \otimes \gamma^\mu \qquad (3.33) \\ &\sim \int \mathrm{d}^d k\, \mathrm{d}^d l \gamma_\nu \frac{\not{l} - \not{p}'}{(l-p')^2} \Gamma_1 \frac{\not{k} - \not{q}}{(k-q)^2} \gamma_\mu \frac{-\gamma^\nu \not{k}}{k^2} \frac{\not{k} + \not{l}}{(k+l)^2} \Gamma_2 \frac{1}{l^2} \otimes \gamma^\mu \\ &\quad + \int \mathrm{d}^d k\, \mathrm{d}^d l 2\not{k} \frac{\not{l} - \not{p}'}{(l-p')^2} \Gamma_1 \frac{\not{k} - \not{q}}{(k-q)^2} \gamma_\mu \frac{1}{k^2} \frac{\not{k} + \not{l}}{(k+l)^2} \Gamma_2 \frac{1}{l^2} \otimes \gamma^\mu, \qquad (3.34) \end{aligned}$$

we observe that in the numerator the term

$$2\not{k}(\not{l} - \not{p}') \sim \gamma^\nu \not{k}(\not{k} + \not{l}) \sim \lambda^2 \tag{3.35}$$

arises that vanishes as λ^2 if all momenta become collinear. This additional factor of λ^2 makes I_{25} in the collinear-collinear region finite. The same modifications can be used to show that I_{26} is IR safe in the collinear-collinear region. In I_{27} there are only three denominators that scale as λ^2. Thus, it is clear that the the collinear-collinear region is finite.

We also investigated the soft-collinear solution $(0, \gamma p')$, however, these do not lead to further singularities, this is why omit their discussion here.

The IR divergence found in the hard-collinear regions seems to imply that the factorization of hard and soft scales is not possible, but this is not the case, it is expected that collinear divergences only affect external legs [54]. It is due to our choice of the Feynman-'t Hooft gauge that we see collinear divergences that affect the full two-loop diagrams. We will make this explicit in the next section.

3.2.4 Absence of collinear divergences

In the preceding section we found that the individual diagrams of the loop corrections to the up-quark penguin exhibit a collinear divergence. As such this seems to imply that this process does not factorize since the (short-distance) OPE coefficient $\widetilde{C}_{i,j}^{(1)}$ in Eqn. (2.7) would be IR divergent. However, collinear divergences are usually a property

of external legs and not of high-energy processes. We chose the Feynman-'t Hooft gauge to write down the amplitudes. The Feynman-'t Hooft gauge leads to a simple gluon propagator but has the usual disadvantage that there are unphysical degrees of freedom contributing to individual diagrams. In the sum of all diagrams (possibly also including ghosts) lead to the cancellation of these unphysical degrees of freedom. This could also lead to the cancellation of the collinear divergences in the two-loop integrals. There are two possibilities to check this conjecture. We either compute the sum of all integrals which expose the collinear divergence or change to a physical gauge in which no unphysical degrees of freedom contribute.

The three diagrams which we found to have collinear divergences in the Feynman-'t Hooft gauge have the general form

$$I_{2j} = \int \mathrm{d}^d l \quad \bar{u}_q(p')\gamma^\mu \frac{\not{l} - \not{p}'}{(l-p')^2} \frac{g_{\mu\nu}}{l^2} \widetilde{\Gamma}^\nu_{2j}(l,q). \tag{3.36}$$

The γ^μ arises through the gluon that couples to the quark line of the massless quark q and $\frac{g_{\mu\nu}}{l^2}$ derives from the gluon propagator in the Feynman-'t Hooft gauge $-i\frac{g_{\mu\nu}}{l^2}$ and leads to the contraction with the remainder $\widetilde{\Gamma}^\nu_{2j}(l,q)$ of the diagram. In a physical gauge [57, 58] the gluon propagator has the form

$$i \sum_{i=1,2} \frac{\epsilon_\mu^{*(i)}(l)\epsilon_\nu{}^{(i)}(l)}{l^2} \tag{3.37}$$

for $l^2 \to 0$. Obviously, the name derives from the fact that only the physical polarizations of the gluon contribute. In addition to the Lorentz condition $l.\epsilon(l) = 0$ the constraint $n_\pm.\epsilon(l) = 0$ holds which proves to be very helpful for the investigation of IR properties of these diagrams. If we replace $g_{\mu\nu}$ by the sum of the polarizations, we obtain

$$I_{2j} = -\int \mathrm{d}^d l \sum_{i=1,2} \bar{u}_q(p') \not{\epsilon}^{*(i)}(l) \frac{\not{l} - \not{p}'}{(l-p')^2} \frac{1}{l^2} \epsilon^{*(i)}_\nu(l) \widetilde{\Gamma}^\nu_{2j}(l,q). \tag{3.38}$$

We then use

$$\not{\epsilon}^{*(i)}(l)(\not{p}' + \not{l}) = -\not{p}'\not{\epsilon}^{*(i)}(l) - \not{l}\not{\epsilon}^{*(i)}(l) + 2p'.\epsilon^{*(i)}(l) + 2l.\epsilon^{*(i)}(l). \tag{3.39}$$

The last term is identical to zero because of the Lorentz condition $l.\epsilon^{(i)}(l) = 0$. The first term will vanish immediately in the integral expression because of the equation of motion $\bar{u}_q(p')\not{p}' = 0$. Furthermore, we find with the Sudakov decomposition $\bar{u}_q(p')\not{l} =$

$\bar{u}_q(p_{\rm cm}n_-)(l_-\not{n}_- + l_+\not{n}_+ + \not{l}_\perp) = \bar{u}_q(p_{\rm cm}n_-)(l_+\not{n}_+ + \not{l}_\perp) \sim \lambda$ and $p'.\epsilon^{(i)}(l) \sim \lambda^2$ hold. Thus, in the physical gauge we gain one power in λ in the numerator which leads to an IR-safe integral. To be explicit

$$I_{2j} = -\int \mathrm{d}^d l \sum_{i=1,2} \bar{u}_q(p') \frac{-\not{l}\not{\epsilon}^{*(i)}(l) + 2p'.\epsilon^{*(i)}(l)}{(l-p')^2} \frac{1}{l^2} \epsilon_\nu^{*(i)}(l) \widetilde{\Gamma}^\nu_{2j}(l,q) \tag{3.40}$$

$$\sim \int \mathrm{d}\lambda \lambda^3 \frac{\lambda}{\lambda^2\lambda^2} \to 0. \tag{3.41}$$

Thus, we observe that the 'physical' diagrams I_{2j} are actually free of IR divergences, it was merely due to our choice of gauge that we found collinear divergences. In the Feynman-'t Hooft gauge this can be shown by considering the sum

$$\sum_{j=1}^{7} I_{2j} + I_{22} = \sum_{j=1}^{7} \int \mathrm{d}^d l \quad \bar{u}_q(p')\gamma^\mu \frac{\not{l} - \not{p}'}{(l-p')^2} \frac{g_{\mu\nu}}{l^2} \widetilde{\Gamma}^\nu_{2j}(l,q) + I_{22} \tag{3.42}$$

$$= \sum_{j\in\{1,2,2,3,4,5,6,7\}} \int \mathrm{d}^d l \quad \bar{u}_q(p') \frac{-(\not{l} - \not{p}') + 2(l_\nu - p'_\nu)}{(l-p')^2} \frac{1}{l^2} \widetilde{\Gamma}^\nu_{2j}(l,q) \tag{3.43}$$

as above $\bar{u}_q(p')(\not{l} - \not{p}') \sim \lambda$, on the other hand the term $\sum_{j\in\{1,2,2,3,4,5,6,7\}}(l_\nu - p'_\nu)\widetilde{\Gamma}^\nu_{2j}(l,q)$ vanishes as λ if $p' \propto l$ because of the (collinear) Ward identity shown in Fig. 3.4. There is one subtlety to this, while the self-energy diagram of the q quark that enters as I_{22} in Eqn. (3.43) carries the typical factor $\frac{1}{2}$ of self-energies. The Ward identity does not include such a factor, this means we have to add a second term I_{22} to the sum. This is possible because these self-energy terms can be factorized or included without invalidating the OPE.

We conclude that there are no physical collinear divergences in the diagrams of the hard process. The only physical collinear divergence appears in I_{22} and is associated to the self-energy of the quark q. In fact even this diagram is not IR-divergent in the case that we consider. Since we set $m_s = 0$ and $p'^2 = 0$, there is no scale in the self-energy diagram and it must be zero in NDR. In reality $m_s \neq 0$ and $p'^2 \neq 0$ is not on-shell. Thus, in the physical process there is no collinear divergence.

3.2.5 IR structure of the Q_{8G} penguins

Hitherto, we limited the IR-structure discussion to the Q_i^u penguin insertions. The NLO corrections to the Q_{8G} penguins are only one-loop diagrams see Fig. A.1 and the expressions in the Feynman-'t Hooft gauge can be found as well in the appendix in A.2. Since

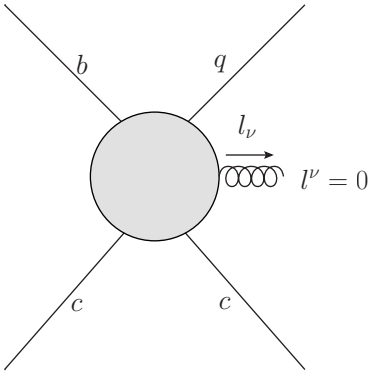

Figure 3.4: The graphical representation of the Ward identity which leads to the absence of collinear divergences in the two-loop diagrams in Figs. 3.2 and A.1.

these integrals are one-loop diagrams the IR divergences are easily identifiable. Soft IR divergences arise if a soft gluon couples to external legs only, but since this only involves external legs these soft divergences factorize. Every diagram in which a gluon couples to the light quark q has a collinear divergence in the Feynman-'t Hooft gauge it may be written as

$$I_{2jG} \int \mathrm{d}^d l \quad \bar{u}_q(p')\gamma^\mu \frac{\not{l} - \not{p}'}{(l-p')^2} \frac{g_{\mu\nu}}{l^2} \widetilde{\Gamma}^\nu_{2jG}(l). \tag{3.44}$$

where we implicitly defined the remainder of the diagram $\widetilde{\Gamma}^\nu_{2jG}(l)$ and $\bar{u}_q(p')$ is the spinor of the light quark. However, if we use the physical gauge as in the preceding section we can show that the hard process is in fact free of these collinear divergences.

We conclude that in the Q_{8G} penguin the soft and hard scales factorize at NLO as well.

3.2.6 Conclusions

The discussion in this section was rather long. Therefore, we summarize the most relevant points in this section. We investigated the IR structure of the two-loop Q_i^u penguin and the one-loop Q_{8G} penguin that both contribute to the penguin pollution. We were interested in the IR structure to prove the factorization of soft and hard scales which is necessary two describe the penguin pollution by an OPE. We found that soft and hard scales factorize.

We first introduced some notions on the IR divergences and the Landau equations. The Landau equations are a necessary criterion for an IR divergence. We solved the Landau equations for the relevant two-loop Q_i^u penguin diagrams and investigated the actual divergence by means of naive and collinear power counting. We only found the standard soft IR divergences that arise if a soft gluon couples to two external legs and

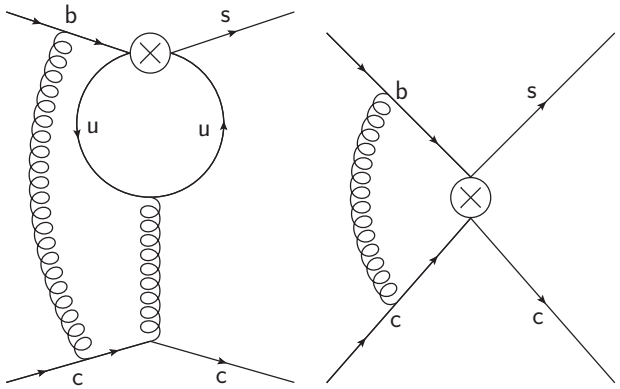

Figure 3.5: All soft divergences factorize they can be matched on diagrams in which the penguin loop is contracted to a point and described by an effective operator.

factorize because of this, see Fig. 3.5. Furthermore, we found collinear divergences in diagrams in which a gluon couples to the light quark q. These divergences correspond to the mass divergences that have been identified by Kinoshita [54]. We then showed in the physical gauge that the collinear divergence is a property of the external q leg and not of the up quark penguin. This can also be understood in terms of a collinear Ward identity in the Feynman-'t Hooft gauge.

The physical picture is that soft gluons can only interact with external, i.e. asymptotic particles because they cannot resolve the short time scale of the hard interaction. Collinear divergences arise if massless particles couple to each other and if their momenta become collinear. This is the case for the gluons that couple the light quark q, all diagrams of the form in Fig. 3.6 exhibit a collinear divergence, yet the sum of all diagrams is IR safe, except for the light quark self-energy I_{22} which, however, factorizes. The remaining divergence is due to the well known property of colored particles that for example a strange quark cannot be distinguished from strange quark accompanied by an infinite number of collinear gluons. Physically, these IR divergences are regularized by hadronization. In contrast, in inclusive cross sections the cancellation of IR divergences is ensured by the Kinoshita-Lee-Nauenberg (KLN) theorem [54, 59] which requires the summation over degenerate final and initial states.

We note that the general IR structure of massive QCD one and two-loop scattering amplitudes has been derived in [60, 61].

We may compare the situation to QCDF where the soft divergences are either absorbable into the form factor or the LCDA, if they cannot be absorbed they are power suppressed [7]. Since our OPE results into four quark operators all soft divergences factorize into the four quark matrix elements. Similarly, the collinear divergence is a property

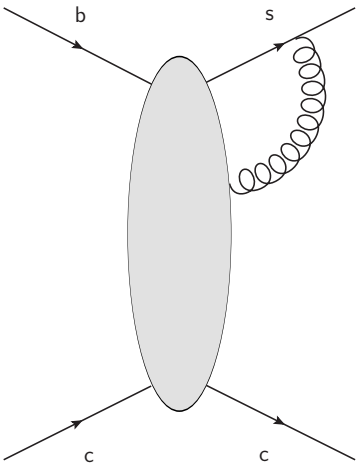

Figure 3.6: Generic diagram with a collinear divergence in the Feynman-'t Hooft gauge. The sum over all diagrams has no collinear divergence.

of q that can be absorbed into the matrix element and that is physically regularized by the hadronization.

3.3 Spectator scattering

In the preceding section we saw that the IR structure of the full and the effective theory can be matched onto each other. Thus, we concluded that the factorization of hard and soft scales is possible. However, we ignored the existence of the second valence quark in the $\bar{B}$ and X meson. To represent this light quark which does not participate directly in the b quark decay we may draw a *spectator* quark in addition to the diagram of the b decay, see Fig. 3.7a. The effects of the spectator quarks are usually included in the matrix elements. However, interactions of the hard process with the spectator quark displayed in Figs. 3.7b and 3.7c could spoil the factorization that is necessary for the OPE. Therefore, we will discuss these interactions in this section.

Let the momentum transferred to the spectator quark be l. This leads to a propagator $1/l^2$ in the expressions that describe spectator scattering perturbatively. Naturally, the question arises what happens for $l^2 = \mathcal{O}\left(\Lambda^2_{\mathrm{QCD}}\right)$ with l being soft or light-like. The region where $l^2 = \mathcal{O}\left(\Lambda^2_{\mathrm{QCD}}\right)$ is not perturbative and may dominate this process, this would imply a failure of our OPE because it does not include spectator scattering. Hence, it is necessary to show that soft spectator scattering is power suppressed.

In addition we will consider hard-collinear spectator scattering. Let us explain this, if the spectator quark is ignored the final meson X receives its full hard momentum, which

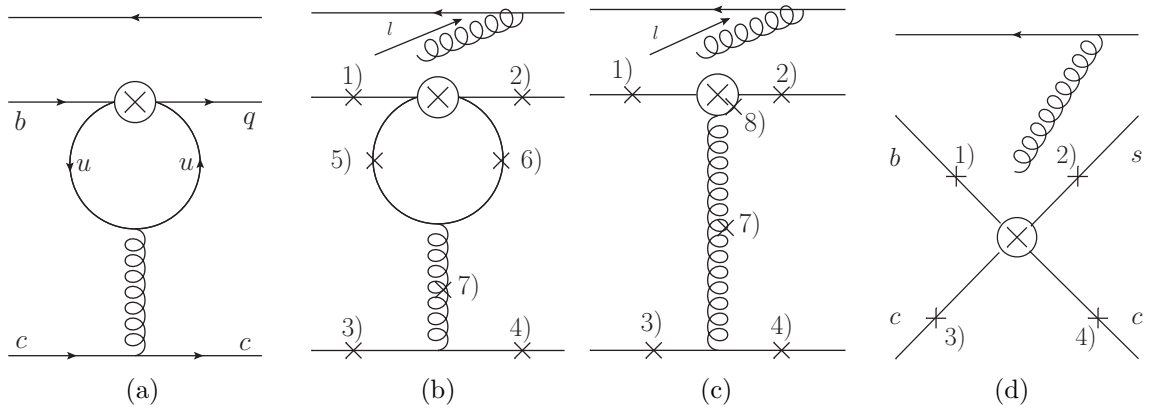

Figure 3.7: Q_2^u penguins with spectator quark and spectator-quark interaction. (a) Leading-order Diagram, including the spectator quark. (b) Leading-order spectator-scattering diagram for the up quark penguin. The crosses (1) to (7) are possible places where the open end of the gluon can be attached. (c) Leading-order spectator-scattering diagram of the Q_{8G} penguin, the crosses (1) to (4), (7) and (8) are possible places where the open end of the gluon can couple to. (d) Spectator-scattering of the full theory is partly factorizable, the crosses (1) to (4) indicate spectator scattering diagrams after the OPE that match the spectator scattering in the full theory.

is $p_X = p_{\rm cm} n_-$, from the light quark q. This kinematical configuration is disfavored w.r.t. the configuration where the energetic X meson is formed by two partons of similar hard momentum. Hence, if the momentum transfer to the spectator quark is hard-collinear, $l \simeq p_{\rm cm}/2n_-$, the hadronization of the X meson is more likely than in the LO diagram where X receives its full hard momentum from light quark q.

The suppression of the asymmetric momentum configuration of the partons can be seen explicitly in the light-cone distribution amplitude (LCDA, the meson wave function integrated over transverse momenta) of a light meson [7]

$$\Phi_X(u) \sim \begin{cases} 1 & \text{for} \quad \text{generic } u, \\ \Lambda_{\rm QCD}/p_{\rm cm} & \text{for} \quad u, \bar{u} \sim \Lambda_{\rm QCD}/p_{\rm cm} \end{cases} \tag{3.45}$$

here u ($\bar{u}$) is the longitudinal momentum fraction carried by the valence (anti-)quark in the meson X. The LCDA describes the probability of forming an X meson from two partons with momentum up_X and $\bar{u}p_X$ ($\bar{u} = 1 - u$). Since the LCDA is of $\mathcal{O}\left(\Lambda_{\rm QCD}/p_{\rm cm}\right)$ in a small region of $\mathcal{O}\left(\Lambda_{\rm QCD}/p_{\rm cm}\right)$ of the u integral (which we, however, do not perform explicitly), the LO process has an *end-point suppression* of $\mathcal{O}\left(\Lambda_{\rm QCD}^2/p_{\rm cm}^2\right)$.

We do not explicitly use the LCDA because the hadronization of the X has a soft overlap with $\bar{B}\psi$ system. Nevertheless, we use the power counting that can be inferred from

the LCDA to investigate the importance of hard-collinear spectator scattering. Consequently, we find that the leading-order process has a suppression factor $\Lambda^2_{\rm QCD}/p^2_{\rm cm}$ because of the asymmetric momentum configuration. In contrast, the hard spectator interactions do not have such a suppression via the LCDA but are at least suppressed by $\Lambda^2_{\rm QCD}/p^2_{\rm cm}$ because there is an additional hard momentum running through the diagram e.g., the off-shellness of the hard-collinear gluon propagator yields $1/l^2 \sim 1/(\Lambda_{\rm QCD} p_{\rm cm})$. Depending on the suppression, hard-collinear spectator scattering might simply be an $\mathcal{O}(\alpha_s^2)$ correction. However, this correction is inconvenient because it would mean that at $\mathcal{O}(\alpha_s^2)$ we would have to introduce six-quark matrix elements. It is preferable if we can show that hard-collinear spectator interactions are power suppressed as we want to show it for soft spectator scattering. We will first discuss soft spectator scattering and then hard-collinear spectator scattering.

Before we go into detail let us clarify our power counting. We considered the LO diagram up to now as a four quark process whereas the spectator scattering process is a six quark diagram. In the amplitude this leads to four and six-quark matrix elements that have mass dimension 6 and 9, respectively. Since both processes contribute to the same amplitude they must have the same mass dimension. The difference in mass dimension of the matrix elements is compensated by the hard-scattering part of the diagrams. This makes the comparison by power counting of these two contributions somewhat intransparent. To circumvent this difficulty, we will just count hard suppression factors. This means that we will only count factors of $1/M$ and $1/p_{\rm cm}$ ignoring powers of $\Lambda_{\rm QCD}$, if all hard contributions are identified, all other contributions are $\mathcal{O}(\Lambda_{\rm QCD})$. In particular, this means that the terms $\mathcal{O}(\Lambda_{\rm QCD})$ that appear in the denominator in some expressions are always canceled by terms $\mathcal{O}(\Lambda_{\rm QCD})$ in the numerator. This method is equivalent to adding another soft-gluon exchange to both processes which connects the spectator current with the LO diagram and adds an integration over soft momentum in the spectator diagram.

From Eqn. (3.45) and the discussion thereafter we find that the LO diagram is suppressed by $1/p^2_{\rm cm}$, the suppression factors of the spectator scattering diagrams labeled by the attachments (1)-(7) in Fig. 3.7b and by (1)-(4),(7), and (8) in Fig. 3.7c are evaluated in what follows.

Soft spectator scattering In the case of soft spectator scattering with $l^2 = \mathcal{O}\left(\Lambda^2_{\rm QCD}\right)$, the insertions (1)-(4) for the Q_i^u and Q_{8G} penguin in Figs. 3.7b and 3.7c, respectively, do not need to be considered. These diagrams have the same end-point suppression as the LO diagram but do not carry any further suppression factor, however, they trivially factorize in the OPE. The corresponding diagrams after the OPE are given by the insertions (1)-(4)

in Fig. 3.7d. The reason is simply that in these diagrams the spectator interacts with the external legs.

The contributions from spectator-quark interactions as given by the insertions (5)-(8) have no possible equivalent at the leading order of the OPE. Therefore, we have to show that these processes are power suppressed by $1/M$ and are described by operators of higher order in the OPE.

For the insertion (5) and (6) in Fig. 3.7b we obtain[2]

$$I_5 = \frac{-2g_s^2\alpha_S}{q^2l^2} I^{\rho\sigma\tau}(-q,l)\,\gamma_\lambda\gamma_\rho\gamma_\mu T^a\gamma_\sigma\gamma_\nu T^b\gamma_\tau\gamma^\lambda(1-\gamma_5)\otimes\gamma^\mu T^a\otimes\gamma_\nu T^b, \quad (3.46)$$

$$I_6 = \frac{-2g_s^2\alpha_S}{q^2l^2} I^{\rho\sigma\tau}(-l,q)\,\gamma_\lambda\gamma_\rho\gamma_\nu T^b\gamma_\sigma\gamma_\mu T^a\gamma_\tau\gamma^\lambda(1-\gamma_5)\otimes\gamma^\mu T^a\otimes\gamma_\nu T^b, \quad (3.47)$$

where we used the "$\otimes$" notation to separate different quark currents. The first Dirac and color structure is sandwiched between the spinors of the b and q quark, the second between the $\bar{c}$ and c spinors and the third between the spinors of the spectator quarks. Furthermore, the up-quark loop becomes a three-point function

$$I^{\rho\sigma\tau}(q,l) = \frac{(2\pi\mu)^{4-d}}{i\pi^2}\int \mathrm{d}^dk \frac{k^\rho+q^\rho}{(k+q)^2}\frac{k^\sigma}{k^2}\frac{k^\tau+l^\tau}{(k+l)^2}. \quad (3.48)$$

This three-point function is IR safe for $l=0$ by naive power counting but has a collinear divergence for light-like but nonzero l. For example, with $l=\bar{u}p_{\mathrm{cm}}n_-$ we infer from section 3.2.3 that we can count $(k_+,k_-,k_\perp)\sim(\lambda^2,1,\lambda)$ and $\mathrm{d}^4k_2\sim\mathrm{d}\lambda\lambda^3$ near the singularity. This leads to a logarithmic divergence

$$I_{\rho\sigma\tau}(q,l)\sim\int\frac{\mathrm{d}\lambda\lambda^3}{(\lambda^2)(\lambda^2)}\sim\int\frac{\mathrm{d}\lambda}{\lambda}. \quad (3.49)$$

Nevertheless, we expect that the divergence is not present in I_5 and I_6 because we usually associate collinear divergences only to external legs. The easiest way to show the absence is again the use of the physical gauge, we rewrite the gluon propagator of the collinear gluon in the physical gauge

$$\frac{-ig_{\mu\nu}}{l^2}\to i\sum_{i=1,2}\frac{\epsilon_\mu^{*(i)}(l)\epsilon_\nu^{(i)}(l)}{l^2}. \quad (3.50)$$

[2]For the insertions (5) and (6) it is also possible to insert the operator Q_1 instead of Q_2 at the effective vertex, however, this only affects the color structure of the diagram and not the power counting. Therefore, we do not treat this here. The suppression of the Q_1 insertions is the sames as for the Q_2 insertion.

Consider now I_5

$$I_5 \propto \sum_{i=1,2} \frac{\epsilon_\nu^{*(i)}(l)\epsilon_\rho{}^{(i)}(l)}{l^2} \int \mathrm{d}^4k \frac{\not{k}-\not{q}}{(k-q)^2}\gamma_\mu \frac{\not{k}}{k^2}\gamma^\nu \frac{\not{k}+\not{l}}{(k+l)^2} \otimes \gamma^\mu \otimes \gamma^\rho \tag{3.51}$$

$$\sim \frac{1}{l^2}\int \mathrm{d}^4k \frac{1}{(k-q)^2}\gamma_\mu \frac{\not{k}}{k^2}\not{\epsilon}^{*(i)} \frac{\not{k}+\not{l}}{(k+l)^2} \tag{3.52}$$

Before, we saw that the measure together with the denominators lead to a logarithmic divergence, we will now show that the numerator scales like λ if the loop momentum becomes collinear to l, for this we use the notation and counting introduced before Eqn. (3.49) and that only the 1 and 2 component of the polarization vector $\epsilon^{(i)}$ are nonzero, consider the numerator

$$\not{k}\not{\epsilon}^{*(i)}(l)(\not{k}+\not{l}) = 2\underbrace{\epsilon^{*(i)}(l).k}_{\sim\lambda}(\not{k}+\not{l}) - \not{\epsilon}^{*(i)}(l)\underbrace{(k^2+\not{k})\not{l}}_{\sim\lambda^2} \sim \epsilon^{*(i)}(l).k_\perp \sim \lambda. \tag{3.53}$$

An equivalent reasoning can be applied to I_6. Hence, the three-point function in I_5 and I_6 is finite for $l^2 = 0$ and has mass dimension one in four dimensions, consequently it scales after renormalizing the UV poles with the largest mass scale that appears in the loop which is $\sqrt{q^2} \sim M$.

$$I^{\rho\sigma\tau}(q,l) \sim \sqrt{q^2} \sim M \tag{3.54}$$

Thus

$$I_5 \sim I_6 \sim \frac{1}{q^2 l^2} I_{\rho\sigma\tau}(q,l) \sim 1/M \tag{3.55}$$

we remind the reader that $l^2 \sim \Lambda^2_{\mathrm{QCD}}$ is canceled by terms of Λ_{QCD} in the denominator. The insertion (7) leads to

$$I_7 = -g_S^2 \frac{P((q+l)^2)}{q^2 l^2} i f^{abc} V_{\mu\nu\rho}(-q,-l,q+l)\gamma^\rho(1-\gamma_5)T^c \otimes \gamma^\mu T^a \otimes \gamma_\nu T^b \tag{3.56}$$

where the three gluon function $V_{\mu\nu\rho}(-q,-l,q+l)$ is defined in Eqn. (A.29) it is linear in its arguments, this implies the scaling

$$V_{\mu\nu\rho}(-q,-l,q+l) \sim \sqrt{q^2} \sim M, \tag{3.57}$$

and the penguin function $P(q^2) \sim [1 + \log(q^2/\mu^2)]$ is given in Eqn. (2.9) and derives from

the evaluation of the up quark loop, we find

$$I_7 \sim \frac{P((q+l)^2)}{q^2 l^2} V_{\mu\nu\rho}(-q,-l,q+l) \sim \frac{1}{M^2} M \sim \frac{1}{M} \tag{3.58}$$

thus if l is soft the insertions (5), (6), and (7) are suppressed by $1/M$. The expressions for the insertions (7) and (8) in Fig. 3.7b are given by

$$I_{7G} = \frac{-i4\alpha_S^2 m_b}{q^2 l^2 (q+l)^2} V_{\mu\nu\rho}(-q,-l,q+l)\sigma^\rho{}_\lambda (q^\lambda + l^\lambda)(1+\gamma_5) T^c i f^{abc} \otimes \gamma^\mu T^a \otimes \gamma^\nu T^b \tag{3.59}$$

$$I_{8G} = i4\alpha_S^2 \frac{m_b}{q^2 l^2} \sigma_{\mu\nu}(1+\gamma_5) T^c i f^{abc} \otimes \gamma^\mu T^a \otimes \gamma^\nu T^b. \tag{3.60}$$

the $1/M$ suppression is quite explicit

$$I_{7G} \sim \frac{m_b}{q^2 l^2 (q+l)^2} V_{\mu\nu\rho}(-q,-l,q+l)(q^\lambda + l^\lambda) \sim \frac{1}{M}, \tag{3.61}$$

$$I_{8G} \sim \frac{m_b}{q^2 l^2} \sim \frac{1}{M}. \tag{3.62}$$

We conclude that soft spectator scattering with a gluon of momentum $l^2 = \mathcal{O}\left(\Lambda_{\rm QCD}^2\right)$ does not impede the OPE. If the gluon couples to external legs it is unsuppressed w.r.t. the LO process but factorizes [insertions (1)-(4) in Figs. 3.7b and 3.7c] and it is $1/M$ suppressed if the gluon couples to internal lines [insertions (5)-(8)]. The soft spectator scattering diagrams have the same suppression from the LCDA as the LO process, namely $1/p_{\rm cm}^2$. The power-counting behavior results from the simple fact, that the external lines have an off-shellness of $\mathcal{O}\left(\Lambda_{\rm QCD}\right)$ that cannot add further suppression factors. On the contrary, the internal lines are off-shell by $\mathcal{O}\left(M\right)$. Thus, the attachment of an additional line results into a $1/M$ suppression.

Hard-collinear spectator scattering After this thorough discussion of soft spectator scattering let us discuss now hard-collinear spectator scattering which is unsuppressed by the LCDA but obtains suppression factors since an additional hard momentum runs through it. We first discuss the spectator scattering in Fig. 3.7b and thereafter the spectator scattering processes in Fig. 3.7c.

The simplest situation are the attachments (1) or (2) in this case the spectator scattering factorizes as in the soft case. The spectator scattering diagrams corresponding to insertions (3) and (4) in Fig. 3.7b are partly factorizable and partly power suppressed. In contrast to soft scattering these diagrams do not factorize entirely because the momentum

transfer through the up-quark loop differs between the full and the effective theory. The momentum transfer is $(q+l)^2$ in the full theory, in contrast in the OPE it is fixed to q^2 in the OPE coefficient $\widetilde{C}_{j,k}$. Let us elucidate this for the insertion (4). Evaluating the diagram with the Q_2 insertion leads to

$$I_4^{full} = -g_S^2 \frac{P[(q+l)^2]}{l^2} \gamma_\mu (1-\gamma_5) T^a \otimes \gamma^\nu T^b \frac{\not{p}_c + \not{l} + m_c}{(p_c+l)^2 - m_c^2} \gamma^\mu T^a \otimes \gamma_\nu T^b. \tag{3.63}$$

where $P(q^2)$ is as before the penguin function from Eqn. (2.9), the $1/l^2$ derives from the propagator of the hard-collinear gluon. In the OPE this process is described by

$$I_4^{OPE} = -g_S^2 \frac{P(q^2)}{l^2} \gamma_\mu (1-\gamma_5) T^a \otimes \gamma^\nu T^b \frac{\not{p}_c + \not{l} + m_c}{(p_c+l)^2 - m_c^2} \gamma^\mu T^a \otimes \gamma_\nu T^b. \tag{3.64}$$

The only element that has changed is that $P[(q+l)^2]$ is replaced by $P(q^2)$. This reflects that we fix the momentum flow from the $b-q$ line to the $\bar{c}-c$ line in the OPE to q^2. The term I_4^{OPE} represents the part that factorizes in the OPE, consequently, the part of spectator scattering that does not factorize is

$$I_4^{full} - I_4^{OPE} = -g_S^2 \frac{P((q+l)^2 - P(q^2)}{l^2} \gamma_\mu (1-\gamma_5) T^a \otimes \gamma^\nu T^b \frac{\not{p}_c + \not{l} + m_c}{(p_c+l)^2 - m_c^2} \gamma^\mu T^a \otimes \gamma_\nu T^b. \tag{3.65}$$

Let us now evaluate this nonfactorizing contribution with power counting, $l \simeq p_{\rm cm}/2n_-$, the difference of the penguin functions gives

$$P((q+l)^2) - P(q^2) = \ln\left(\frac{(q+l)^2}{q^2}\right) \simeq \frac{2q.l}{q^2} \sim \frac{p_{\rm cm}}{M} \tag{3.66}$$

Additionally, the charm-quark propagator scales as

$$\frac{\not{p}_c + \not{l} + m_c}{(p_c+l)^2 - m_c^2} \sim \frac{\not{p}_c}{2p_c.l} \sim \frac{E_c}{E_c p_{\rm cm}} \sim \frac{1}{p_{\rm cm}}. \tag{3.67}$$

In order to find the scaling of the charm propagator we exploited the fact that the largest component of the charm four vector is given by the charm quark energy $E_c > m_c$. If we combine these scalings we obtain

$$I_4^{full} - I_4^{OPE} \sim \frac{P((q+l)^2 - P(q^2)}{l^2} \frac{\not{p}_c + \not{l} + m_c}{(p_c+l)^2 - m_c^2} \sim \frac{p_{\rm cm}}{M p_{\rm cm}} \frac{1}{p_{\rm cm}} \sim \frac{1}{p_{\rm cm} M}, \tag{3.68}$$

similarly we derive

$$I_3^{full} - I_3^{OPE} = -g_S^2 \frac{P((q+l)^2 - P(q^2)}{l^2} \gamma_\mu (1-\gamma_5) T^a \otimes \gamma^\mu T^a \frac{-\not{p}_{\bar{c}} - \not{l} + m_c}{(p_{\bar{c}}+l)^2 - m_c^2} \gamma^\nu T^b \otimes \gamma_\nu T^b$$
$$\sim \frac{P((q+l)^2 - P(q^2)}{l^2} \frac{-\not{p}_{\bar{c}} - \not{l} + m_c}{(p_{\bar{c}}+l)^2 - m_c^2} \sim \frac{p_{\rm cm}}{M p_{\rm cm}} \frac{1}{p_{\rm cm}} \sim \frac{1}{p_{\rm cm} M}, \tag{3.69}$$

hence, the nonfactorizing part of the insertions (3) and (4) is suppressed by $\frac{p_{\rm cm}}{M}$ w.r.t the LO process.

The contributions from spectator-quark interactions as given by the insertions (5), (6) and (7) have no possible equivalent at the leading order of the OPE.

The expression for insertions (5) and (6) were given in Eqns. (3.46) and (3.47), since $l^2 \sim p_{\rm cm}\Lambda_{\rm QCD}$ the three point function has the scaling $I^{\rho\sigma\tau}(q,l) \sim \sqrt{q^2} \sim M$. This implies the following scaling for the insertions (5) and (6)

$$I_5 \sim I_6 \sim \frac{I^{\rho\sigma\tau}(q,l)}{q^2 l^2} \sim \frac{M}{M^2 p_{\rm cm}\Lambda_{\rm QCD}} \sim \frac{1}{M p_{\rm cm}} \tag{3.70}$$

From Eqn. (3.56) we derive

$$I_7 \sim \frac{P((q+l)^2)}{q^2 l^2} V_{\mu\nu\rho}(-q,-l,q+l) \sim \frac{1}{M^2 p_{\rm cm}\Lambda_{\rm QCD}} M \sim \frac{1}{M p_{\rm cm}} \tag{3.71}$$

We have now discussed all hard-collinear insertions in Fig. 3.7b. We found that they do not spoil factorization. Insertions (1), (2) and a part of (3) and (4) also appear in the effective theory and therefore factorize. Insertions (5), (6), (7) and the other part of (3) and (4) are power-suppressed by $p_{\rm cm}/M$ w.r.t. the LO term which has a suppression of $\mathcal{O}\left(1/p_{\rm cm}^2\right)$.

Hard-collinear spectator scattering for the Q_{8G} penguin: We still have to discuss the hard-collinear spectator scattering for the chromomagnetic penguin Q_{8G} shown in Fig. 3.7c. The treatment has great similarities to the previous discussion, thus the discussion will be quite short. In the OPE the LO process has the amplitude

$$I_G = i \frac{\alpha_s}{\pi} \frac{m_b}{q^2} \sigma^{\mu\nu} q_\nu (1+\gamma_5) T^a \otimes \gamma_\mu T^a. \tag{3.72}$$

The insertions (1) and (2) in Fig. 3.7c trivially factorize and can be matched on the insertions (1) and (2) in the OPE in Fig. 3.7d as in the case of the up-quark penguin.

Similarly, the insertions (3) and (4) partly factorize and the nonfactorizing part is power suppressed. We find for the insertions (3) and (4) the expressions

$$I_{3G} = \frac{-i4\alpha_S^2 m_b}{l^2(q+l)^2}\sigma_{\mu\lambda}(q^\lambda + l^\lambda)(1+\gamma_5)T^a \otimes \gamma^\mu T^a \frac{-\not{p}_{\bar{c}} - \not{l} + m_c}{(p_{\bar{c}}+l)^2 - m_c^2}\gamma_\nu T^b \otimes \gamma^\nu T^b \quad (3.73)$$

$$I_{4G} = \frac{-i4\alpha_S^2 m_b}{l^2(q+l)^2}\sigma_{\mu\lambda}(q^\lambda + l^\lambda)(1+\gamma_5)T^a \otimes \gamma_\nu T^b \frac{\not{p}_c + \not{l} + m_c}{(p_c+l)^2 - m_c^2}\gamma^\mu T^a \otimes \gamma^\nu T^b. \quad (3.74)$$

For example, let us treat I_{3G}. The difference between the full and the effective theory is the different momentum transfer from the $b-q$ to the $\bar{c}-c$ line. In analogy with Eqn. (3.65), we find the nonfactorizing part to be

$$I_{3G}^{\text{full}} - I_{3G}^{\text{OPE}} = \frac{-i4\alpha_S^2 m_b}{l^2}\sigma_{\mu\lambda}\left[\frac{q^\lambda + l^\lambda}{(q+l)^2} - \frac{q^\lambda}{q^2}\right](1+\gamma_5)T^a \otimes \gamma^\mu T^a \frac{-\not{p}_{\bar{c}} - \not{l} + m_c}{(p_{\bar{c}}+l)^2 - m_c^2}\gamma_\nu T^b \otimes \gamma^\nu T^b \quad (3.75)$$

which leads to the scaling

$$I_{3G}^{\text{full}} - I_{3G}^{\text{OPE}} \sim \frac{1}{l^2}\left[\frac{q^\lambda + l^\lambda}{(q+l)^2} - \frac{q^\lambda}{q^2}\right]\frac{-\not{p}_{\bar{c}} - \not{l} + m_c}{(p_{\bar{c}}+l)^2 - m_c^2} \quad (3.76)$$

$$\sim \frac{1}{p_{\text{cm}}}\frac{p_{\text{cm}}}{M}\frac{1}{p_{\text{cm}}} \sim \frac{1}{M p_{\text{cm}}}. \quad (3.77)$$

An equivalent procedure leads to

$$I_{4G}^{\text{full}} - I_{4G}^{\text{OPE}} \sim \frac{1}{M p_{\text{cm}}}. \quad (3.78)$$

The insertions (7) and (8) do not have an equivalent after the OPE but this is not fatal since we can use Eqns. (3.59) and (3.60) to show that they are power suppressed

$$I_{7G} \sim \frac{m_b}{q^2 l^2 (q+l)^2} V_{\mu\nu\rho}(-q,-l,q+l)(q^\lambda + l^\lambda) \sim \frac{m_b}{M^2 p_{\text{cm}} \Lambda_{\text{QCD}} M^2} MM \sim \frac{1}{M p_{\text{cm}}}, \quad (3.79)$$

$$I_{8G} \sim \frac{m_b}{q^2 l^2} \sim \frac{1}{M p_{\text{cm}}}. \quad (3.80)$$

Conclusion about spectator scattering Soft spectator scattering with external lines is unsuppressed w.r.t. the LO process but factorizes [insertions (1) - (4) in Figs. 3.7b and 3.7c]. Soft spectator scattering with internal lines is power suppressed by $1/M$ w.r.t. to the LO [insertions (5) - (8)]. Under the assumption that we can use the LCDA of the X meson to evaluate the suppression of the LO process, we find that it is suppressed by $1/p_{\text{cm}}^2$ due to the end-point suppression of the LCDA. In contrast, hard-collinear spectator scattering is

unsuppressed by the LCDA but these interactions either fully factorize [insertions (1) and (2)], factorize partly and are $p_{\rm cm}/M$ suppressed w.r.t. the LO process otherwise [insertions in (3) and (4)], or are simply power suppressed by $p_{\rm cm}/M$ (w.r.t. the LO process) [(5)-(7) in Fig. 3.7b and (7) and (8) in Fig. 3.7c]. Furthermore, hard-collinear spectator scattering has a suppression from $\alpha_S(\sqrt{l^2})$. The suppression of hard-collinear spectator scattering relies on the assumption $p_{\rm cm} \ll M$. Since in reality $p_{\rm cm}/M \sim 1/2$ we justify our choice in more detail. Given that $p_{\rm cm} \approx 1.7$ GeV is not such a large scale the discussion about hard-collinear spectator scattering is somewhat academical from the start. In reality, the end-point suppression is probably weaker than assumed above. Furthermore, the LCDA should have its largest contribution for $l \simeq p_{\rm cm}/2 \approx 0.85$ GeV, when the momentum of the valence quarks in the X meson is completely symmetric. This is in fact barely a hard momentum. Here, it is convenient that we showed that soft spectator scattering with $l^2 \sim \Lambda^2_{\rm QCD}$ is suppressed by $1/M$, hence, also counting $p_{\rm cm} \sim \Lambda_{\rm QCD}$ leads to a viable OPE.

In QCDF $p_{\rm cm} \sim m_b \sim M$ is employed, this is why hard-collinear spectator scattering of the Q_2^u penguin is unsuppressed in reference [62]. However, they find that it only yields a tiny contribution because of numerical cancellations. In fact, in the case of hard-collinear spectator scattering, it is possible to separate the hadronization of X meson from the $\bar{B} \to \psi$ transition. The reason is that also the spectator quark becomes energetic. This means that the X meson is only connected via energetic lines with the $\bar{B} \to \psi$ system. Hence, we may invoke the color transparency argument to argue that the X has no soft overlap with the $\bar{B} \to \psi$ system. This means that assuming $p_{\rm cm} \sim m_b \sim M$ it should be possible to calculate hard-spectator scattering by

$$\langle J/\psi X|Q_i^u|\bar{B}\rangle\big|_{\text{hard-collinear Sp. Sc.}} = \langle J/\psi|(\bar{c}c)_V(\bar{p}b)_{V-A}|\bar{B}\rangle(m_X^2)\int \mathrm{d}u\, T_i(u)\,\phi_X(u), \quad (3.81)$$

where T_i^u is the hard-scattering kernel that connects the $\bar{B} \to \psi$ transition and the quark fields that create the X meson and $\langle J/\psi|(\bar{c}c)_V(\bar{p}b)_{V-A}|\bar{B}\rangle(m_X^2)$ describes the $\bar{B} \to \psi$ transition. However, we will not pursue this further here, because the hadronic quantity $\langle J/\psi|(\bar{c}c)_V(\bar{p}b)_{V-A}|\bar{B}\rangle(m_X^2)$ is unknown.

Consequently, we find that the interactions with the spectator quark are suppressed by $p_{\rm cm}/M$ and by $1/M$ and do not obstruct the OPE.

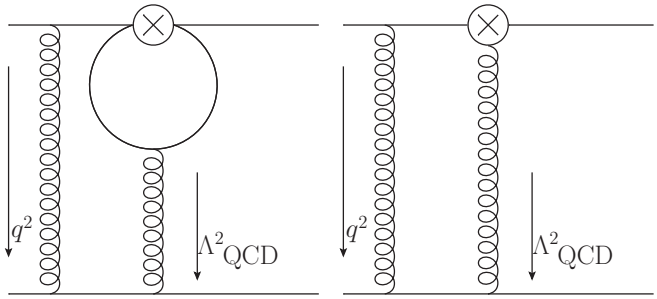

(a) Q_2 insertion. (b) Q_{8G} insertion.

Figure 3.8: The NLO diagrams where the momentum that flows through the penguin loop is soft and the additional gluon is hard. This NLO contribution is suppressed by $1/M^3$.

3.4 Soft penguins

There is the possibility at NLO that the hard momentum does not run through the penguin but runs through another gluon as depicted in Fig. 3.8 in this case the penguin cannot be described by an OPE because it is soft. We will now show that this process is power suppressed and does not impede the OPE. We will discuss the soft penguin in Fig. 3.8a, the discussion for the soft Q_{8G} penguin is analogous. There are four possible diagrams in which a hard gluon connects the the $b-q$ line with the $\bar{c}-c$ line, these are I_{13}, I_{14}, I_{23} and I_{24}. We will explain for the diagram I_{13} in Fig. 3.8a how the suppression arises. The three other cases are analogous. The full diagram in Fig. 3.8a corresponds to computing:

$$I_{13} = \tilde{G}\mathcal{C}_{13}\int \mathrm{d}^d k_1\,\mathrm{d}^d k_2 \quad \Gamma_1 \frac{\not{k}_1}{k_1^2}\gamma_\mu \frac{\not{k}_1+\not{k}_2}{(k_1+k_2)^2}\Gamma_2 \frac{\not{k}_2+\not{p}'+m_b}{(k_2+p')^2-m_b^2}\gamma_\nu \frac{1}{(k_2-q)^2}\frac{1}{k_2^2} \otimes\gamma^\mu \frac{\not{p}_c-\not{k}_2+m_c}{(p_c-k_2)^2-m_c^2}\gamma^\nu \tag{3.82}$$

the k_1 integral is trivial and leads to (inserting the effective operator Q_2 and the corresponding counter term)

$$\begin{aligned} I_{13} &= \tilde{G}\mathcal{C}_{13}\int^{\Lambda_{\rm QCD}} \mathrm{d}^4 k_2 \quad \frac{4}{3}\left[\log\left(\frac{\mu^2}{k_2^2}\right)+i\pi+\frac{2}{3}\right]\left(g^{\mu\rho}-\frac{k_2^\mu k_2^\rho}{k_2^2}\right)\gamma_\rho(1-\gamma_5) \\ &\quad \times \frac{\not{k}_2+\not{p}'+m_b}{(k_2+p')^2-m_b^2}\gamma_\nu \frac{1}{(k_2-q)^2}\otimes\gamma^\mu\frac{\not{p}_c-\not{k}_2+m_c}{(p_c-k_2)^2-m_c^2}\gamma_\nu \end{aligned} \tag{3.83}$$

we are only interested in the region where $k_2^2 \sim \Lambda_{\rm QCD}^2$ is small, since the integral is IR finite in this region we set $d = 4$. Let us only consider the scaling of the diagram, we therefore neglect the Dirac and color structure. The different components then scale as

$$\begin{gathered} \mathrm{d}^4 k_2 \sim \Lambda_{\rm QCD}^4, \qquad \log\left(\frac{\mu^2}{k_2^2}\right) \sim \log\left(\frac{M^2}{\Lambda_{\rm QCD}^2}\right), \qquad \frac{k_2^\mu k_2^\rho}{k_2^2} \sim 1, \\ \frac{\not{k}_2 + \not{p}' + m_b}{(k_2+p')^2 - m_b^2} \sim \frac{1}{M}, \qquad \frac{1}{(k_2-q)^2} \sim \frac{1}{M^2}, \qquad \frac{\not{p}_c - \not{k}_2 + m_c}{(p_c-k_2)^2 - m_c^2} \sim \frac{1}{\Lambda_{\rm QCD}}. \end{gathered} \tag{3.84}$$

By multiplying all factors we then derive the scaling of I_{13} to be

$$I_{13} \sim \log\left(\frac{M^2}{\Lambda_{\rm QCD}^2}\right) \frac{\Lambda_{\rm QCD}^3}{M^3} \tag{3.85}$$

In any of the four diagrams there is always a hard gluon and a bottom or light quark q that are off-shell by M^2, if the penguin loop is soft. Hence, these diagrams all have the following scaling

$$I_{13} \sim I_{14} \sim I_{23} \sim I_{24} \sim \frac{\Lambda_{\rm QCD}^3}{M^3} \tag{3.86}$$

w.r.t. to the LO penguin in the region where $k_2 \sim \Lambda_{\rm QCD}$. The same line of arguments is effective for the soft Q_{8G} penguins at NLO shown in Fig. 3.8b. In other words, these NLO diagrams are suppressed for small loop momentum k_2 and described by operators of higher order in the OPE.

3.5 Additional partons

In Fig. 3.9, we show a tree-level diagram that contributes to the process $\bar{B} \to \psi X$. The up quark pair of the effective vertex does not contribute to a loop correction but takes part in the hadronization of the X meson. This diagram contributes to the penguin pollution p_f but is not described by the OPE at LO. Similar to the soft penguin process in the preceding section, this diagram is suppressed by

$$\frac{1}{M^3}. \tag{3.87}$$

The suppression is due to the off-shell b propagator and the gluon propagator with virtuality $q^2 \sim M^2$. The alternative diagrams where the hard gluon is attached to one of the light quarks, q, $\bar{u}$ or u have the same suppression. Even though the OPE has only a

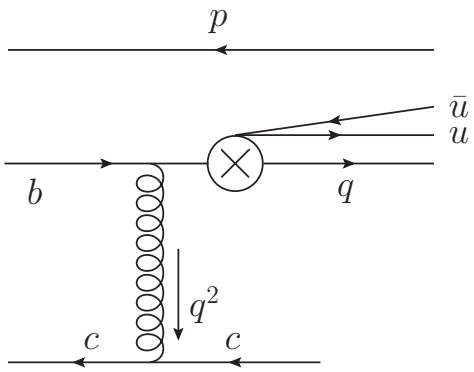

Figure 3.9: A higher Fock state contributions to the process $\bar{B} \to \psi X$. The light meson is formed by four quarks, the quarks q and $\bar{p}$ carry the quantum numbers of the X meson. This contribution is not loop suppressed.

validity up to terms $1/M$ this process in which the X hadronizes from the partons $\bar{p}q\bar{u}u$ is worth mentioning. The reason is that this process does not carry the typical loop-suppression factor $1/(16\pi^2)$ because it is a tree-level diagram. For the Q_{8G} penguin this is not the case, it carries a loop-suppression factor in the operator, see Eqn. (1.37). Therefore, we solely need to consider the contribution of diagram 3.9 where additional hard or soft partons contribute to the hadronization of the X meson. In the limit $p_{\text{cm}} \gg \Lambda_{\text{QCD}}$ we can describe these contributions with a higher order term in the Fock state expansion of the X meson [63]

$$|X(p_{\text{cm}})\rangle \simeq |\bar{p}q\rangle + \mathcal{O}\left(\frac{1}{p_{\text{cm}}}\right)|\bar{p}qg\rangle + \cdots + \mathcal{O}\left(\frac{1}{p_{\text{cm}}^3}\right)|\bar{p}q\bar{u}u\rangle + \ldots . \tag{3.88}$$

The hadronization of several energetic partons to one hadron is suppressed by orders of $1/p_{\text{cm}}$ with respect to the LO process in which the hadron is only formed by an energetic quark pair. Hence, the hadronization of an energetic quark configuration $\bar{p}q\bar{u}u$ into the X meson has a $1/M^3$ suppression from the hard-scattering graph in Eqn. (3.87) and a suppression from the coefficient in the Fock-state expansion.

Nonetheless, $p_{\text{cm}} \gg \Lambda_{\text{QCD}}$ is a rather academic limit, the realistic value $p_{\text{cm}} = 1.7$ GeV divided to three or four partons results into an average energy of $400 - 600\text{MeV} \sim \Lambda_{\text{QCD}}$ which means that the partons rather are soft. If all partons are soft, this cannot be described by the Fock-state expansion anymore. However, this configuration violates the starting assumption that a coherent configuration of soft particles cannot mediate a hard process. In this case this means that four soft (anti-)quarks do not hadronize into an energetic meson.

The remaining possibility is that two or three soft partons contribute to the hadroniza-

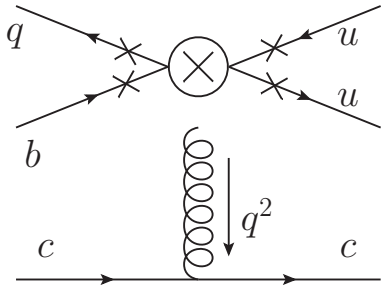

Figure 3.10: Exchange diagrams with up quarks created at the effective vertex in the full theory. The OPE makes it apparent that these diagrams are strongly suppressed.

tion of one or two energetic partons. In this case, all soft partons must end up in the same final meson to conserve all quantum numbers. The quantitative evaluation of this situation is not really possible because soft partons defy theoretical description. However, the qualitative picture is that, since this configuration only covers a small subspace of the possible phase-space configurations this leads to a suppression. This may be seen in Eqn. (3.88) considering the limit where some parton momenta go to zero. In this case the term $|\bar{p}q\bar{u}u\rangle$ still has a suppression of $\mathcal{O}\left(\frac{1}{p_{\rm cm}^3}\right)$. We conclude that additional partons do not lead to a dominant contribution because the hard-scattering part is suppressed by

$$\frac{\Lambda_{\rm QCD}^3}{M^3} \lesssim \frac{1}{16\pi^2} \tag{3.89}$$

and because the hadronization of several partons into an X meson is suppressed.

3.6 Exchange diagrams with up quarks

In the case that the light quark at the effective vertex q is equal to the spectator quark p in the $\bar{B}$ meson, $p = q$, *exchange* and *annihilation* processes[3] are possible. We show an exchange diagram in Fig. 3.10. We limit the discussion to exchange processes, the discussion of annihilation processes is equivalent. Furthermore, we only discuss the case that an up-quark pair is created at the effective vertex.

In the tree-level processes that we hitherto considered the spectator quark takes part in the hadronization of one of the final state mesons (the X meson), in contrast, in exchange diagrams the spectator quark is annihilated at the effective vertex. The exchange diagrams in which light (up) quarks are produced at the effective vertex in Fig. 3.10, are terms

[3]Exchange diagrams are possible for $\bar{B}_p$ decays with $p \in \{d, s\}$, annihilation type diagrams are possible for B^- decays. In this case the $\bar{u}$ and q quark in Fig. 3.10 must be interchanged.

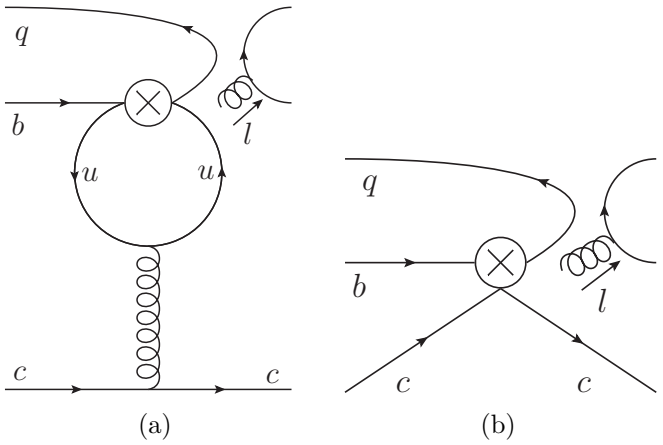

Figure 3.11: (a) Penguin annihilation diagram in the full theory. (b) The penguin annihilation diagram becomes an exchange diagram in the OPE.

$\mathcal{O}\left(\Lambda^3_{\rm QCD}/M^3\right)$. This suppression is due to the gluon with virtuality $q^2 = M^2$ and one off-shell fermion propagator that adds a suppression $1/M$. This off-shell fermion propagator arises when the open gluon in Fig. 3.10 is attached to any of the crosses. The suppression factor $\Lambda^3_{\rm QCD}/M^3$ is essentially the same as in the case of the soft penguins in section 3.4 or higher Fock states in section 3.5. Hence, the OPE makes explicit that exchange and annihilation processes in which light quarks are created at the effective vertex are negligible after the scales $M \sim \sqrt{q^2}$ are integrated out.

3.7 Penguin annihilation diagrams

If the light quark q at the effective vertex is equal to the spectator quark p in the $\bar{B}$ meson, $p = q$ also *penguin annihilation* processes are possible. We show an example in Fig. 3.11a in the full theory and in Fig. 3.11b in the effective theory. This process arises if the up quarks that are created at the effective vertex contribute via a loop correction and the large momentum q^2 flows through this loop. In contrast to the exchange diagrams discussed in the previous section these diagrams are not suppressed in the OPE. However, in $\bar{B} \to \psi X$ decays these diagrams are only relevant if the X meson has a flavor singlet component, e.g. $X = \eta^{(\prime)}$, $\phi(1020)$ but not π^0 nor $\rho^0(770)$.

From a phenomenological point of view one may claim that these diagrams are suppressed by the OZI rule [64–66] but we avoid to invoke the OZI rule because of its phenomenological origin. Furthermore, also the penguins in Fig. 2.1 for which we developed our OPE have OZI-rule suppression. Thus, using the OZI rule only for penguin annihilation processes would be inconsistent. We pursue our discussion of penguin annihilation

diagrams independently of the OZI rule.

The diagram in Fig. 3.11a is matched on Fig. 3.11b in the effective theory. The isolated $\bar{q}q$ line carries the momentum of the meson X. Therefore, there must be a hard gluon with momentum $l \simeq p_X$ that connects this line to the rest of the diagram. In fact the momentum configuration is very similar to the one in hard-collinear spectator scattering in section 3.3 and the penguin annihilation diagrams factorize as hard-collinear spectator scattering. The processes that are integrated out with the OPE have an p_{cm}/M suppression. Hence, penguin annihilation diagrams do not impede the factorization, they become exchange processes where charm quarks are produced at the effective vertex by the OPE.

In contrast to the exchange processes discussed in the previous section 3.6, the exchange processes in Fig. 3.11b are not suppressed. The exchange processes due to the penguin annihilation processes are not the only exchange processes, in addition there are exchange processes due to the current-current operators Q_i^c. Consequently, whenever the X meson has a flavor-singlet component, the decay amplitude receives contributions from exchange processes in addition to the tree-level decays where the spectator quark does not take part at the effective vertex. This means that every four-quark operator contributes with two different Wick contractions to a matrix element. In t_f this derives from the current-current operators Q_i^c, in p_f it derives from the penguin annihilation processes that are integrated out in the OPE.

Thus, penguin annihilation diagrams are unproblematic in the proof of the OPE, however, they influence the phenomenology because they lead to additional Wick contractions for every four-quark operator.

3.8 OPE in $\bar{B} \to D\bar{D}$

We intentionally limited the discussion of the OPE to the decays $\bar{B} \to \psi X$ up to now and disregarded possible differences for $\bar{B} \to D\bar{D}$ decays which we will discuss now. $\bar{B} \to D\bar{D}$ and $\bar{B} \to \psi X$ decays are driven by the same quark-level process. However, in $\bar{B} \to D\bar{D}$ decays the charm quarks hadronize into separate mesons, see Fig. 3.12, whereas they form a charmonium in $\bar{B} \to \psi X$ decays. This raises the question whether there is still a large momentum flow through the up-quark penguin shown in Fig. 3.12b. Therefore, we analyze the momentum flow in the decay. The hard energy release stems from the decay of the b quark and the spectator quark can only contribute via soft interactions. This can be seen from the light-cone distribution amplitude (LCDA) of the $\bar{B}$ meson [7]. Let ξ be

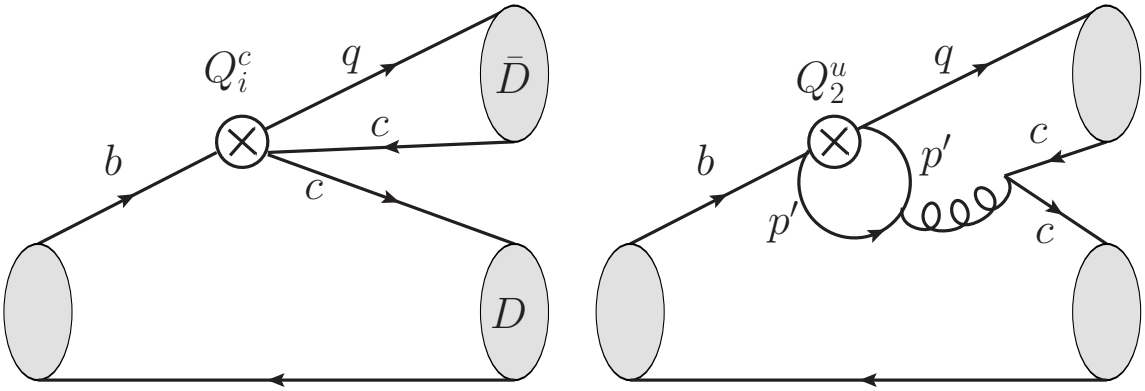

(a) Q_i^c contribution to the decay $\bar{B} \to D\bar{D}$

(b) Q_2^u contribution to the decay $\bar{B} \to D\bar{D}$ in the full theory.

Figure 3.12: Full-theory contributions to the decay $\bar{B} \to D\bar{D}$. The insertion of the operator Q_2^u is integrated out in the OPE, this exploits that the momentum transfer through the up quark loop and the gluon must be $\mathcal{O}(m_B^2)$. On the quark level, it is the same penguin diagram that we discussed so far in $\bar{B} \to \psi X$ decays. The difference is that the charm quarks do not hadronize into a charmonium but into a $D\bar{D}$ pair.

the momentum of the spectator quark normalized to the $\bar{B}$ momentum, then

$$\Phi_B(\xi) \sim \begin{cases} m_b/\Lambda_{\text{QCD}}; & \xi \sim \Lambda_{\text{QCD}}/m_b, \\ 0; & \xi \sim 1. \end{cases} \tag{3.90}$$

Hence, it is not possible that the spectator quark carries hard momentum, the same is true for the spectator quarks of the D mesons in the heavy quark limit. In reality the suppression might not be as strong as in the case of $\bar{B}$ mesons, since m_c is rather an intermediate mass than a heavy mass but we maintain the the heavy quark limit for m_c. In the opposite limit $m_c \to 0$, $\bar{B} \to D\bar{D}$ decays could be treated in QCDF but this description fails.

It follows that in any $D\bar{D}$ production process the charm quarks must carry the momentum of the D mesons up to soft corrections. We are now able to derive the kinematic configuration for the mesons and quarks. Four-momentum conservation implies

$$p_B = \begin{pmatrix} m_B \\ 0 \\ 0 \\ 0 \end{pmatrix}, \quad p_D = \begin{pmatrix} E_D \\ 0 \\ 0 \\ -p_{\text{cm}} \end{pmatrix} \quad \text{and} \quad p_{\bar{D}} = \begin{pmatrix} E_{\bar{D}} \\ 0 \\ 0 \\ p_{\text{cm}} \end{pmatrix} \tag{3.91}$$

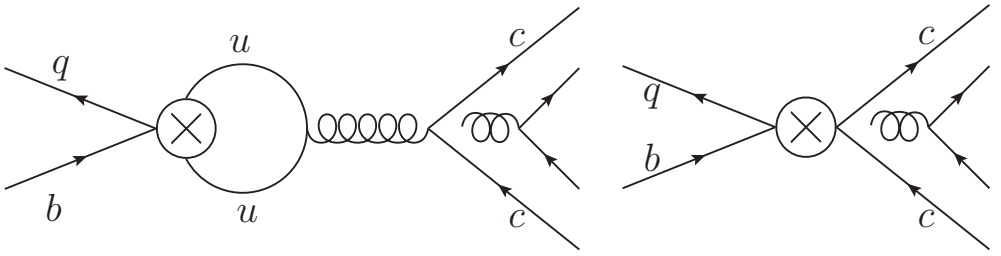

(a) (b)

Figure 3.13: The penguin annihilation diagram in the full theory (a) becomes an exchange diagram after the OPE (b). Since we discuss $\bar{B} \to D\bar{D}$ decays here, we arrange the quark lines differently than in $\bar{B} \to D\bar{D}$ decays.

with $E_D = \sqrt{m_D^2 + p_{\text{cm}}^2}$. The center-of-mass momentum is

$$p_{\text{cm}} \equiv \frac{1}{2m_{\bar{B}}}\sqrt{(m_{\bar{B}}^2 - (m_{\bar{D}} + m_D)^2)(m_{\bar{B}}^2 - (m_{\bar{D}} - m_D)^2)} \approx \frac{1}{2}\sqrt{m_{\bar{B}}^2 - 4m_D^2} \tag{3.92}$$

and a typical value is $p_{\text{cm}} = 1.9$ GeV. Thus, on the quark level the LCDAs imply

$$p_b = \frac{m_b}{2}(n_+ + n_-), \quad p_{\bar{c}} \simeq p_{\bar{D}}, \quad p_c \simeq p_D, \quad q \simeq (p_{\bar{c}} + p_c) \simeq E_D(n_+ + n_-). \tag{3.93}$$

Hence, $q^2 \simeq 4E_D^2 \simeq m_B^2$ represents a large scale that makes the OPE possible and we can come to the modifications that are necessary to perform the proof.

The proof of factorization is almost identical to the proof in the previous sections. One fundamental difference is that in a $\bar{B} \to D\bar{D}$ decay, p' is soft in contrast to $\bar{B} \to \psi X$ decays in which it is $p_{\text{cm}} n_+$. We will now discuss the implications of this.

The proof of factorization of hard and soft scales is independent of the actual hadrons and the value of the momentum p' is not essential. Hence, soft and hard scales also factorize in $\bar{B} \to D\bar{D}$ just as in discussed in section 3.2. Similarly, the discussion about *soft* spectator scattering is in one-to-one correspondence to the discussion in section 3.3. In $\bar{B} \to \psi X$ decays, the discussion about *hard-collinear* spectator scattering is necessary because of the LCDA of the X meson disfavors an asymmetric momentum configuration. In $\bar{B} \to D\bar{D}$ decays hard-collinear spectator scattering is penalized by the D meson LCDA and therefore absent. Soft penguins have a suppression of $\mathcal{O}\left(\Lambda_{\text{QCD}}^3/M^3\right)$ in analogy to section 3.4. Similarly, the full-theory exchange diagrams where an up-quark pair is created at the effective vertex in Fig. 3.10 are suppressed as in $\bar{B} \to \psi X$ decays.

Penguin annihilation processes in $\bar{B} \to D\bar{D}$ decays have the same kinematic configuration as soft spectator scattering. Consequently, they factorize as soft spectator scattering

in section 3.3. This becomes clear when we consider the penguin annihilation diagram that is integrated out with the OPE in Fig. 3.13a the gluon that creates the pair of light valence quarks only needs to be soft $l^2 = \mathcal{O}\left(\Lambda^2_{\rm QCD}\right)$. The momentum transfer through the effective vertex is $q^2 \sim m_B^2$. Hence, the penguin annihilation processes do not impede factorization. Nevertheless their phenomenological role in $\bar{B} \to D\bar{D}$ decays is more pronounced than $\bar{B} \to \psi X$ decays. Since the charm quarks hadronize into different D mesons, it suffices that the final $D\bar{D}$ state is a CP eigenstate to have a contribution from the penguin annihilation process. In contrast to $\bar{B} \to \psi X$ decays where penguin annihilation diagrams are only possible if X has a flavor singlet component. The implications of this will become clearer in the chapter on phenomenology.

We conclude that the OPE is also applicable to $\bar{B} \to D\bar{D}$ decays but that there are some differences between $\bar{B} \to \psi X$ and $\bar{B} \to D\bar{D}$ decays: The momentum transfer $q^2 \sim m_B$ is larger in $\bar{B} \to D\bar{D}$ decays. From the LCDA of the D mesons we conclude that light quark q must be soft, as a consequence hard-collinear spectator scattering is absent in $\bar{B} \to D\bar{D}$ decays because it is penalized by the D meson LCDAs. The penguin annihilation processes in $\bar{B} \to D\bar{D}$ decays factorize like soft-spectator scattering.

3.9 Conclusion of the factorization chapter

In this chapter, we showed that the penguin diagrams in Fig. 2.1 can be described by the OPE that we suggested in the previous Chapter 2. The demonstration of factorization first specialized to $\bar{B} \to \psi X$ decays and then generalized to $\bar{B} \to D\bar{D}$ decays which only requires little additional considerations.

We consider all possible contributions to the full-theory matrix element and discuss their equivalents in the effective theory. The proof of the OPE makes it clear that all full-theory contributions are either: a) perturbative computable and described by the Wilson coefficients $\widetilde{C}_{i,j}$, b) nonperturbative but included in the matrix elements, or c) suppressed by $\Lambda_{\rm QCD}/M$ ($p_{\rm cm}/M$ in the case of hard-collinear spectator scattering in $\bar{B} \to \psi X$ decays). The large scale $M = \sqrt{q^2}$ is defined by means of the momentum transfer q^2 that is transferred from the b quark to the $\bar{c}c$ pair in the quark-level transition $b \to c\bar{c}q$. The soft effects are characterized by the hadronic scale $\Lambda_{\rm QCD}$. The OPE results into four-quark operators because the hadronization of the final state particles in $\bar{B} \to \psi X$ and $\bar{B} \to D\bar{D}$ cannot be separated.

We first showed that it is possible to separate soft and hard scales in the quark-level transition $b \to c\bar{c}q$. The IR divergences that we found all factorize into the matrix

elements. In fact, none of the IR divergences that we found would be present if we would maintain the quarks off-shell by $\mathcal{O}(\Lambda_{\rm QCD})$ and the quark q massive. However, the factorization of scales must be independent of these soft scales. Therefore, the soft scales were set to zero at the cost of obtaining IR divergences that can be absorbed in the matrix elements and are physically regularized by hadronization.

Subsequently, we discussed soft and hard-collinear spectator scattering and showed that interactions with the spectator quark do not invalidate the OPE. We also considered the soft penguins in which q^2 does not flow through the penguin that we describe by the OPE. These processes are suppressed by $\Lambda_{\rm QCD}^3/M^3$ because of two off-shell propagators. Higher Fock states and the exchange diagrams where up quarks are created at the effective vertex have the same suppression for the same reason. At last we discussed penguin annihilation diagrams these factorize like hard-collinear spectator scattering in $\bar{B} \to \psi X$ decays and do not invalidate the OPE.

The quark q must be soft in $\bar{B} \to D\bar{D}$ decays because of the D meson LCDA. This results into a larger value of q^2 than in $\bar{B} \to \psi X$ decays and leads to the absence of hard-collinear spectator scattering. The penguin annihilation diagrams factorize as soft spectator scattering in $\bar{B} \to D\bar{D}$ decays.

Higher order terms are suppressed by $\frac{\Lambda_{\rm QCD}}{M} \sim \frac{1}{10}$ or by $\mathcal{O}\left(\frac{p_{\rm cm}}{M} \sim \frac{1}{2}\right)$. This suppression could in some terms be compensated by large factors in the expansion such that formally suppressed terms are larger than expected. In this case, it is important to recall that the most significant contribution to the penguin p_f actually does not derive from the up-quark or chromomagnetic penguin but from the top-quark penguins, see Eqn. (2.12). Consequently, even if in some cases the corrections to the up-quark or chromomagnetic penguin of $\frac{\Lambda_{\rm QCD}}{M}$ are sizable, this has only a small influence on the overall result.

Chapter 4

Phenomenology

With the OPE for the penguin pollution at hand we are now able to make predictions for *CP*-violating observables and to determine a first-principles theory error on the extraction of the mixing angles ϕ_d and ϕ_s in the decays $\bar{B}_d \to J/\psi K_S$, $\bar{B}_s \to J/\psi\phi$, and $\bar{B}_s \to D_s^+ D_s^-$.

The derivation of these results still needs some work. With the OPE we could show that all contributions in $b \to c\bar{c}q$ decay amplitudes are mediated by the operators in equations 2.1 and 2.2. These operators have perturbative coefficients but the matrix elements of theses operators have not yet been discussed. We will discuss how these matrix elements can be controlled with $1/N_C$ counting.

4.1 Preparations

4.1.1 Computation of the remaining Wilson coefficients

For simplicity, we have neglected the insertion of the penguin operators into the penguin diagrams in the proof of the OPE. The proof of the OPE in Chapter 3 is independent of the particular color or Dirac structure of the inserted operator. Therefore, we can compute now the full coefficient instead of the counting $C_1, C_2 \sim \mathcal{O}(1)$ and $C_3, C_4, C_5, C_6 \sim \mathcal{O}(\alpha_S)$ which we used in Chapter 2. We count all Wilson coefficients to be $\mathcal{O}(1)$. Consequently, we also include penguin mixing into the running of the Wilson coefficients. As a result the matrix elements in the amplitude are full NLO matrix elements. We compute the $Q_i^{\rm nc}$ insertions into the penguin diagram in Fig. 2.1a and find the following additional coefficients for the OPE in Eqn. (2.7)

$$\widetilde{C}_{4,8V} = \widetilde{C}_{6,8V} = \frac{\alpha_S}{4\pi}\left[\frac{8}{3}\ln\frac{q^2}{\mu^2} - 3G_X(0) - G_X(s_b)\right] \tag{4.1}$$

$$\widetilde{C}_{3,8V} = \frac{\alpha_S}{4\pi}\left[\frac{4}{3}\ln\frac{q^2}{\mu^2} + \frac{4}{3} - G_X(0) - G_X(s_b)\right] \tag{4.2}$$

with $s_b = m_b^2/q^2$ and $G_X(s) = G(s - i\epsilon, 1)$

$$G(s,1) = -4\int_0^1 \mathrm{d}u u(1-u)\ln\left[s - u(1-u)\right]. \tag{4.3}$$

and

$$G(0,1) = \frac{10}{9} + \frac{2}{3}i\pi, \qquad G(1,1) = \frac{34}{9} - \frac{2}{3}\sqrt{3}\pi. \tag{4.4}$$

These results and the notation agree with the results of the penguins P_4^u and P_6^u in QCDF from [8]. Note, that $P(q^2) = \frac{\alpha_S}{4\pi}\left[\frac{2}{3}\ln\frac{q^2}{\mu^2} + \frac{2}{3} - G_X(0)\right]$. Hence, the penguin operator insertions into the penguin diagram lead to nonvanishing coefficients $\widetilde{C}_{j,8V}$ for $j \in \{3,4,6\}$.

4.2 *CP* violation

In this section, we give the expressions of C_f, S_f and $A_{\Delta\Gamma_s}$ as a function of a_f and the numerical values of the CKM parameters that we use for the evaluation of our formulae.

4.2.1 Observables

Up to now, we evaluated C_f, S_f, and $A_{\Delta\Gamma}$ only in the limit $a_f \to 0$. We generalize the expressions now for $a_f \neq 0$. For a decay of a $\bar{B}_p$ meson via the quark level process $b \to c\bar{c}q$ we use λ_f from Eqn. (1.27) to rewrite the *CP*-violating observables in Eqn. (1.23) as

$$\begin{aligned}
C_f &= 2\frac{\mathrm{Im}(a_f)\mathrm{Im}(\epsilon_q)}{1 + 2\mathrm{Re}(a_f)\mathrm{Re}(\epsilon_q)) + |a_f^2\epsilon_q^2|} \simeq 2\mathrm{Im}(a_f)\mathrm{Im}(\epsilon_q), && (4.5)\\
S_f &= \eta_f\frac{-\sin(\phi_p) + 2\mathrm{Re}(a_f)\mathrm{Im}(\epsilon_q e^{-i\phi_p}) + |a_f^2|\mathrm{Im}(\epsilon_q^2 e^{-i\phi_p})}{1 + 2\mathrm{Re}(a_f)\mathrm{Re}(\epsilon_q) + |a_f^2\epsilon_q^2|} && (4.6)\\
&\simeq -\eta_f[\sin(\phi_p) - 2\mathrm{Re}(a_f)\mathrm{Im}(\epsilon_q)\cos(\phi_p)], && (4.7)\\
A_{\Delta\Gamma_s} &= -\eta_f\frac{\cos(\phi_s) + 2\mathrm{Re}(a_f)\mathrm{Re}(\epsilon_q e^{-i\phi_s}) + |a_f^2|\mathrm{Re}(\epsilon_q^2 e^{-i\phi_s})}{1 + 2\mathrm{Re}(a_f)\mathrm{Re}(\epsilon_q) + |a_f^2\epsilon_q^2|} && (4.8)\\
&\simeq -\eta_f[\cos(\phi_s) + 2\mathrm{Re}(a_f)\mathrm{Im}(\epsilon_q)\sin(\phi_s)]. && (4.9)
\end{aligned}$$

The $\simeq$ approximations correspond to an expansion in $|\epsilon_q a_f|$ and are valid up to terms $\mathcal{O}\left(|\epsilon_q a_f|^2\right)$. We set $\phi_p = \phi_s$ in $A_{\Delta\Gamma}$ because $A_{\Delta\Gamma}$ is only observable for B_s decays. The

CP-violating observables are not independent of each other but obey the relation

$$C_f^2 + S_f^2 + A_{\Delta\Gamma}^2 = 1 \tag{4.10}$$

for every decay separately. The reason for this is that only the absolute value and the phase of λ_f are physical, after setting $|q/p| = 1$ which is a very good approximation for neutral $\bar{B}$ decays.

We note that C_f and S_f are quasi-independent functions in terms of a_f, whereas C_f measures $\mathrm{Im}(a_f)$, S_f measures a combination of $\sin(\phi_p)$ and $\mathrm{Re}(a_f)$. In the literature [34, 67], the observables are often expressed in terms of the absolute value and the phase of a_f instead as functions of imaginary and real parts. However, this disguises the quasi-independence. Physically, it may seem unrealistic that the imaginary part is gigantic whereas the real part vanishes but mathematically real and imaginary part are independent quantities and we adopt this more careful point of view.

4.2.2 Observable shifts

Since we are interested in the corrections that arise due to a nonzero penguin it is useful to introduce the observable shifts [30, 33]

$$\Delta S_f \equiv S_f + \eta_f \sin(\phi_p), \qquad \Delta A_{\Delta\Gamma} \equiv A_{\Delta\Gamma} + \eta_f \cos(\phi_s) \tag{4.11}$$

these are less dependent on the actual value of ϕ_p. Alternatively, one can express the contributions of the penguin-to-tree ratio a_f to the observable S_f as a shift of the angle [31] ϕ_p, which is defined as follows

$$\Delta\phi_p \equiv -\arg\left(\frac{1+\epsilon_q a_f}{1+\epsilon_q^* a_f}\right) \tag{4.12}$$

this leads to

$$\tan(\Delta\phi_p) = -\frac{2\mathrm{Re}(a_f)\mathrm{Im}(\epsilon_q) + |a_f|^2\mathrm{Im}({\epsilon_q}^2)}{1 + 2\mathrm{Re}(a_f)\mathrm{Re}(\epsilon_q) + |a_f|^2\mathrm{Re}({\epsilon_q}^2)} \tag{4.13}$$

and one may rewrite $S_f \simeq -\eta_f \sin(\phi_p + \Delta\phi_p)$. If we once more expand in $|\epsilon_q a_f|$ we obtain

$$\tan(\Delta\phi_p) \simeq -2\mathrm{Re}(a_f)\mathrm{Im}(\epsilon_q) \tag{4.14}$$

which is certainly a good approximation for $q = s$.

4.2.3 Numerical Values

We use the standard Wolfenstein parametrization of the CKM matrix as in reference [21]. The numerical values are taken from CKMfitter collaboration [22][1]. For the numerical analysis we use the global fit results

$$\lambda = 0.22543, \quad A = 0.8227, \quad \bar{\rho} = 0.1504, \quad \bar{\eta} = 0.3540. \tag{4.15}$$

The ratio $\epsilon_q = \lambda_{uq}/\lambda_{cq}$ specifies the CKM parameters that contribute to the *CP*-violating observables,

$$\epsilon_d = \frac{V_{ud}^* V_{ub}}{V_{cd}^* V_{cb}}, \qquad \epsilon_s = \frac{V_{us}^* V_{ub}}{V_{cs}^* V_{cb}}. \tag{4.16}$$

Their size is given by $|\epsilon_d| = R_u = 0.385^{+0.0070}_{-0.0068}$ and $|\epsilon_s| = R_u\lambda^2 = 0.0196$, here R_u is one side of the unitarity triangle. The phases are

$$\arg(\epsilon_d) = 180^\circ - \gamma, \qquad \arg(\epsilon_s) = -\gamma. \tag{4.17}$$

The current best-fit values for the angles are

$$\alpha = (90.4^{+2.0}_{-1.0})^\circ, \quad \beta = (22.62^{+0.44}_{-0.42})^\circ, \quad \gamma = (67.0^{+2.0}_{-0.9})^\circ, \quad \beta_s = (1.078^{+0.021}_{-0.024})^\circ. \tag{4.18}$$

The direct measurements are most precise for the angle β. The angle β_s, on the other hand, is very strongly constrained by the global fit.

4.3 Phenomenology in $\bar{B} \to \psi X$

In this section we will present the *CP*-violating observables in $\bar{B} \to \psi X$ decays. Here, the $\bar{B}$ meson, with $\bar{B} \in \{B^-, \bar{B}_d, \bar{B}_s\}$, decays into a charmonium $\psi \in \{\eta_c(1S), J/\psi(1S), \chi_{c0}(1P), \chi_{c1}(1P), \psi(2S)\}$ and X is either a light pseudoscalar meson $X = P$ with $P \in \{\pi^0, \pi^-, K_S, K^-, \eta, \eta'(958)\}$ or a light vector meson $X = V$ with $V \in \{\rho^0(770), \rho^-(770), K^*(892), \phi(1020)\}$.

The prediction of the *CP*-violating observables leads in particular to a first-principles theoretical uncertainty on the extraction of the UT angles β and β_s in the decays $\bar{B}_d \to J/\psi K_S$ and $\bar{B}_s \to J/\psi\phi$, respectively. The *CP*-violating observables are determined with the ratio $a_f = p_f/t_f$. Thanks to our OPE, we can write $a_f = p_f/t_f$ as a function of Wilson coefficients and matrix elements of local four-quark operators. Whereas the

[1] See update on homepage, fit from EPS 2015

Wilson coefficients are determined using perturbation theory, the matrix elements are treated with $1/N_C$ counting. Before we apply the $1/N_C$ counting in the determination of a_f, we test its validity with the branching ratios.

After the derivation of the decay amplitude, we discuss some of its aspects in $1/N_C$ counting and then give the numerical results. Subsequently, we compare our results to the available measurements and to other theoretical estimates.

4.3.1 Decay amplitude

In this section we explain the details of the numerical evaluation of the decay amplitude in $\bar{B} \to \psi X$ decays. From the Hamiltonian in Eqn. (1.30) and the OPE in Eqn. (2.7), we derive the decay amplitude

$$\mathcal{A}(\bar{B} \to f) = \lambda_{cq} t_f + \lambda_{uq} p_f \tag{4.19}$$

with

$$\begin{aligned} t_f &= -\mathrm{i}\frac{G_F}{\sqrt{2}}\Big[\; (a_1 + a_3 + a_5)\,\langle Q_{0V}\rangle + (2C_2 + C_{8V} - C_{8G}\widetilde{C}_{8G,8T})\,\langle Q_{8V}\rangle \\ &\quad -(a_1 + a_3 - a_5)\,\langle Q_{0A}\rangle - (2C_2 + 2C_4 - 2C_6)\,\langle Q_{8A}\rangle + C_{8G}\widetilde{C}_{8G,8T}\,\langle Q_{8T}\rangle\Big], \qquad (4.20) \\ p_f &= -\mathrm{i}\frac{G_F}{\sqrt{2}}\Big[\; (a_3 + a_5)\,\langle Q_{0V}\rangle + (2C_2\widetilde{C}_{2,8V} + C_{8V} - C_{8G}\widetilde{C}_{8G,8T})\,\langle Q_{8V}\rangle \\ &\quad -(a_3 - a_5)\,\langle Q_{0A}\rangle - (2C_4 - 2C_6)\,\langle Q_{8A}\rangle + C_{8G}\widetilde{C}_{8G,8T}\,\langle Q_{8T}\rangle\Big]. \qquad (4.21) \end{aligned}$$

We use the shorthand-notation $\langle Q\rangle \equiv \langle f|Q|\bar{B}\rangle$, and the standard Wilson coefficient combinations $a_i \equiv C_i + \frac{1}{N_C}C_{i+1}$ for $i \in \{1,3,5\}$, moreover, we defined

$$C_{8V} \equiv 2C_4 + 2C_6 + 2C_3\widetilde{C}_{3,8V} + 2C_4\widetilde{C}_{4,8V} + 2C_6\widetilde{C}_{6,8V} + C_{8G}\widetilde{C}_{8G,8T}. \tag{4.22}$$

We evaluate the Wilson coefficients in the NDR scheme at the scale $\mu = m_{J/\psi} = \sqrt{q^2}$. They have the values

$$\begin{aligned} C_2 &= 1.10, \\ C_1 &= -0.23, \quad C_4 = -0.04, \quad C_6 = -0.05, \\ C_{8V} &= -0.16, \quad 2C_2\widetilde{C}_{2,8V} = -0.01 - 0.07\mathrm{i}, \quad C_{8G}\widetilde{C}_{8G,8T} = 0.02, \\ C_3 &= 0.01, \quad C_5 = 0.01. \end{aligned} \tag{4.23}$$

We will mainly use the $1/N_C$ counting to order the matrix elements in size but it is also possible to attribute a $1/N_C$ counting to the Wilson coefficients [44]

$$C_2 \sim \mathcal{O}(1), \qquad C_1, C_4, C_6, C_{8V} \sim \frac{1}{N_C}, \qquad C_3, C_5 \sim \frac{1}{N_C^2}. \tag{4.24}$$

Hence, the size of the Wilson coefficient is in principle as the $1/N_C$ ordering implies but perturbative effects lead to a variation from the $1/N_C$ expectation.

With Eqn. (2.11) we write

$$\langle Q_{8T} \rangle = \langle Q_{8V} \rangle \left(1 + \mathcal{O}\left(\frac{p_{\rm cm}}{m_b}\right)\right) \tag{4.25}$$

to reduce the number of matrix elements by one in Eqns. (4.20) and (4.21). The suppression of $\mathcal{O}\left(\frac{p_{\rm cm}}{m_b}\right)$ is not very small but the Wilson coefficient of $\langle Q_{8T} \rangle$ is small, $\left|\frac{C_{8G}\widetilde{C}_{8G,8T}}{C_{8V}}\right| = 0.1$, such that we incur an $\mathcal{O}(5\%)$ error on p_f. We treat the term $\mathcal{O}\left(\frac{p_{\rm cm}}{m_b}\right)$ as a theoretical uncertainty and omit it in the following expressions but take it into account in the numerical result.

We remain with the matrix elements $\langle Q_j \rangle$ with $j \in \{0V, 0A, 8V, 8A\}$ which we estimate in the following by means of color counting [12, 40, 43, 44], see also section 1.2.2. It is convenient to define the factorized color-singlet matrix element $V_0 \equiv -i \langle Q_{0V} \rangle$, for example, in the decay mode $\bar{B}_d \to J/\psi K^0$ we obtain (See appendix B.1 for more details)

$$\begin{aligned}
V_0 &\equiv -\mathrm{i} \left\langle J/\psi K^0 \right| Q_{0V} \left| \bar{B}_d \right\rangle_{\rm fact.} && (4.26)\\
&= -\mathrm{i} \left\langle J/\psi K^0 \right| (\bar{c}c)_{V-A} (\bar{s}b)_{V-A} \left| \bar{B}_d \right\rangle_{\rm fact.} && (4.27)\\
&= -\mathrm{i} \langle J/\psi | \, \bar{c}\gamma_\mu(1-\gamma_5)c \, |0\rangle \left\langle K^0 \right| \bar{s}\gamma^\mu(1-\gamma_5)b \left| \bar{B}_d \right\rangle && (4.28)\\
&= 2 f_{J/\psi} m_{B_d} p_{\rm cm} F_1^{BK}(m_{J/\psi}^2). && (4.29)
\end{aligned}$$

This means, if we neglect the gluon exchange between the $\bar{c}c$ and $\bar{s}b$ current, the matrix element $\langle Q_{0V} \rangle$ can be computed. Corrections to this require the exchange of at least two gluons between the currents which leads to suppression of $1/N_C^2$ of these corrections. In every decay mode separately, we normalize the matrix elements to V_0 and define the normalized hadronic matrix elements v_0, v_8, a_0 and a_8 as

$$\langle Q_{0V} \rangle \equiv V_0 \, v_0, \quad \langle Q_{0A} \rangle \equiv V_0 \, a_0, \quad \langle Q_{8V} \rangle \equiv V_0 \, v_8, \quad \langle Q_{8A} \rangle \equiv V_0 \, a_8. \tag{4.30}$$

The matrix element $\langle Q_{0V} \rangle$ represents the leading term in $1/N_C$, the color counting of the

normalized matrix elements is

$$v_0 = 1 + \mathcal{O}\left(\frac{1}{N_C^\alpha}\right), \quad a_0 = \mathcal{O}\left(\frac{1}{N_C^\alpha}\right), \quad v_8 = \mathcal{O}\left(\frac{1}{N_C}\right), \quad a_8 = \mathcal{O}\left(\frac{1}{N_C}\right). \tag{4.31}$$

with $\alpha = 1$ if X has a color singlet component and $\alpha = 2$ if not (as in the example for $\bar{B}_d \to J/\psi K_S$). Thus, we obtain[2]

$$\begin{aligned} t_f &= \frac{G_F}{\sqrt{2}} V_0 \left[(a_1 + a_3 + a_5)v_0 + (2C_2 + C_{8V})v_8 \right. \\ &\qquad \left. -(a_1 + a_3 - a_5)a_0 - (2C_2 + 2C_4 - 2C_6)a_8\right], \end{aligned} \tag{4.32}$$

$$\begin{aligned} p_f &= \frac{G_F}{\sqrt{2}} V_0 \left[\; (a_3 + a_5)v_0 + (2C_2\widetilde{C}_{2,8V} + C_{8V})v_8 \right. \\ &\qquad \left. -(a_3 - a_5)a_0 - (2C_4 - 2C_6)a_8\right], \end{aligned} \tag{4.33}$$

and identify the dominating terms in the amplitudes by means of the $1/N_C$ counting

$$t_f = \frac{G_F}{\sqrt{2}} V_0 \left[a_1 v_0 + 2C_2(v_8 - a_8) + \mathcal{O}\left(1/N_C^2\right)\right] \qquad \sim \mathcal{O}\left(\frac{1}{N_C}\right), \tag{4.34}$$

$$p_f = \frac{G_F}{\sqrt{2}} V_0 \left[(a_3 + a_5)v_0 + (2C_2\widetilde{C}_{2,8V} + C_{8V})v_8 + \mathcal{O}\left(1/N_C^3\right)\right] \sim \mathcal{O}\left(\frac{1}{N_C^2}\right), \tag{4.35}$$

with $v_0 = 1$ and the expectation $0 \leq v_8, a_8 \leq 1/N_C$. The comparison of these expressions with the experimental branching ratios allows a test of the $1/N_C$ counting. For this test we compare the theoretical amplitude in LO of the $1/N_C$ counting

$$A(\bar{B} \to f) = \frac{G_F}{\sqrt{2}} V_0 \lambda_{cq} \left[a_1 + 2C_2(v_8 - a_8)\right], \tag{4.36}$$

with the experimental amplitude

$$\mathcal{A}_{\text{exp}}(\bar{B} \to f) \equiv \sqrt{8\pi m_{\bar{B}}^2 \mathcal{B}(\bar{B} \to f)\tau_{\bar{B}}/p_{\text{cm}}}. \tag{4.37}$$

This leads to bounds on $|v_8 - a_8|$ which are given in Tab. 4.1. The fact that in no decay mode $|v_8 - a_8|$ is larger than $1/N_C = 1/3$ is a good confirmation of the $1/N_C$ counting. The bounds in Tab. 4.1 do not constrain $|v_8|$ and $|a_8|$ separately. Thus, they do not exclude that $|v_8|$ and $|a_8|$ interfere negatively, such that they are larger than the combination $|v_8 - a_8|$. However, in most decays the bound $|v_8|, |a_8| \leq 1/3$ holds as long as $|v_8|, |a_8| \leq 2|v_8 - a_8|$. Consequently, $|v_8| > 1/3$ or $|a_8| > 1/3$ would require some fine

[2]Note that the parameters a_1–a_6 are the Wilson-coefficient combinations known from the literature. a_0 and a_8, on the other hand, are normalized hadronic matrix elements.

Decay	$\min(\lvert v_8 - a_8\rvert)$	$\max(\lvert v_8 - a_8\rvert)$
$\bar{B}_d \to J/\psi\pi^0$	0.05	0.18
$\bar{B}_d \to J/\psi K_S$	0.07	0.19
$\bar{B}_d \to J/\psi\eta$	0.06	0.18
$\bar{B}_d \to J/\psi\eta'$	0.05	0.17
$\bar{B}_d \to \eta_c K_S$	0.05	0.17
$\bar{B}_d \to \eta_c K^*$	0.04	0.16
$\bar{B}_d \to \psi(2S) K_S$	0.10	0.22
$\bar{B}_d \to \chi_{c1}\pi^0$	0.02	0.15
$\bar{B}_d \to \chi_{c1} K_S$	0.02	0.14
$\bar{B}_s \to J/\psi K_S$	0.06	0.18
$\bar{B}_s \to J/\psi\eta$	0.10	0.22
$\bar{B}_s \to J/\psi\eta'$	0.10	0.23
$\bar{B}_s \to \psi(2S)\eta$	0.17	0.29
$\bar{B}_s \to \psi(2S)\eta'$	0.12	0.24
$\bar{B}_d \to (J/\psi\rho^0)^0$	0.04	0.16
$\bar{B}_d \to (J/\psi\rho^0)^\parallel$	0.02	0.14
$\bar{B}_d \to (J/\psi\rho^0)^\perp$	0.04	0.16
$\bar{B}_d \to (J/\psi K^*)^0$	0.04	0.17
$\bar{B}_d \to (J/\psi K^*)^\parallel$	0.02	0.14
$\bar{B}_d \to (J/\psi K^*)^\perp$	0.03	0.15
$\bar{B}_d \to (\psi(2S) K^*)^0$	0.04	0.16
$\bar{B}_d \to (\psi(2S) K^*)^\parallel$	0.00	0.12
$\bar{B}_d \to (\psi(2S) K^*)^\perp$	0.05	0.17
$\bar{B}_s \to (J/\psi\phi)^0$	0.03	0.15
$\bar{B}_s \to (J/\psi\phi)^\parallel$	0.01	0.13
$\bar{B}_s \to (J/\psi\phi)^\perp$	0.03	0.15
$\bar{B}_s \to (J/\psi K^*)^0$	0.03	0.15
$\bar{B}_s \to (J/\psi K^*)^\parallel$	0.01	0.13
$\bar{B}_s \to (J/\psi K^*)^\perp$	0.04	0.16

Table 4.1: Upper and lower values that are allowed for the normalized hadronic matrix element combination $|v_8 - a_8|$ by the experimental branching ratio $\mathcal{B}(\bar{B}_p \to f)$. None of the combinations is larger than our expectation of $\mathcal{O}(1/N_C)$. The experimental uncertainties are not included but their inclusion does not change the fundamental picture.

tuning of these matrix elements to conform with the bound from the branching ratio. We see this as evidence that $1/N_C$ counting is applicable in $\bar{B} \to \psi X$ decays and use (for exceptions see below)

$$|v_0| = 1, \quad a_0 = 0, \quad \text{and} \quad 0 \leq |v_8|, |a_8| \leq \frac{1}{N_C}. \tag{4.38}$$

with $N_C = 3$ for the numerical evaluation of $a_f = p_f/t_f$. We set $|v_0| = 1$ and $|a_0| = 0$ because the omission of $\mathcal{O}\left(1/N_C^{\alpha}\right)$ terms in these quantities induces an error $\mathcal{O}\left(1/N_C^{\alpha+1}\right)$ on t_f and $\mathcal{O}\left(1/N_C^{\alpha+2}\right)$ on p_f. This uncertainty is negligible, since the uncertainty due to the values of v_8 and a_8 is $\mathcal{O}\left(1/N_C\right)$.

Interestingly, in the decays $\bar{B}_d \to \chi_{c0} K^{(*)}$ the singlet matrix element $\langle Q_{V0} \rangle$ vanishes at LO in $1/N_C$. The quantum numbers $J^{PC} = 0^{++}$ of the χ_{c0} do not permit that a vector or axial current generates a χ_{c0}

$$\langle \chi_{c0} | \, \gamma_\mu (1 \pm \gamma_5) \, |0\rangle = 0. \tag{4.39}$$

In these decays

$$t_f = \frac{G_F}{\sqrt{2}} \, 2C_2 \left(\langle Q_{V8} \rangle - \langle Q_{A8} \rangle \right) \tag{4.40}$$

is the leading contribution in $1/N_C$, this allows the determination of $| \langle Q_{V8} \rangle - \langle Q_{A8} \rangle |$ up to $\mathcal{O}\left(10\%\right)$. Normalizing to a typical value $\frac{G_F}{\sqrt{2}} V_0 = 3 \times 10^{-5}$ GeV we obtain for $\bar{B}_d \to J/\psi K_S$

$$\frac{| \langle Q_{V8} \rangle - \langle Q_{A8} \rangle |}{V_0} = |v_8 - a_8| = 0.04. \tag{4.41}$$

This value $|v_8 - a_8|$ is on the low side of the ranges in Tab. 4.1 and may be seen as an additional confirmation of the $1/N_C$ counting. However, it is unclear whether χ_{c0} can be related this easily to the other charmonium decays.

Since the factorized singlets V_0 are absent in decays where the charmonium is a χ_{c0}, we cannot normalize the matrix elements to V_0 in these decays. However, the absence of V_0 also means that the decay amplitude is largely determined by $\langle Q_{V8} \rangle$ and $\langle Q_{A8} \rangle$. The size of $| \langle Q_{V8} \rangle - \langle Q_{A8} \rangle |$ can be determined as in Eqn. (4.41), we use this to set the following limit on the matrix elements

$$| \langle Q_{V8} \rangle |, | \langle Q_{A8} \rangle | \leq x | \langle Q_{V8} \rangle - \langle Q_{A8} \rangle |. \tag{4.42}$$

We set $x = 2$ by arguing that the matrix elements should not too fine-tuned, i.e. that their combination $| \langle Q_{V8} \rangle - \langle Q_{A8} \rangle |$ should not be a lot smaller than the individual matrix

elements $|\langle Q_{V8}\rangle|$ and $|\langle Q_{A8}\rangle|$.

In the case that the charmonium is an η_c, the factorized singlet $\langle Q_{V0}\rangle|_{\text{fact.}}$ vanishes. In contrast, $\langle Q_{A0}\rangle|_{\text{fact.}}$ is nonzero because η_c is a pseudoscalar particle. Therefore, we normalize the matrix elements to $\langle Q_{A0}\rangle|_{\text{fact.}}$ instead to $\langle Q_{V0}\rangle|_{\text{fact.}}$ and the $1/N_C$ counting of the normalized color singlet matrix elements is modified, we use $|a_0| = 1$ and $v_0 = 0$.

For the numerical evaluation we need to determine the factorized color singlets V_0 in every decay. For their determination, we use the form factors from references [68–75] and evaluate them at the charmonium mass m_ψ. Furthermore, we use the decay constants [76–78]

$$f_{J/\psi} = 0.405 \pm 0.005 \text{ GeV}, \quad f_{\psi(2S)} = 0.288 \pm 0.002 \text{ GeV}, \quad f_{\eta_c} = 0.387 \pm 0.007 \text{ GeV}. \tag{4.43}$$

In decays that involve the χ_{c1}, we estimate the decay constant to be $f_{\chi_{c1}} = 0.45$ GeV. To our knowledge there is no numerical value of the χ_{c1} decay constant available in the literature. This is why we choose a typical value that tends to overestimate the real value. The results in Tab. 4.2 are to good approximation linear in the decay constant and can be simply rescaled by $f_{\chi_{c1}}/(0.45 \text{ GeV})$ to obtain a result for the other values.

In all decays we require that the theoretical amplitude as a function of Wilson coefficients and (normalized) matrix elements obeys the experimental constraint from the branching ratio

$$\lambda_{cq} t_f + \lambda_{uq} p_f \stackrel{!}{=} \mathcal{A}_{\text{exp}}(\bar{B} \to f), \tag{4.44}$$

with $\mathcal{A}_{\text{exp}}$ defined in Eqn. (4.37). We leave the phases of the normalized matrix elements free and exploit that the overall phase of an amplitude is unphysical and can be chosen to be zero. The size of the normalized matrix elements is left free in the ranges given in and below Eqn. (4.38).

With the given experimental bound, the decay-specific singlets V_0, the bounds in Eqn. (4.38) and the Wilson coefficients in Eqn. (4.23) we derive the *CP*-violating coefficients that we discuss in the next section.

4.3.2 $\bar{B} \to \psi X$ results

The results for the *CP*-violating coefficients are given in Tabs. 4.2–4.5. Several comments apply

- The expected value for $-\eta_f A_{\Delta\Gamma_s} = \cos(\phi_s) = 0.99929 \pm 0.00003$ is very close to 1. Consequently, the values for $10^3 \times \max(|\Delta A_{\Delta\Gamma_s}|)$ in Tabs. 4.3 and 4.5 are lower

Final State Unit	$\max(\lvert\Delta\phi_d\rvert)$ 1°	$\max(\lvert\Delta S_f\rvert)$ 10^{-2}	$\max(\lvert C_f\rvert)$ 10^{-2}
$\bar{B}_d \to J/\psi\pi^0$	15	16	27
$\bar{B}_d \to J/\psi K_S$	0.68	0.84	1.13
$\bar{B}_d \to J/\psi\eta$	15	17	25
$\bar{B}_d \to J/\psi\eta'$	17	19	30
$\bar{B}_d \to \eta_c K_S$	0.92	1.13	1.59
$\bar{B}_d \to \psi(2S)K_S$	0.69	0.85	1.17
$\bar{B}_d \to \chi_{c0}K_S$	2.15	2.70	3.85
$\bar{B}_d \to \chi_{c1}\pi^0$	21	25	39
$\bar{B}_d \to \chi_{c1}K_S$	1.08	1.35	1.78

Table 4.2: *CP*-violating parameters in $\bar{B}_d \to \psi P$ decays (P is a pseudoscalar meson). The maximum size of the hadronic phase shift $\Delta\phi_d$, the maximal shift of the mixing-induced *CP* asymmetry S_f and of the direct *CP* asymmetry C_f. The values are functions of the penguin-to-tree ratio a_f which is computed by means of the OPE and the $1/N_C$ counting.

Final State Unit	$\max(\lvert\Delta\phi_s\rvert)$ 1°	$\max(\lvert\Delta S_f\rvert)$ 10^{-2}	$\max(\lvert C_f\rvert)$ 10^{-2}	$\max(\Delta A_{\Delta\Gamma_s}\rvert)$ 10^{-3}
$\bar{B}_s \to J/\psi K_S$	14	24	23	38
$\bar{B}_s \to J/\psi\eta$	0.57	0.99	0.95	0.33
$\bar{B}_s \to J/\psi\eta'$	0.55	0.95	0.91	0.32
$\bar{B}_s \to \psi(2S)\eta$	0.40	0.70	0.68	0.24
$\bar{B}_s \to \psi(2S)\eta'$	0.52	0.91	0.88	0.31

Table 4.3: *CP*-violating parameters in $\bar{B}_s \to \psi P$ decays. For more explanations, see caption of Tab. 4.2.

bounds for $-\eta_f A_{\Delta\Gamma_s}$, if they are larger than 0.71×10^{-3}.

- In decays $\bar{B}_p \to \psi V$ in which V and ψ are vector mesons[3] the final state has three possible polarizations. We classify these by the polarization of the final state mesons [79]. Either both vector mesons are longitudinally polarized (0), or they are transversely polarized and the polarization vectors are either perpendicular ($\perp$) or parallel ($\parallel$). The factorizable part of the singlet matrix elements $\langle Q_{V0}\rangle$ is evaluated according to reference [80].

- If $V = K^*$ we assume that the K^* is reconstructed via $(K_S\pi^0)$. Only this reconstruction allows to measure S_f (and $A_{\Delta\Gamma}$). If the K^* is reconstructed via $(K^\pm\pi^\mp)$ the *CP* asymmetry is time-independent and only direct *CP* violation is possible be-

[3]The charmonia $\eta_c(1S)$ and χ_{c0} are no vector meson but pseudoscalar and scalar mesons, respectively.

Final State Unit	$\max(\lvert\Delta\phi_d\rvert)$ 1°	$\max(\lvert\Delta S_f\rvert)$ 10^{-2}	$\max(\lvert C_f\rvert)$ 10^{-2}
$\bar{B}_d \to (J/\psi\rho^0)^0$	18	20	29
$\bar{B}_d \to (J/\psi\rho^0)^\parallel$	20	25	37
$\bar{B}_d \to (J/\psi\rho^0)^\perp$	18	20	30
$\bar{B}_d \to (J/\psi K^*)^0$	0.85	1.06	1.41
$\bar{B}_d \to (J/\psi K^*)^\parallel$	1.00	1.22	2.03
$\bar{B}_d \to (J/\psi K^*)^\perp$	0.93	1.16	1.54
$\bar{B}_d \to \eta_c K^*$	0.96	1.17	1.63
$\bar{B}_d \to \chi_{c0} K^*$	1.81	2.27	3.24
$\bar{B}_d \to (\psi(2S)K^*)^0$	0.93	1.15	1.53
$\bar{B}_d \to (\psi(2S)K^*)^\parallel$	1.47	1.84	2.57
$\bar{B}_d \to (\psi(2S)K^*)^\perp$	0.85	1.05	1.40

Table 4.4: *CP*-violating parameters in $\bar{B}_d \to \psi V$ decays. For more explanations, see caption of Tab. 4.2.

cause the final state is no *CP* eigenstate. Hence, only the prediction for C_f is valid in this situation.

- The charged B^- mesons cannot decay into *CP* eigenstates. This situation is similar to the situation when the K^* is reconstructed via $K^\pm\pi^\mp$. The *CP* asymmetry is time-independent and only direct *CP* violation is possible. Thus, only the coefficient of direct *CP* violation C_f can be measured. The results for B^- decays are not listed because they can be obtained by using isospin symmetry. For example, we derive from Tab. 4.2

$$\max(|C_{B^-\to J/\psi\pi^-}|) = 27 \times 10^{-2}. \tag{4.45}$$

- The dominant theory uncertainty of the results derives from the $1/N_C$ estimate of v_8 because the penguin p_f is dominated by v_8. Hence, the allowed value of $|v_8|$ which we set to $1/N_C$ determines to a large extent the size of a_f. The size of t_f is determined by the branching ratio with $t_f \approx \mathcal{A}_{\text{exp.}}/\lambda_{cq}$. All other uncertainties are subdominant. These are uncertainties from the branching ratios, CKM parameters and higher-order terms of the OPE and the $\mathcal{O}\left(p_{\text{cm}}/m_b\right)$ term in Eqn. (4.25).

4.3.3 Comparison to experimental measurements

Of the results given in the previous section the most remarkable results are ΔS_f, respectively $\Delta\phi_p$, in $\bar{B}_d \to J/\psi K_S$, $\bar{B}_d \to J/\psi\pi^0$, and $\bar{B}_s \to J/\psi\phi$. We compare them to the

Final State Unit	$\max(\lvert\Delta\phi_s\rvert)$ 1°	$\max(\lvert\Delta S_f\rvert)$ 10^{-2}	$\max(\lvert C_f\rvert)$ 10^{-2}	$\max(\Delta A_{\Delta\Gamma_s}\rvert)$ 10^{-3}
$\bar{B}_s \to (J/\psi\phi)^0$	0.98	1.70	1.61	0.68
$\bar{B}_s \to (J/\psi\phi)^\parallel$	1.12	1.96	2.18	0.93
$\bar{B}_s \to (J/\psi\phi)^\perp$	0.99	1.73	1.64	0.69
$\bar{B}_s \to (J/\psi K^*)^0$	20	35	35	82
$\bar{B}_s \to (J/\psi K^*)^\parallel$	28	47	48	140
$\bar{B}_s \to (J/\psi K^*)^\perp$	18	30	29	59

Table 4.5: *CP*-violating parameters in $\bar{B}_s \to \psi V$ decays. For more explanations, see caption of Tab. 4.2

experimental values, we distinguish: Single-experiment measurements, the world-average of a measurement and the expected SM value. We cite BABAR, Belle, LHCb or CMS for single-experiment determinations, for the global fit of an observable we cite the heavy flavor averaging group (HFAG) [29] and we use the global fit to the CKM matrix which represents the SM expectation of CKM parameters from the CKMfitter group [22].

The measurement of $S_{J/\psi K_S}$ in $\bar{B}_d$ decays represents the best determination of the UT angle β. The most precise determination by a single experiment has been achieved by the LHCb collaboration [81], we compare their determination to a global fit of all $S_{J/\psi K_S}$ measurements by HFAG and a fit of CKMfitter of $\sin(2\beta)$ excluding measurements of $S_{J/\psi K_S}$,

$$\begin{aligned}
&\text{LHCb:} && S_{J/\psi K_S} &&= 0.731 \pm 0.035 \pm 0.020,\\
&\text{HFAG:} && S_{J/\psi K_S} &&= 0.691 \pm 0.017,\\
&\text{CKMfitter (excl. } J/\psi K_S\text{)}: && \sin(2\beta) &&= 0.748 \pm 0.032,\\
&\text{Theory uncertainty:} && \Delta S_{J/\psi K_S} &&= \pm 0.008.
\end{aligned} \tag{4.46}$$

The single-experiment determination of LHCb has still a relatively large uncertainty of $\pm 0.035 \pm 0.020$. With the LHCb upgrade this should should reduce to ± 0.008 [82] and is then of the same size as our theory error. The difference of the HFAG and the CKMfitter results should be in the absence of penguin pollution and of NP only attributable to experimental uncertainties. Currently, these two values only deviate slightly (1–2 σ) from each other.

In $\bar{B}_s \to J/\psi\phi$ there are three possible polarizations of the final state 0, $\perp$, or $\parallel$ which lead to three separate and polarization-dependent measurements of ϕ_s but it is not yet possible to separate these measurements with significance.

$$\begin{array}{lrcl}
\text{LHCb:} & S_{J/\psi\phi} & = & 0.058 \pm 0.049, \\
\text{CMS:} & S_{J/\psi\phi} & = & 0.075 \pm 0.102, \\
\text{HFAG:} & S_{J/\psi\phi} & = & 0.034 \pm 0.033, \\
\text{CKMfitter:} & \sin(2\beta_s) & = & 0.038 \pm 0.001, \\
\text{Theory uncertainty:} & \Delta S_{(J/\psi\phi)^0} & = & \pm 0.017.
\end{array} \tag{4.47}$$

The direct measurements of $\phi_s = -2\beta_s$ by CMS [83] and by LHCb [84] and the global fit of all direct measurements (HFAG) are still compatible with zero and with the SM expectation (CKMfitter).

The *CP*-violating observables in $\bar{B}_d \to J/\psi\pi^0$ decays have been measured by Belle [85] and BABAR [86].

$$\begin{array}{lrcllcl}
\text{Belle:} & S_{J/\psi\pi^0} & = & -0.65 \pm 0.22, & C_{J/\psi\pi^0} & = & -0.08 \pm 0.17, \\
\text{BABAR:} & S_{J/\psi\pi^0} & = & -1.23 \pm 0.21, & C_{J/\psi\pi^0} & = & -0.20 \pm 0.19, \\
\text{CKMfitter (incl. } J/\psi K_S): & \sin(2\beta) & = & 0.701 \pm 0.011, & & & \\
\text{Theory uncertainty:} & \Delta S_{J/\psi\pi^0} & = & \pm 0.16, & |C_{J/\psi\pi^0}| & \leq & 0.27.
\end{array} \tag{4.48}$$

In this mode in particular the value of $S_{J/\psi\pi^0}$ is interesting. Our results for $B_d \to J/\psi\pi^0$ favor the Belle measurement over the BABAR result. The BABAR result is outside the physical range – which is $|S_{J/\psi\pi^0}| \leq 1$ – but implies that $S_{J/\psi\pi^0}$ should be minimal. The measurements of C_f in $B_s \to J/\psi K^*$ decays [87] agrees with our prediction Tab. 4.5. Furthermore, the measurements of S_f and C_f for the $B_d \to J/\psi\rho^0$ polarization amplitudes [88] comply with the ranges in Tab. 4.4.

The current measurements of *CP*-violating observables in Cabibbo-favored decays (governed by $b \to \bar{c}cs$ and involving ϵ_s) have larger uncertainties than our predicted theory error. We observe no tension between theory prediction (CKMfitter + our uncertainties in Tabs. 4.2– 4.5).

In Cabibbo-suppressed decays (governed by $b \to \bar{c}cd$ and involving ϵ_d) our uncertainties are in the same range as the experimental uncertainty. There is a long-standing discrepancy between BABAR and Belle in the measurement of $S_{J/\psi\pi^0}$, our result is compatible with Belle. We observe no other discrepancy between experiment and theory.

4.3.4 Comparison to the literature

The BSS idea [11] has already been applied to predict the size of the penguin pollution in $\bar{B}_d \to J/\psi K_S$ [89]. However, the estimate of this paper misses the dominant contribution

Reference	$\Delta S_{J/\psi K_S}$	$\Delta\phi_d$	Method
This thesis	$\lvert\Delta S\rvert \leq 0.008$	$\lvert\Delta\phi_d\rvert \leq 0.7°$	OPE
[34]	-0.01 ± 0.01	$-1.1° \pm 0.7°$	SU(3) flavor
[33]	$\lvert\Delta S\rvert \lesssim 0.01$	$\lvert\Delta\phi_d\rvert \lesssim 0.8°$	SU(3) flavor
[32]	0.00 ± 0.02	$0.0° \pm 1.6°$	U-spin
[31]	$[-0.05, -0.01]$	$[-3.9, -0.8]°$	U-spin
[89]	$-(2 \pm 2) \cdot 10^{-4}$	$0.0° \pm 0.0°$	BSS

Table 4.6: Evaluation of the penguin pollution in $\bar{B}_d \to J/\psi K_S$ in the literature. The values quoted in gray have been determined from the values in the literature in black. The BSS determination missed the dominant contribution from the top penguins.

from the top penguins. Additionally, they make the assumption that (we use our notation) $v_8 = |v_8 - a_8|$. This means they assume a lower value for the matrix element than we and in addition they assume that the phase is small because of the light-cone sum rules (LCSR) calculation in reference [90]. However, the LCSR calculation misses the prediction of the branching ratio $\mathcal{B}(\bar{B}_d \to J/\psi K_S)$ by a factor of two. Therefore, this does not seem to be a reliable estimate.

The only reliable estimate is $v_8 \sim \mathcal{O}(1/N_C)$, consequently, it is a matter of taste which value of v_8 one uses in the BSS approach. Our aim was to find a bound on the penguin pollution, therefore, we used the conservative bound $|v_8| \leq 1/N_C$. With less conservative assumptions it is possible to obtain stronger bounds at the risk of overestimating the theoretical predictability. This is done in reference [89], yet, the omission of the top penguins is certainly incorrect and leads to the very small value given in Tab. 4.6.

The estimates of $\Delta\phi_d$ in reference [31, 34] and of $\Delta S_{J/\psi K_S}$ in reference [32, 33] rely on flavor symmetries, either $SU(3)_F$ or U-spin (a $SU(2)$ subgroup of $SU(3)_F$ that rotates down quarks into strange quarks). Even though we think that the use of flavor symmetries in principle is a viable approach, we would like to state some caveats. Experimentally, the U-spin estimates rely on the measurement of S_f in control modes, these are primarily $\bar{B}_d \to J/\psi\pi^0$ and $\bar{B}_s \to J/\psi K_S$. However, the branching ratios of these control modes are Cabibbo suppressed because the leading contribution is $\propto \lambda_{cd}$ instead of $\propto \lambda_{cs}$, this leads to the suppression $|\lambda_{cd}/\lambda_{cs}|^2 = 0.05$. Consequently, the control channels have lower statistics. Furthermore and more importantly, flavor symmetries are not exact and the breaking of the flavor symmetry between a signal and control channel can neither experimentally nor theoretically be determined. The usual expectation is that these effects are $\mathcal{O}(m_s/\Lambda_{\text{QCD}}) = 30\%$ but it is not possible to show that this is the case for the penguin pollution.

References [31, 34] model the breaking of the flavor symmetry with naive factorization

but this cannot be correct because the decays have large nonfactorizable contributions. Furthermore, the use of naive factorization leads to a pseudo-sensitivity which relates the branching ratio and the coefficient C_f to the penguin pollution. This yields an additional bound on the penguin pollution. However, this bound is spurious and, in fact, absent if flavor symmetry breaking is correctly parametrized.

In reference [33] a fit based on (generically broken) $SU(3)_F$ flavor symmetry is performed. We think that this is the correct way to describe the decays with flavor symmetries. However, also in this case there is no possibility to extract the $SU(3)_F$ breaking parameters that contribute to the penguin pollution. By means of the flavor symmetry it is possible to extract the size of the penguin pollution. However, the error on this determination cannot be rigorously determined but must be implemented by assuming a reasonable value of maximal $SU(3)_F$ breaking. The maximal value of $|\Delta S_{J/\psi K_S}|$ obtained by reference [33] given in Tab. 4.6 is centered around zero. This is a consequence of including generic $SU(3)_F$ breaking. In contrast references [31, 34] obtain a central value of $\Delta\phi_d$ that is shifted from zero. This is due to the use of naive factorization to estimate flavor-symmetry breaking and the resulting additional spurious constraint on the penguin pollution.

We conclude that flavor symmetries are another viable method to estimate the penguin pollution. This method requires the correct implementation of flavor symmetry breaking which leads to a residual theoretical uncertainty.

4.4 Results for $\bar{B} \to D\bar{D}$ decays

This section is dedicated to the phenomenology in $\bar{B} \to D\bar{D}$ decays. There are ten decay channels with $\bar{B} \in \{B^-, \bar{B}_d, \bar{B}_s\}$, $D \in \{D^+, D^0, D_s^+\}$, and $\bar{D} \in \{D^-, \bar{D}^0, D_s^-\}$. The most important representative of these decays is the decay $\bar{B}_s \to D_s^+ D_s^-$ because it allows similarly to $\bar{B}_s \to J/\psi\phi$ the extraction of the $\bar{B}_s - B_s$ mixing phase ϕ_s. This is in particular interesting because the final state $D_s^+ D_s^-$ does not require an angular analysis. Furthermore, the influence of the penguin pollution is different in $\bar{B}_s \to J/\psi\phi$ and $\bar{B}_s \to D_s^+ D_s^-$, which allows a completely independent determination of ϕ_s.

In section 3.8 we discussed that the OPE can also be applied to the penguin pollution in $\bar{B} \to D\bar{D}$ decays. In $\bar{B} \to D\bar{D}$ decays the charm quarks end up in different mesons, as a consequence, we will discuss exchange and penguin annihilation diagrams in detail. Moreover, this results into a more elaborate discussion of subleading $1/N_C$ terms than in $\bar{B} \to \psi X$ decays.

First, we discuss the generic structure of the decay amplitude in $\bar{B} \to D\bar{D}$ decays. Subsequently, we establish the $1/N_C$ counting of the individual contributions and test the expected $1/N_C$ behavior. Finally, we derive the CP-violation observables and compare them to the available measurements. At last we compare our results to discussions in the literature.

4.4.1 The $\bar{B} \to D\bar{D}$ decay amplitude

We explained in section 3.8 that the OPE is also applicable to the penguin pollution in $\bar{B} \to D\bar{D}$ decays. From the OPE it follows that at LO in $\frac{\Lambda_{\rm QCD}}{M}$, $M \sim m_B$ all processes are mediated by the operator basis in Eqns. (2.1) and (2.2). In the preceding section we have seen that in fact the basis in Eqn. (2.1) is sufficient if certain terms $\mathcal{O}\left(\frac{p_{\rm cm}}{M}\right)$ are neglected using Eqn. (2.11). In $\bar{B} \to D\bar{D}$ decays this situation is even simpler, since

$$\langle Q_{8T} \rangle = \langle Q_{8V} \rangle \left[1 + \mathcal{O}\left(\frac{\Lambda_{\rm QCD}}{m_b} \right) \right]. \tag{4.49}$$

The terms $\mathcal{O}\left(\frac{\Lambda_{\rm QCD}}{M}\right)$ derive from the momentum p' of the light quark q which is soft in $\bar{B} \to D\bar{D}$ decays. Thus, the basis in Eqn. (2.1) is sufficient to describe all $\bar{B} \to D\bar{D}$ decays and we may write the decay amplitude in $\bar{B} \to D\bar{D}$ decays as

$$\mathcal{A}(\bar{B} \to f) = \lambda_{cq} t_f + \lambda_{uq} p_f, \tag{4.50}$$

with

$$\begin{aligned} t_f &= -\mathrm{i}\frac{G_F}{\sqrt{2}} [\ (a_1 + a_3 + a_5) \langle Q_{0V} \rangle + (2C_2 + C_{8V}) \langle Q_{8V} \rangle \\ &\quad -(a_1 + a_3 - a_5) \langle Q_{0A} \rangle - (2C_2 + 2C_4 - 2C_6) \langle Q_{8A} \rangle], \qquad (4.51) \\ p_f &= -\mathrm{i}\frac{G_F}{\sqrt{2}} \Big[\ (a_3 + a_5) \langle Q_{0V} \rangle + (2C_2 \widetilde{C}_{2,8V} + C_{8V}) \langle Q_{8V} \rangle \\ &\quad -(a_3 - a_5) \langle Q_{0A} \rangle - (2C_4 - 2C_6) \langle Q_{8A} \rangle]. \qquad (4.52) \end{aligned}$$

There are two possibilities how the operators can be Wick-contracted in $\bar{B} \to D\bar{D}$ matrix elements. We give the two corresponding diagrams in Fig. 4.1. If the q quark from the $b \to c\bar{c}q$ transition hadronizes into the $\bar{D}$ this is the tree insertion which we denote by an index T. If the spectator quark p in the $\bar{B}_p$ meson is equal to q, $p = q$, exchange diagrams are possible denoted by an index E. We split t_f and p_f up into the contributions

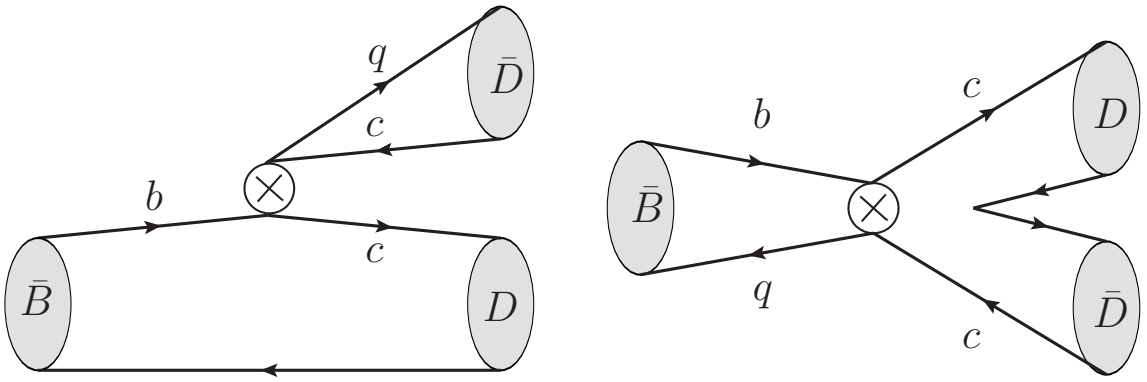

(a) T insertion. (b) E insertion.

Figure 4.1: In the effective theory, there are only two possible insertions of the operators in $\bar{B} \to D\bar{D}$ matrix elements. If q hadronizes in $\bar{D}$ this is the tree-level (T) insertion. If the spectator quark is annihilated at the effective vertex this is the exchange (E) insertion.

that derive from T and E insertions

$$t_f = t_f^{\mathrm{T}} + t_f^{\mathrm{E}}, \qquad p_f = p_f^{\mathrm{T}} + p_f^{\mathrm{E}} \tag{4.53}$$

and refer to t_f^{T}, t_f^{E}, p_f^{T}, and p_f^{E} as *effective parameters* [44]. They are given by

$$\begin{aligned}
t_f^{\mathrm{T}} &\equiv \frac{G_F}{\sqrt{2}}\big[\ (a_1+a_3+a_5)\langle Q_{0V}\rangle_{\mathrm{T}} + (2C_2+C_{8V})\langle Q_{8V}\rangle_{\mathrm{T}} \\
&\qquad -(a_1+a_3-a_5)\langle Q_{0A}\rangle_{\mathrm{T}} - (2C_2+2C_4-2C_6)\langle Q_{8A}\rangle_{\mathrm{T}}\big]\,, && (4.54)\\
p_f^{\mathrm{T}} &\equiv \frac{G_F}{\sqrt{2}}\Big[\ (a_3+a_5)\langle Q_{0V}\rangle_{\mathrm{T}} + (2C_2\widetilde{C}_{2,8V}+C_{8V})\langle Q_{8V}\rangle_{\mathrm{T}} \\
&\qquad -(a_3-a_5)\langle Q_{0A}\rangle_{\mathrm{T}} - (2C_4-2C_6)\langle Q_{8A}\rangle_{\mathrm{T}}\big]\,, && (4.55)\\
t_f^{\mathrm{E}} &\equiv \frac{G_F}{\sqrt{2}}\big[\ (a_1+a_3+a_5)\langle Q_{0V}\rangle_{\mathrm{E}} + (2C_2+C_{8V})\langle Q_{8V}\rangle_{\mathrm{E}} \\
&\qquad -(a_1+a_3-a_5)\langle Q_{0A}\rangle_{\mathrm{E}} - (2C_2+2C_4-2C_6)\langle Q_{8A}\rangle_{\mathrm{E}}\big]\,, && (4.56)\\
p_f^{\mathrm{E}} &\equiv \frac{G_F}{\sqrt{2}}\Big[\ (a_3+a_5)\langle Q_{0V}\rangle_{\mathrm{E}} + (2C_2\widetilde{C}_{2,8V}+C_{8V})\langle Q_{8V}\rangle_{\mathrm{E}} \\
&\qquad -(a_3-a_5)\langle Q_{0A}\rangle_{\mathrm{E}} - (2C_4-2C_6)\langle Q_{8A}\rangle_{\mathrm{E}}\big]\,, && (4.57)
\end{aligned}$$

The expressions of t_f^{T} and t_f^{E} (p_f^{T} and p_f^{E}) are identical except for the index of the matrix elements denoted by T and E. Whether an effective parameter is nonzero in a specific decay depends on whether the T or E Wick contraction contributes to the specific decay. We list this for all $\bar{B} \to D\bar{D}$ decays in Tab. 4.7.

We did not consider this decomposition before because all $\bar{B} \to \psi X$ decays have

Mode	q	$t_f^{\rm T}$	$t_f^{\rm E}$	$p_f^{\rm T}$	$p_f^{\rm E}$	Class
$B^- \to D^0 \bar{D}^-$	d	$\times$		$\times$		A
$B^- \to D^0 D_s^-$	s	$\times$		$\times$		A
$\bar{B}^0 \to D_+ D_s^-$	s	$\times$		$\times$		A
$\bar{B}_s \to D_s^+ D^-$	d	$\times$		$\times$		A
$\bar{B}^0 \to D^0 \bar{D}^0$	d		$\times$		$\times$	B
$\bar{B}^0 \to D_s^+ D_s^-$	d		$\times$		$\times$	B
$\bar{B}_s \to D^+ D^-$	s		$\times$		$\times$	B
$\bar{B}_s \to D^0 \bar{D}^0$	s		$\times$		$\times$	B
$\bar{B}^0 \to D^+ D^-$	d	$\times$	$\times$	$\times$	$\times$	C
$\bar{B}_s \to D_s^+ D_s^-$	s	$\times$	$\times$	$\times$	$\times$	C

Table 4.7: The parametrization of the $\bar{B} \to D\bar{D}$ decay amplitudes in terms of the effective parameters $t_f^{\rm T}$, $t_f^{\rm E}$, $p_f^{\rm T}$, and $p_f^{\rm E}$. An $\times$ indicates that a effective parameter contributes to a decay, $q \in \{d, s\}$ specifies q in λ_{cq} and λ_{uq}. The classes are defined after Eqn. (4.57).

leading contributions from $t_f^{\rm T}$ and $p_f^{\rm T}$. Only those decays in which X has a flavor singlet component also receive contributions from $t_f^{\rm E}$ and $p_f^{\rm E}$ but this can be neglected in the determination of *CP*-violating observables. In contrast, inspecting Tab. 4.7 we observe that the $\bar{B} \to D\bar{D}$ decays can be grouped into three classes. We call these classes A, B and C. The decays of class A only obtain contributions from effective parameters with T insertions, the decays of class B only obtain contributions from E insertions and the decays of class C obtain contributions from T and E insertions. Hence, in $\bar{B} \to D\bar{D}$ decays some modes are dominated by E insertions and the E insertions are decisive for the determination of the *CP*-violating observables.

A further advantage of the decomposition into T and E insertions becomes clear when we consider the effective parameters in $1/N_C$ counting. To allow a transparent discussion of N_C effects of T insertions, it is preferable to switch to another operator basis in which the color-singlet operators create the final $\bar{D}$ mesons as color singlets. This basis is

$$\begin{aligned} Q_0 &= (\bar{c}b)_{(V-A)}(\bar{q}c)_{(V-A)}, \\ Q_8 &= (\bar{c}T^a b)_{(V-A)}(\bar{q}T^a c)_{(V-A)}, \\ Q_{S0} &= -2(\bar{c}b)_{(S-P)}(\bar{q}c)_{(S+P)}, \\ Q_{S8} &= -2(\bar{c}T^a b)_{(S-P)}(\bar{q}T^a c)_{(S+P)}. \end{aligned} \tag{4.58}$$

It is equivalent to the basis in Eqn. (2.1) after Fierz transformation and use of the color

algebra. For example, one rewrites Q_{8V} as

$$Q_{8V} = \frac{1}{2N_C}\left(C_F Q_0 - Q_8 + C_F Q_{S0} - Q_{S8}\right), \tag{4.59}$$

where $N_C = 3$ is the number of colors and $C_F = \frac{N_C^2-1}{2N_C}$. With this basis we rewrite t_f^{T} and p_f^{T} as

$$\begin{aligned} t_f^{\mathrm{T}} &= -\mathrm{i}\tfrac{G_F}{\sqrt{2}}\left[(a_2+a_4)\langle Q_0\rangle_{\mathrm{T}} + (2C_1+2C_3)\langle Q_8\rangle_{\mathrm{T}} + a_6\langle Q_{S0}\rangle_{\mathrm{T}} + 2C_5\langle Q_{S8}\rangle_{\mathrm{T}}\right], \\ p_f^{\mathrm{T}} &= -\mathrm{i}\tfrac{G_F}{\sqrt{2}}\left[(a_4 + C_F/(2N_C)C_{8\tilde{V}})\langle Q_0\rangle_{\mathrm{T}} + (2C_3 - C_{8\tilde{V}}/(2N_C))\langle Q_8\rangle_{\mathrm{T}}\right. \\ &\quad \left. + (a_6 + C_F/(2N_C)C_{8\tilde{V}})\langle Q_{S0}\rangle_{\mathrm{T}} + (2C_5 - C_{8\tilde{V}}/(2N_C))\langle Q_{S8}\rangle_{\mathrm{T}}\right]. \end{aligned} \tag{4.60}$$

Here, it is convenient to introduce the Wilson coefficient combinations $a_{2i} \equiv C_{2i} + \frac{1}{N_C}C_{2i-1}$ for $i \in \{1,2,3\}$ and $C_{8\tilde{V}} \equiv 2C_2\widetilde{C}_{2,8V} + 2C_3\widetilde{C}_{3,8V} + 2C_4\widetilde{C}_{4,8V} + 2C_6\widetilde{C}_{6,8V} + C_{8G}\widetilde{C}_{8G,8T}$.

We will now discuss the $1/N_C$ counting of the effective parameters to clarify why the decomposition into effective parameters is reasonable. For this we recall, that the $1/N_C$ ordering of the Wilson coefficients has been given in the $\bar{B} \to \psi X$ phenomenology section. Numerically, we evaluate the Wilson coefficients at the scale $\mu = m_b$ in $\bar{B} \to D\bar{D}$ decays.

We discuss the $1/N_C$ counting of the T matrix elements first. We normalize them to the factorized color singlet matrix element which is given by

$$-\mathrm{i}V_0 \equiv -\mathrm{i}\left\langle \bar{D}D|Q_0|\bar{B}\right\rangle_{\mathrm{T}}\Big|_{\mathrm{fact.}} = f_{\bar{D}}F_0^{\bar{B}D}(m_{\bar{D}}^2)(m_B^2 - m_D^2). \tag{4.61}$$

This leads to the definition of the normalized matrix elements q_0, q_8, s_0, and s_8

$$\left\langle \bar{D}D|Q_0|\bar{B}\right\rangle_{\mathrm{T}} \equiv V_0 q_0 \tag{4.62}$$

$$\left\langle \bar{D}_q D|Q_{S0}|\bar{B}\right\rangle_{\mathrm{T}} \equiv V_0 \chi_{\bar{D}_q} s_0 \tag{4.63}$$

$$\left\langle \bar{D}D|Q_8|\bar{B}\right\rangle_{\mathrm{T}} \equiv V_0 q_8 \tag{4.64}$$

$$\left\langle \bar{D}_q D|Q_{S8}|\bar{B}\right\rangle_{\mathrm{T}} \equiv V_0 \chi_{\bar{D}_q} s_8. \tag{4.65}$$

In Eqn. (4.63) the factor

$$\chi_{\bar{D}_q} \equiv \frac{2m_{\bar{D}_q}^2}{(\overline{m_b} - \overline{m_c})(\overline{m_c} - \overline{m_q})} \tag{4.66}$$

is due to the equations of motions that are used to compute the naively factorized *scalar-penguin* matrix element $\langle Q_{S0}\rangle|_{\mathrm{fact.}} = \chi_{\bar{D}_q}V_0$. In $\chi_{\bar{D}_q}$ the masses $\overline{m}_b, \overline{m}_c, \overline{m}_q$ and $\overline{m}_{q'}$ are the $\overline{MS}$ masses of the b, c, and q quark, respectively. q is the non-charm quark in the $\bar{D}$ meson. We normalize the scalar octet matrix element $\left\langle \bar{D}_q D|Q_{S8}|\bar{B}\right\rangle_{\mathrm{T}}$ to the scalar

singlet, consequently also a factor factor $\chi_{\bar{D}_q}$ enters Eqn. (4.65). The $1/N_C$ counting of the normalized matrix elements is

$$q_0 = 1 + \mathcal{O}\left(\frac{1}{N_C}\right), \quad s_0 = 1 + \mathcal{O}\left(\frac{1}{N_C}\right), \quad q_8 = \mathcal{O}\left(\frac{1}{N_C}\right), \quad s_8 = \mathcal{O}\left(\frac{1}{N_C}\right). \quad (4.67)$$

Altogether, we obtain the $1/N_C$ scaling

$$\frac{t_f^{\mathrm{T}}}{V_0} = \frac{G_F}{\sqrt{2}}\left[(a_2 + a_4)q_0 + a_6\chi_D s_0\right] + \mathcal{O}\left(\frac{1}{N_C^2}\right) \sim \mathcal{O}(1), \quad (4.68)$$

$$\frac{p_f^{\mathrm{T}}}{V_0} = \frac{G_F}{\sqrt{2}}\left[(a_4 + \frac{C_F}{2N_C}C_{8\tilde{V}})q_0 + (a_6 + \frac{C_F}{2N_C}C_{8\tilde{V}})\chi_D s_0\right] + \mathcal{O}\left(\frac{1}{N_C^2}\right) \sim \mathcal{O}\left(\frac{1}{N_C}\right). \quad (4.69)$$

In $\bar{B} \to D\bar{D}$ decays of the first class we can hence compute the decay amplitude in LO in $1/N_C$.

For the discussion of the the E matrix elements we maintain the operator basis in Eqn. (2.1) because in this basis the dominant contributions to t_f^{E} and p_f^{E} are very transparent. The LO term in $1/N_C$ vanishes

$$\langle D\bar{D}|Q_{0V}|\bar{B}_q\rangle_{\mathrm{E}}\big|_{\mathrm{fact}} = \langle D\bar{D}|(\bar{c}c)_V|0\rangle\langle 0|(\bar{q}b)_A|\bar{B}_q\rangle \quad (4.70)$$

$$= if_B F^{D\bar{D}}(m_{\bar{B}}^2)(m_D^2 - m_{\bar{D}}^2) \quad (4.71)$$

$$= 0. \quad (4.72)$$

This is due to current conservation as it has been also noted in references [91, 92]. Hence, there is no factorizable exchange matrix element to which the E matrix elements can be normalized and all E matrix elements are of the same order in $1/N_C$. Thus, the $1/N_C$ counting expectation is

$$\langle Q_{0V}\rangle_{\mathrm{E}} \sim \langle Q_{0A}\rangle_{\mathrm{E}} \sim \langle Q_{8V}\rangle_{\mathrm{E}} \sim \langle Q_{8A}\rangle_{\mathrm{E}}. \quad (4.73)$$

This leads to

$$t_f^{\mathrm{E}} = \frac{G_F}{\sqrt{2}}\left[2C_2(\langle Q_{8V}\rangle_{\mathrm{E}} - \langle Q_{8A}\rangle_{\mathrm{E}})\right]\left(1 + \mathcal{O}\left(\frac{1}{N_C}\right)\right) \quad (4.74)$$

$$p_f^{\mathrm{E}} = \frac{G_F}{\sqrt{2}}\left[(2C_2\widetilde{C}_{2,8V} + C_{8V})\langle Q_{8V}\rangle_{\mathrm{E}}\right]\left(1 + \mathcal{O}\left(\frac{1}{N_C}\right)\right) \quad (4.75)$$

These relations are in fact even better obeyed than up to terms $\mathcal{O}(1/N_C)$ but rather up to $\mathcal{O}(10\%)$ since the Wilson coefficients of the neglected terms are smaller than the N_C

counting implies because of perturbative effects. For example, in $t_f^{\rm E}$ the neglected terms $\mathcal{O}\left(a_1/(2C_2)\right)$ are formally $\mathcal{O}\left(1/N_C\right)$ but in fact smaller. We conclude that there are only two E matrix elements that contribute significantly to the decay amplitudes. The effective parameter $t_f^{\rm E}$ receives the main contribution from $\langle Q_{8V}\rangle_{\rm E} - \langle Q_{8A}\rangle_{\rm E}$ which has the normal $V-A$ structure of the weak interaction. The subleading term $p_f^{\rm E}$ receives its dominant contribution from $\langle Q_{8V}\rangle_{\rm E}$.

This ends the discussion about the structure of $\bar{B} \to D\bar{D}$ decay amplitudes, thanks to the OPE we found that all $\bar{B} \to D\bar{D}$ transitions are mediated by the operators given in Eqn. (2.1) or alternatively in Eqn. (4.58). Exchange processes are important $\bar{B} \to D\bar{D}$ decays this is why we separated the matrix elements in T and E insertions. We then proceeded with evaluating the T and E matrix elements in $1/N_C$ counting. We find a surprisingly simple situation. Namely, that $t_f^{\rm T}$ and $p_f^{\rm T}$ are dominated by q_0 and s_0 and that $t_f^{\rm E}$ and $p_f^{\rm E}$ are dominated by $\langle Q_{8V}\rangle$ and $\langle Q_{8A}\rangle$. This may seem idle since we only reexpressed the four unknown effective parameters $t_f^{\rm T}$, $p_f^{\rm T}$, $t_f^{\rm E}$ and $p_f^{\rm E}$ by four a priori unknown normalized matrix elements. However, the advantage is that we can order the normalized matrix elements in size by $1/N_C$ counting and can test this $1/N_C$ counting with the branching ratios. If the branching ratios follow the $1/N_C$ counting we can confidently apply it to determine the *CP*-violating observables.

Test of N_C counting Let us test the $1/N_C$ counting in $\bar{B} \to D\bar{D}$ decays. The LO amplitude in $1/N_C$ is

$$\mathcal{A}_{\rm LO}(\bar{B} \to D\bar{D}\ ) = \frac{G_F}{\sqrt{2}}\lambda_{cq} a_2 V_0 q_0, \tag{4.76}$$

with $q_0 = 1$ for all decays that get contributions from $t_f^{\rm T}$. The terms $t_f^{\rm E}$ and p_f are subleading in $1/N_C$. We show $|\mathcal{A}_{\rm LO}(\bar{B} \to D\bar{D}\ )/\mathcal{A}_{\rm exp}(\bar{B} \to D\bar{D}\ )|$ in Fig. 4.2. We observe that $\mathcal{A}_{\rm LO}$ generally overestimates the experimental branching ratio. However, except in the decay modes $\bar{B}_d \to D^+D^-$ and $\bar{B}_s \to D_s^+D_s^-$ the experimental amplitude lies within the range expected from $1/N_C$ counting.

It is also possible to include some subleading terms in $1/N_C$. The inclusion of the terms $\propto s_0$ with $s_0 = 1$ is trivial. In addition, we may extract the size of $t_f^{\rm E} = 2C_2\langle Q_{8V}\rangle_{\rm E} - \langle Q_{8A}\rangle_{\rm E}$ from the class B decays. We use

$$\langle Q_{8V}\rangle_{\rm E} - \langle Q_{8A}\rangle_{\rm E} = -(2.3 \pm 0.2) \times 10^{-6}\ \text{GeV}. \tag{4.77}$$

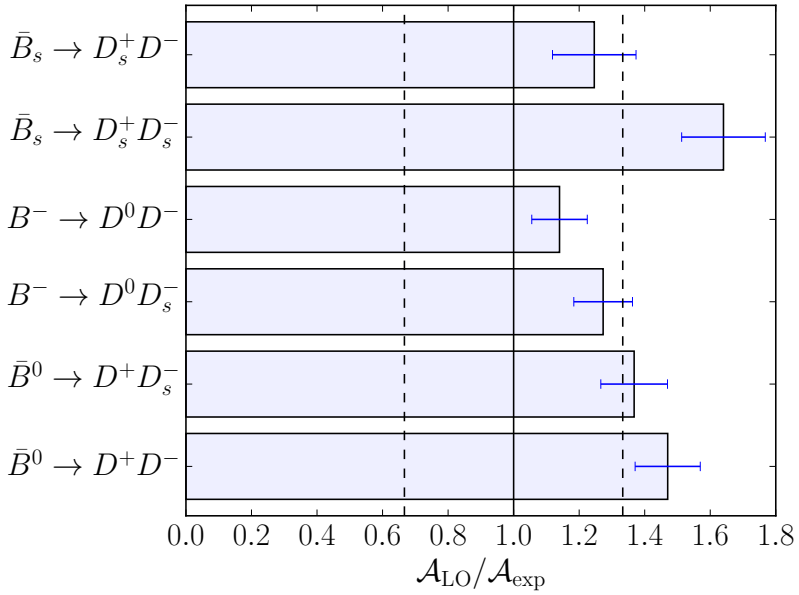

Figure 4.2: Check of the $1/N_C$ counting. The leading order term of the decay amplitude in $1/N_C$ is given by $\mathcal{A}_{\rm LO} = \frac{G_F}{\sqrt{2}}|\lambda_c|a_2 V_0$. The LO term overestimates the experimental amplitude in general. Uncertainties due to the input parameters (branching ratios, decay constants and form factors) are indicated by the error bars. The range that is expected from $1/N_C$ counting is limited by the dashed lines.

The relative phase $\arg(t_f^{\rm E}/t_f^{\rm T}) = \pi$ is deduced from the fact that the isospin sum rule[4]

$$\mathcal{A}_{\rm exp}(\bar{B}_d \to D^+ D^-) = \mathcal{A}_{\rm exp}(\bar{B}^- \to D^0 D^-) + \mathcal{A}_{\rm exp}(\bar{B}_d \to D^0 \bar{D}^0) \tag{4.78}$$

can only be satisfied if $\arg(t_f^{\rm E}/t_f^{\rm T}) \approx \pi$. We then use

$$t_f^{\rm T} = \frac{G_F}{\sqrt{2}}\lambda_{cq} V_0 \left[(a_2 + a_4)q_0 + a_6 \chi_D s_0\right], \qquad t_f^{\rm E} = \frac{G_F}{\sqrt{2}} 2C_2 \left[\langle Q_{8V}\rangle_{\rm E} - \langle Q_{8A}\rangle_{\rm E}\right] \tag{4.79}$$

to determine the ratios $|\mathcal{A}_{\rm NLO}/\mathcal{A}_{exp}|$ which are displayed in Fig. 4.3. The inclusion of the first order subleading $1/N_C$ terms leads to a better agreement between experiment and $1/N_C$ counting. There is one unknown subleading $1/N_C$ correction. These are the terms $\mathcal{O}\left(\frac{1}{N_C}\right)$ in $q_0 = 1 + \mathcal{O}\left(\frac{1}{N_C}\right)$. Our interpretation of the situation is that $1/N_C$ counting is effective but that all terms of the subleading $1/N_C$ contributions interfere negatively with the LO contribution in $1/N_C$. Furthermore, since also in Fig. 4.3 the experimental

[4]This sum rule is valid since we neglect the processes where up quarks are produced at the effective vertex as discussed in sections 3.6 and 3.8.

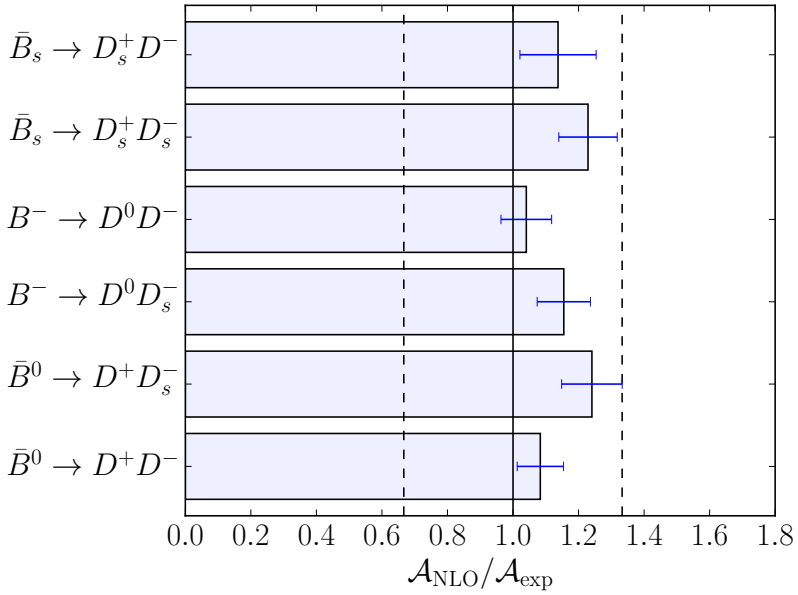

Figure 4.3: Check of the $1/N_C$ counting including subleading terms in $1/N_C$. All theoretical values overestimate the experimental values but all ratios are within the expected range.

amplitudes are still overestimated by the $1/N_C$ counting this means that the term $\mathcal{O}\left(\frac{1}{N_C}\right)$ in $q_0 = 1 + \mathcal{O}\left(\frac{1}{N_C}\right)$ most likely has a negative sign.

4.4.2 *CP*-violating parameters in $\bar{B} \to D\bar{D}$ decays

The test of the $1/N_C$ counting makes us confident that we can apply it to estimate the matrix elements. With these estimates we derive the *CP*-violating observables in the classes A, B, and C.

In the decays of class A only the effective parameters t_f^{T} and p_f^{T} contribute. Thus, the numerical evaluation can be done as in the $\bar{B} \to \psi X$ section. We write $a_f = \frac{p_f^{\mathrm{T}}}{t_f^{\mathrm{T}}}$ and require that

$$\mathcal{A}(\bar{B} \to f) = \lambda_{cq} t_f^{\mathrm{T}} + \lambda_{uq} p_f^{\mathrm{T}} \stackrel{!}{=} \mathcal{A}_{\mathrm{exp}}. \tag{4.80}$$

within the experimentally allowed 1σ range of $\mathcal{A}_{\mathrm{exp}}$. We allow that the normalized hadronic matrix elements vary in the ranges implied by $1/N_C$ counting in Eqn. (4.67)

$$0 \leq ||q_0| - 1| \leq \frac{1}{N_C}, \quad ||s_0| - 1| \leq \frac{1}{N_C}, \quad 0 \leq |q_8| \leq \frac{1}{N_C}, \quad 0 \leq |s_8| \leq \frac{1}{N_C}, \tag{4.81}$$

	$B^- \to D^0 D^-$	$B^- \to D^0 D_s^-$	$\overline{B}_d \to D^+ D_s^-$	$\bar{B}_s \to D_s^+ D^-$
$\max(C_f) \times 10^2$	4.5	0.75	0.80	5.0
$\min(C_f) \times 10^2$	-11	-0.30	-0.35	-12

Table 4.8: Results for the extremal values of the direct *CP*-violating observable C_f in class A decays.

with $N_C = 3$. We obtain the results for C_f in Tab. 4.8.

In the decays of class B, we obtain

$$a_f = \frac{p_f^{\mathrm{E}}}{t_f^{\mathrm{E}}} = \frac{(2C_2\widetilde{C}_{2,8V} + C_{8V})\,\langle Q_{8V}\rangle_{\mathrm{E}}}{(2C_2 + 2C_{8V})(\langle Q_{8V}\rangle_{\mathrm{E}} - \langle Q_{8A}\rangle_{\mathrm{E}})}. \tag{4.82}$$

The size of the penguin pollution is dominated by the ratio

$$x \equiv \frac{\langle Q_{8V}\rangle_{\mathrm{E}}}{\langle Q_{8V}\rangle_{\mathrm{E}} - \langle Q_{8A}\rangle_{\mathrm{E}}}. \tag{4.83}$$

Even though the value of $|\,\langle Q_{8V}\rangle_{\mathrm{E}} - \langle Q_{8A}\rangle_{\mathrm{E}}\,|$ can be obtained from the branching ratios, we do not need it to determine the penguin pollution because the penguin pollution is only dependent on x. Yet, there is no experimental information on x. We exclude that the matrix elements are fine-tuned and therefore impose $|x| \leq 2$. Thus, we derive the maximal size of the *CP*-violating observables in class B decays with $|x| \leq 2$. They are given in the first two columns of Tab. 4.9.

The results for the class C decays $\bar{B}_d \to D^+ D^-$ and $\bar{B}_s \to D_s^+ D_s^-$ are given in the third and fourth column of Tab. 4.9. They are derived by combining the methods for class A and class B decays. However, it is necessary to use $\langle Q_{8V}\rangle_{\mathrm{E}} - \langle Q_{8A}\rangle_{\mathrm{E}}$ determined in Eqn. (4.77).

To interpret the results in Tabs. 4.8 and 4.9 the following remarks should be taken into account:

- We derive the values by extremizing the observables as functions of the normalized matrix elements which are only allowed to float in the ranges given by Eqn. (4.81) and for class B and C decays by $|x| \leq 2$. The bounds in Tabs. 4.8 and 4.9 arise if $||q_0| - 1| = ||s_0| - 1| = |q_8| = |s_8| = 1/3$ and $|x| = 2$, the phases of the normalized matrix elements then arrange such that the constraint from the branching ratio in Eqn. (4.80) is satisfied and the observable under consideration becomes maximal.

- Therefore, the dominant uncertainty is induced by the $1/N_C$ counting, the second largest source of uncertainty are the branching ratios which still have relatively large

Decay mode	$\bar{B}_d \to D_s^+ D_s^-$ $\bar{B}_d \to D^0 \bar{D}^0$	$\bar{B}_s \to D^0 \bar{D}^0$ $\overline{B}_s \to D^+ D^-$	$\bar{B}_d \to D^+ D^-$	$\bar{B}_s \to D_s^+ D_s^-$
$\max(C_f) \times 10^2$	$12.5 \cdot \lvert\frac{x}{2}\rvert$	$0.65 \cdot \lvert\frac{x}{2}\rvert$	-16	1.0
$\min(C_f) \times 10^2$	$-12.5 \cdot \lvert\frac{x}{2}\rvert$	$-0.65 \cdot \lvert\frac{x}{2}\rvert$	8.0	-0.65
$\max(\Delta S_f) \times 10^2$	$9.5 \cdot \lvert\frac{x}{2}\rvert$	$0.65 \cdot \lvert\frac{x}{2}\rvert$	-1.0	1.20
$\min(\Delta S_f) \times 10^2$	$-8.0 \cdot \lvert\frac{x}{2}\rvert$	$-0.65 \cdot \lvert\frac{x}{2}\rvert$	-13.0	0.0
$\max(\Delta\phi_p)$ in $^\circ$	$7.0 \cdot \lvert\frac{x}{2}\rvert$	$0.40 \cdot \lvert\frac{x}{2}\rvert$	11	-0.05
$\min(\Delta\phi_p)$ in $^\circ$	$-7.5 \cdot \lvert\frac{x}{2}\rvert$	$-0.40 \cdot \lvert\frac{x}{2}\rvert$	0.1	-0.80
$\max(\Delta A_{\Delta\Gamma}) \times 10^3$		$0.25 \cdot \lvert\frac{x}{2}\rvert$		0.0
$\min(\Delta A_{\Delta\Gamma}) \times 10^3$		$-0.25 \cdot \lvert\frac{x}{2}\rvert$		-0.40

Table 4.9: CP violation observables in decays of class B and C. In the decays of class B in the first two columns the result heavily depends on the assumption that $|\langle Q_{8V}\rangle_{\rm E} / (\langle Q_{8V}\rangle_{\rm E} - \langle Q_{8A}\rangle_{\rm E})| = |x| \leq 2$.

errors. Other uncertainties, due to higher order terms in the OPE or the CKM input are neglected.

- Similarly, the ad hoc choice of $|x| \leq 2$ represents a large uncertainty in class B decays. For a different choice of x one may rescale the *CP* asymmetries in Tab. 4.9 as it is indicated by the factor $\cdot|\frac{x}{2}|$. The results in class C decays are less susceptible to the maximal value of $|x|$ because $p_f^{\rm E}$ is subleading w.r.t. $p_f^{\rm T}$.

- The slight differences in isospin related decays $B^- \to D^0 D^-$ and $\bar{B}_d \to D^+ D_s^-$ are due to the different input parameters (masses, branching ratios)

4.4.3 Comparison to experimental measurements

The *CP*-violating observables that have been measured up to date are given in Tab. 4.10, all measurements are in agreement with our predictions except for the Belle measurement of $S(\bar{B} \to D^+ D^-)$ and $C(\bar{B} \to D^+ D^-)$ [93], which disagrees with the BABAR measurement [94] and is 0.5σ out of the physical range given by $S_f^2 + C_f^2 \leq 1$.

4.4.4 Comparison to the literature

There are only few discussions about the size of *CP* violation in $\bar{B} \to D\bar{D}$ decays, these are [67, 96–98]. References [67, 98] discuss $\bar{B} \to D\bar{D}$ decays using the approximate flavor $SU(3)_F$ symmetry. In this case the same comments as in section 4.3.4 apply. Namely, that the use of naive factorization to parametrize $SU(3)_F$ breaking [67] is questionable and

Mode	S_f	C_f	$A_{\Delta\Gamma}$	Reference
$\bar{B}_s \to D_s^+ D_s^-$	-0.02 ± 0.17	0.09 ± 0.20	-0.995 ± 0.019	LHCb [95]
$\bar{B}_d \to D^+ D^-$	-0.62 ± 0.21	0.08 ± 0.17		BABAR [94]
$\bar{B}_d \to D^+ D^-$	-1.06 ± 0.22	-0.43 ± 0.17		Belle [93]
$\bar{B}_d \to D_s^+ D^-$		0.01 ± 0.03		Belle [93]
$B^- \to D^0 D^-$		-0.03 ± 0.07		PDG [28]

Table 4.10: Experimentally measured *CP*-violating observables in different $\bar{B} \to D\bar{D}$ modes. The measurements are in good agreement with our predictions except for the Belle measurement of $C(\bar{B}_d \to D^+D^-)$ and $S(\bar{B}_d \to D^+D^-)$ in the third line. Yet, this one is also in tension with the BABAR measurement in the second line and 0.5 standard deviations out of the physical range. Statistical and systematic errors are added in quadrature. In general the errors are statistically dominated.

that the implementation of flavor $SU(3)_F$ with generic $SU(3)_F$ breaking [98] is a viable method but has residual theoretical uncertainties because of unknown $SU(3)_F$ breaking.

The authors in references [96, 97] deal with *CP* violation in $\bar{B}_d \to D^+D^-$ and $\bar{B}_s \to D_s^+ D_s^-$. They use the BSS mechanism and naive factorization to compute the penguin-to-tree ratio a_f. Since their and our approach may seem somewhat similar, let us stress the differences here.

The first important point is that without invoking the OPE a calculation of the up-quark penguin is moot. Moreover, in [96, 97] the charm-quark penguin is calculated perturbatively. This is not correct since the OPE necessarily fails for the charm-quark penguin and thus the charm-quark penguin is not computable perturbatively. A further difference is that we consider the matrix elements in $1/N_C$ counting. While this comprises also naive factorization it is better motivated within QCD and includes 'nonfactorizable' contributions. The use of naive factorization in $\bar{B} \to D\bar{D}$ decays sets 'nonfactorizable' contributions to zero which seems incorrect in view of the tests of the $1/N_C$ counting in Figs. 4.2 and 4.3.

Chapter 5

Conclusion

In this thesis we achieved first-principles predictions of CP-violating observables in $\bar{B} \to \psi X$ and $\bar{B} \to D\bar{D}$ decays. Since these decays are governed by the quark-level process $b \to c\bar{c}q$ with $q \in \{d, s\}$, there exist no first-principles predictions from QCD factorization or other QCD based methods. Among the investigated decays are the modes $\bar{B}_d \to J/\psi K_S$, $\bar{B}_s \to J/\psi\phi$ and $\bar{B}_s \to D_s^+ D_s^-$ which are the best channels for the direct measurement of the UT parameters β and β_s. The extraction of these parameters is subject to theoretical uncertainties due to higher-order corrections in the decay amplitude, the so-called penguin pollution. We derived first-principles expressions for the penguin pollution with an operator-product expansion (OPE) and evaluated the matrix elements with $1/N_C$ counting.

The OPE exploits that there is a large momentum transfer $q^2 \sim m_\psi^2, m_b^2$ from the decaying b quark to the $\bar{c}c$ pair. This momentum transfer allows the expansion of the nonlocal and nonperturbative matrix elements in $\Lambda_{\rm QCD}/M$ with $M = \sqrt{q^2}$. The hard effects can be described by a perturbative Wilson coefficient, the soft effects are either described by matrix elements of local four-quark operators or suppressed by $\Lambda_{\rm QCD}/M$. In $\bar{B} \to \psi X$ decays, hard-collinear spectator interactions have a weaker suppression of $p_{\rm cm}/M$ but are not expected to invalidate our results ($p_{\rm cm}$ is the center-of-mass momentum of the X meson in the $\bar{B}$ meson rest frame).

For the proof of the OPE we showed the factorization of soft and hard scales, the suppression of spectator interactions, and the suppression of further soft effects. We also explained how the OPE is applicable to $\bar{B} \to D\bar{D}$ decays.

We evaluate the four-quark matrix elements with $1/N_C$ counting and test whether the matrix elements obey the $1/N_C$ counting with the branching ratios. Nevertheless, the determination of the matrix elements with $1/N_C$ counting represents the largest uncer-

tainty in our approach. From the results given in the phenomenology section, the most important results are the phase-shifts due to SM higher-order corrections $\Delta\phi_d = \phi_d - 2\beta$ and $\Delta\phi_s = \phi_s + 2\beta_s$ that are maximally possible. We find

	Bound			Decay
	$\lvert\Delta\phi_d\rvert$	$\leq$	$0.7°$	$\bar{B}_d \to J/\psi K_S$,
	$\lvert\Delta\phi_s\rvert$	$\leq$	$1.0°$	$\bar{B}_s \to (J/\psi\phi)^0$,
$-0.8° \leq$	$\Delta\phi_s$	$\leq$	$0.0°$	$\bar{B}_s \to D_s^+ D_s^-$.

This means that the theoretical uncertainty on the extraction of β is $\pm 0.35°$ in $\bar{B}_d \to J/\psi K_S$ and of β_s is $\pm 0.2°$ in $\bar{B}_s \to D_s^+ D_s^-$. The uncertainty in the extraction of β_s in $\bar{B}_s \to J/\psi\phi$ is larger with $\pm 0.5°$. In the future, also the decays $\bar{B}_s \to D^+ D^-$ and $\bar{B}_s \to \bar{D}^0 D^0$ will be interesting, since they also allow a very precise determination of β_s. Unfortunately, their statistics is 20 times smaller than that of the channel $\bar{B}_s \to D_s^+ D_s^-$.

The validity of our predictions will be probed in the decays where the penguin pollution is not Cabibbo suppressed, i.e. in the decays that are governed by the quark-level process $b \to \bar{c}cd$. In these decays the *CP* violating parameters are possibly sizable and could deviate from our predictions.

The measurement of $S_{J/\psi\pi^0}$ at the BABAR experiment and the measurements of $S_{D^+D^-}$ and $C_{D^+D^-}$ in the decay $\bar{B}_d \to D^+ D^-$ at the Belle experiment are in 1-2σ tension with our predictions. All other measurements are in agreement with our predictions. Thus, there is currently no sign of new physics but the experimental uncertainties still leave room for deviations from the SM.

Outlook

The OPE simplifies the structure of the decay amplitude but the evaluation of the four-quark matrix elements remains as the largest uncertainty. The calculation of the matrix elements on the lattice is not feasible because there is a large momentum transfer. It might be possible to obtain better constraints on the matrix elements by employing flavor symmetries, such as $SU(3)_F$, but we do not think that this will lead to massive improvements. The use of flavor symmetries is a complementary approach with the main disadvantage that the breaking of $SU(3)_F$ is inaccessible.

A more rigorous proof of the OPE might be possible by establishing a genuine effective theory in which no particles are allowed to have an off-shellness of q^2. In this effective theory only soft light quarks and soft gluons remain. The off-shellness of the charm

quarks should also be at most $\mathcal{O}\left(\Lambda^2_{\rm QCD}\right)$. It could be that this theory is identical to the soft-collinear effective theory (SCET) [99], however, the hadronic currents should not be separated as it is done in SCET. Therefore, this effective theory also results into four-quark matrix elements that need to be matched on the physical matrix elements that can be estimated via $1/N_C$ counting. In principle, these effective-theory matrix elements should only contain soft effects. Therefore, it might even be possible to compute these matrix elements on the lattice in the far future.

The future experimental situation will be mainly influenced by the LHCb and Belle II experiments. While the Belle II experiment is currently still under construction, the LHCb experiment restarted data taking this summer, after the first long shutdown of the LHC ended this year. During its lifetime, the sensitivity of the LHCb experiment will reach the same level as the theoretical uncertainties. Prospectively, the LHCb experiment will reach the 1° sensitivity on the ϕ_s extraction in $\bar{B}_s \to J/\psi\phi$ in Run 3 during the years 2019-2021 [82]. The experimental uncertainty of the UT angle β will be $\sigma_\beta \approx 0.3^\circ$ at about 50 fb^{-1} in the years 2024-2026. Thanks to global fits and results on ϕ_s from the ATLAS and CMS experiment the global experimental uncertainties will be smaller before that time. LHCb has only very limited sensitivity to uncharged light mesons, in particular, the final state $J/\psi\pi^0$ is probably not accessible at the LHCb experiment. Therefore, only when the Belle II experiment is operating new competitive measurements of *CP*-violating observables with π^0 in the final state will become available.

Acknowledgments – Danksagung

Ich danke der Graduiertenschule KSETA, die diese Arbeit finanziert hat.

Während der Promotion haben mich viele Menschen begleitet und unterstützt dafür bin ich sehr dankbar. Als erstes möchte ich meinem Doktorvater Ulrich Nierste danken. Er hat durch sein Engagement für KSETA meine Dokotorandenstelle eingeworben. Vor allem aber bin ich ihm dankbar dafür, dass er mich an das Thema dieser Arbeit herangeführt hat und mich während meiner Promotion stets unterstützt hat. In dieser Zeit habe ich ihn als exzellenten Physiker schätzen gelernt.

Ich danke Kirill Melnikov dafür, dass er zugestimmt hat meine Arbeit als Korreferent zu bewerten. Durch seine Anmerkungen und durch die Diskussion mit ihm habe ich noch weitere wertvolle Einblicke erhalten.

Christoph Wiegand, Martin Spinrath und Stefan Schacht möchte ich herzlich für das Probelesen der Doktorarbeit und wertvolle Verbesserungsvorschläge danken. Stefan Schacht möchte ich weiterhin dafür danken, dass er mir bei Problemen mit der Programmiersprache Python und bei physikalischen Fragestellungen geholfen hat.

Des Weiteren, danke ich meinen Bürokollegen Otto Eberhardt, Markus Bobrowski und Paul Tremper für die gute Büroatmosphäre, die ich immer sehr genossen habe.

Ich möchte auch allen anderen Kollegen vom TTP danken, insbesondere den Systemadministratoren und den Sekretärinnen Frau Lepold, Frau Junge und Frau Schorn.

Dank des Rückhalts und der Förderung durch meine Eltern, Ernst und Marie-Luise, bin ich zu dem Menschen geworden, der ich heute bin, dafür bin ich ihnen zu tiefst dankbar.

Als letztes möchte ich meiner Freundin Isabel für ihre stete Unterstützung danken und dafür, dass sie mein Leben schön macht.

Appendix A

Details to Factorization

A.1 Two-loop integrals

$$I_{13} = -\frac{g_S^4}{(2\pi)^8}\mathcal{C}_{13}\int \mathrm{d}^d k\,\mathrm{d}^d l\,\Gamma_1\frac{\not k-\not q}{(k-q)^2}\gamma_\mu\frac{\not k+\not l}{(k+l)^2}\Gamma_2\frac{\not l+\not p_b+m_b}{(l+p_b)^2-m_b^2}\gamma_\nu\frac{1}{l^2}\frac{1}{(l+q)^2} \quad (A.1)$$
$$\otimes\gamma^\mu\frac{\not{-p}_{\bar c}-\not l+m_c}{(p_c+l)^2-m_c^2}\gamma^\nu$$

$$I_{15} = -\frac{g_S^4}{(2\pi)^8}\frac{\mathcal{C}_{15}}{q^2}\int \mathrm{d}^d k\,\mathrm{d}^d l\Gamma_1\frac{\not k-\not q}{(k-q)^2}\gamma_\mu\frac{\not k}{k^2}\gamma_\nu\frac{\not k+\not l}{(k+l)^2}\Gamma_2\frac{\not l+\not p_b+m_b}{(\not l+\not p_b)^2-m_b^2}\gamma^\nu\frac{1}{l^2}\otimes\gamma^\mu \quad (A.2)$$

$$I_{16} = \frac{g_S^4}{(2\pi)^8}\frac{\mathcal{C}_{16}}{q^2}\int \mathrm{d}^d k\,\mathrm{d}^d l\,\Gamma_1\frac{\not k+\not l}{(k+l)^2}\gamma_\nu\frac{\not k}{k^2}\gamma_\mu\frac{\not k-\not q}{(k-q)^2}\Gamma_2\frac{\not p_b+\not l+m_b}{(p_b+l)^2-m_b^2}\gamma^\nu\frac{1}{l^2}\otimes\gamma^\mu \quad (A.3)$$

$$I_{17} = -\frac{g_S^4}{(2\pi)^8}\frac{\mathcal{C}_{17}}{q^2}\int \mathrm{d}^d k\,\mathrm{d}^d l\quad\Gamma_1\frac{\not k-\not q}{(k-q)^2}\gamma^\rho\frac{\not k+\not l}{(k+l)^2}\Gamma_2\frac{\not l+\not p_b+m_b}{(l+p_b)^2-m_b^2}\gamma^\nu$$
$$\otimes\frac{1}{(q+l)^2}\frac{1}{l^2}V_{\mu\nu\rho}(-q,-l,l+q)\gamma^\mu \quad (A.4)$$

$$I_{23} = -\frac{g_S^4}{(2\pi)^8}\mathcal{C}_{23}\int \mathrm{d}^d k\,\mathrm{d}^d l\quad\gamma_\nu\frac{\not l+\not p'}{(l+p')^2}\frac{1}{l^2}\Gamma_1\frac{\not k+\not l}{(k+l)^2}\gamma^\mu\frac{\not k+\not q}{(k+q)^2}\Gamma_2\frac{1}{(q-l)^2}$$
$$\otimes\gamma^\mu\frac{\not l-\not p_{\bar c}+m_c}{(l-p_{\bar c})^2-m_c^2}\gamma^\nu \quad (A.5)$$

$$I_{24} = -\frac{g_S^4}{(2\pi)^8}\mathcal{C}_{24}\int \mathrm{d}^d k\,\mathrm{d}^d l\quad\gamma_\nu\frac{\not l+\not p'}{(l+p')^2}\frac{1}{l^2}\Gamma_1\frac{\not k+\not l}{(k+l)^2}\gamma^\mu\frac{\not k+\not q}{(k+q)^2}\Gamma_2\frac{1}{(q-l)^2}$$
$$\otimes\gamma^\nu\frac{\not p_c-\not l+m_c}{(p_c-l)^2-m_c^2}\gamma^\mu \quad (A.6)$$

$$I_{25} = \frac{g_S^4}{(2\pi)^8}\frac{\mathcal{C}_{25}}{q^2}\int \mathrm{d}^d k\,\mathrm{d}^d l \quad \gamma_\nu \frac{\not{l}-\not{p}'}{(l-p')^2}\frac{1}{l^2}\Gamma_1\frac{\not{k}-\not{q}}{(k-q)^2}\gamma_\mu\frac{\not{k}}{k^2}\gamma^\nu\frac{\not{k}+\not{l}}{(k+l)^2}\Gamma_2\otimes\gamma^\mu \tag{A.7}$$

$$I_{26} = -\frac{g_S^4}{(2\pi)^8}\frac{\mathcal{C}_{26}}{q^2}\int \mathrm{d}^d k\,\mathrm{d}^d l \quad \gamma_\nu \frac{\not{l}-\not{p}'}{(l-p')^2}\frac{1}{l^2}\Gamma_1\frac{\not{k}+\not{l}}{(k+l)^2}\gamma^\nu\frac{\not{k}}{k^2}\gamma_\mu\frac{\not{k}-\not{q}}{(k-q)^2}\Gamma_2\otimes\gamma^\mu \tag{A.8}$$

$$\begin{aligned} I_{27} = &-\frac{g_S^4}{(2\pi)^8}\frac{\mathcal{C}_{27}}{q^2}\int \mathrm{d}^d k\,\mathrm{d}^d l \quad \gamma^\rho \frac{\not{l}+\not{p}'}{(l+p')^2}\frac{1}{l^2}\Gamma_1\frac{\not{k}+\not{l}}{(k+l)^2}\gamma^\nu\frac{\not{k}+\not{q}}{(k+q)^2}\Gamma_2 \\ &\otimes\frac{1}{(q-l)^2}V_{\mu\nu\rho}(-q,q-l,l)\gamma^\mu \end{aligned} \tag{A.9}$$

$$\begin{aligned} I_{35} = &-\frac{g_S^4}{(2\pi)^8}\mathcal{C}_{35}\int \mathrm{d}^d k\,\mathrm{d}^d l \quad \Gamma_1\frac{\not{k}}{k^2}\gamma_\nu\frac{\not{k}+\not{l}}{(k+l)^2}\gamma_\mu\frac{\not{k}+\not{q}}{(k+q)^2}\Gamma_2\frac{1}{(q-l)^2}\frac{1}{l^2} \\ &\otimes\gamma^\nu\frac{\not{p}_c-\not{l}+m_c}{(p_c-l)^2-m_c^2}\gamma^\mu \end{aligned} \tag{A.10}$$

$$\begin{aligned} I_{36} = &-\frac{g_S^4}{(2\pi)^8}\mathcal{C}_{36}\int \mathrm{d}^d k\,\mathrm{d}^d l \quad \Gamma_1\frac{\not{k}}{k^2}\gamma_\nu\frac{\not{k}+\not{l}}{(k+l)^2}\gamma_\mu\frac{\not{k}+\not{q}}{(k+q)^2}\Gamma_2\frac{1}{(q-l)^2}\frac{1}{l^2} \\ &\otimes\gamma^\mu\frac{\not{l}-\not{p}_{\bar{c}}+m_c}{(l-p_{\bar{c}})^2-m_c^2}\gamma^\nu \end{aligned} \tag{A.11}$$

$$\begin{aligned} I_{37} = &-\frac{g_S^4}{(2\pi)^8}\frac{\mathcal{C}_{37}}{q^2}\int \mathrm{d}^d k\,\mathrm{d}^d l \quad \Gamma_1\frac{\not{k}}{k^2}\gamma^\nu\frac{\not{k}+\not{q}}{(k+q)^2}\Gamma_2\frac{1}{(q-l)^2}\frac{1}{l^2}V_{\mu\nu\rho}(-l,q,l-q) \\ &\otimes\gamma^\rho\frac{\not{l}-\not{p}_{\bar{c}}+m_c}{(l-p_{\bar{c}})^2-m_c^2}\gamma^\mu \end{aligned} \tag{A.12}$$

$$I_{56} = \frac{g_S^4}{(2\pi)^8}\frac{\mathcal{C}_{56}}{q^2}\int \mathrm{d}^d k\,\mathrm{d}^d l \quad \Gamma_1\frac{\not{k}}{k^2}\gamma^\nu\frac{\not{l}}{l^2}\gamma_\mu\frac{\not{q}-\not{l}}{(q-l)^2}\gamma_\nu\frac{\not{k}+\not{q}}{(k+q)^2}\Gamma_2\frac{1}{(k+l)^2}\otimes\gamma^\mu \tag{A.13}$$

$$\begin{aligned} I_{57} = &-\frac{g_S^4}{(2\pi)^8}\frac{\mathcal{C}_{57}}{q^2}\int \mathrm{d}^d k\,\mathrm{d}^d l \quad \Gamma_1\frac{\not{k}}{k^2}\gamma^\rho\frac{\not{k}+\not{l}}{(k+l)^2}\gamma^\nu\frac{\not{k}+\not{q}}{(k+q)^2}\Gamma_2 \\ &\otimes\frac{1}{(q-l)^2}\frac{1}{l^2}V_{\mu\nu\rho}(-q,q-l,l)\gamma^\mu \end{aligned} \tag{A.14}$$

Some notation has been introduced, we stripped the integral expressions from the spinors and separated the two quark currents with a "$\otimes$" instead. The first current is sandwiched between $\bar{u}_q(p')$ and $u(p_b)$, the second current is sandwiched between $\bar{v}_c(p_{\bar{c}})$ and $u_c(p_c)$. Furthermore we used the insertion of an generic operators $Q = \Gamma_1 V_1 \otimes \Gamma_2 V_2$

instead of specific Dirac and color structure. We also factored out the color structures

$$\mathcal{C}_{15} = V_1 T^a T^b V_2 T^b \otimes T^a, \tag{A.15}$$
$$\mathcal{C}_{16} = V_1 T^b T^a V_2 T^b \otimes T^a, \tag{A.16}$$
$$\mathcal{C}_{13} = V_1 T^a V_2 T^b \otimes T^a T^b. \tag{A.17}$$
$$\mathcal{C}_{25} = T^b V_1 T^a T^b V_2 \otimes T^a, \tag{A.18}$$
$$\mathcal{C}_{26} = T^b V_1 T^b T^a V_2 \otimes T^a, \tag{A.19}$$
$$\mathcal{C}_{23} = T^b V_1 T^a V_2 \otimes T^a T^b, \tag{A.20}$$
$$\mathcal{C}_{24} = T^b V_1 T^a V_2 \otimes T^b T^a, \tag{A.21}$$
$$\mathcal{C}_{56} = V_1 T^b T^a T^b V_2 \otimes T^a, \tag{A.22}$$
$$\mathcal{C}_{35} = V_1 T^b T^a V_2 \otimes T^b T^a, \tag{A.23}$$
$$\mathcal{C}_{36} = V_1 T^a T^b V_2 \otimes T^a T^b, \tag{A.24}$$
$$\mathcal{C}_{17} = i V_1 T^b T^c V_2 \otimes f^{abc} T^a, \tag{A.25}$$
$$\mathcal{C}_{27} = i T^c V_1 T^b V_2 \otimes f^{abc} T^a, \tag{A.26}$$
$$\mathcal{C}_{57} = i V_1 T^c T^b V_2 \otimes f^{abc} T^a, \tag{A.27}$$
$$\mathcal{C}_{37} = i V_1 T^b V_2 \otimes f^{abc} T^c T^a. \tag{A.28}$$

We use the tree-gluon vertex functions

$$V_{\mu_1\mu_2\mu_3}(k,l,k_3) \equiv g_{\mu_1\mu_2}(k-l)_{\mu_3} + g_{\mu_2\mu_3}(l-k_3)_{\mu_1} + g_{\mu_3\mu_1}(k_3-k)_{\mu_2}. \tag{A.29}$$

A.2 The Q_{8G} penguins

$$I_{17G} = \frac{\alpha_S^2 m_b}{(2\pi^2)^2 q^2}\mathcal{C}_G \int \mathrm{d}^d l \frac{1}{l^2}\ \sigma_{\rho\lambda}\frac{q^\lambda + l^\lambda}{(q+l)^2}(1+\gamma_5)\frac{\not{p}_b + \not{l} + m_b}{(p_b+l)^2 - m_b^2}\gamma^\nu \otimes V_{\mu\nu\rho}(-q,-l,q+l)\gamma^\mu \tag{A.30}$$

$$I_{18G} = -\frac{\alpha_S^2 m_b}{(2\pi^2)^2 q^2}\mathcal{C}_G \int \mathrm{d}^d l \frac{1}{l^2}\sigma_{\mu\nu}(1+\gamma_5)\frac{\not{p}_b + \not{l} + m_b}{(p_b+l)^2 - m_b^2}\gamma^\nu \otimes \gamma^\mu \tag{A.31}$$

$$I_{27G} = \frac{\alpha_S^2 m_b}{(2\pi^2)^2 q^2}\mathcal{C}_G \int \mathrm{d}^d l \frac{1}{l^2}\gamma^\rho \frac{\not{l} - \not{p}'}{(l-p')^2}\sigma^{\nu\lambda}\frac{q^\lambda + l^\lambda}{(q+l)^2}(1+\gamma_5)V_{\mu\nu\rho}(-q,q+l,-l)\otimes\gamma^\mu \tag{A.32}$$

$$I_{28G} = -\frac{\alpha_S^2 m_b}{(2\pi^2)^2 q^2}\mathcal{C}_G \int \mathrm{d}^d l \frac{1}{l^2}\gamma^\nu \frac{\not{l} - \not{p}'}{(l-p')^2}\sigma_{\mu\nu}(1+\gamma_5)\otimes\gamma^\mu \tag{A.33}$$

$$I_{37G} = -\frac{\alpha_S^2 m_b}{(2\pi^2)^2 q^2}\mathcal{C}_G \int \mathrm{d}^d l \frac{1}{l^2}\frac{1}{(q+l)^2}\sigma^{\rho\lambda}q_\lambda(1+\gamma_5)V_{\mu\nu\rho}(l,-q-l,q) \otimes\gamma^\mu\frac{\not{p}_c + \not{l} + m_c}{(p_c+l)^2 - m_c^2}\gamma^\nu \tag{A.34}$$

$$I_{38G} = -\frac{\alpha_S^2 m_b}{(2\pi^2)^2}\mathcal{C}_G \int \mathrm{d}^d l \frac{1}{l^2}\frac{1}{(q+l)^2}\sigma_{\mu\nu}(1+\gamma_5)\otimes\gamma^\mu\frac{\not{p}_c + \not{l} + m_c}{(p_c+l)^2 - m_c^2}\gamma^\nu \tag{A.35}$$

$$I_{78G} = \frac{2C_F}{N_C}\frac{\alpha_S^2 m_b}{(2\pi^2)^2 q^2}\mathcal{C}_G \int \mathrm{d}^d l \frac{1}{l^2}\frac{1}{(q+l)^2}\sigma_{\nu\rho}(1+\gamma_5)V_{\mu\nu\rho}(-q,q+l,-l)\otimes\gamma^\mu \tag{A.36}$$

$$\mathcal{C}_G = \frac{N_C}{2}T^a \otimes T^a \tag{A.37}$$

$$C_F = \frac{N_C^2 - 1}{2N_C} \tag{A.38}$$

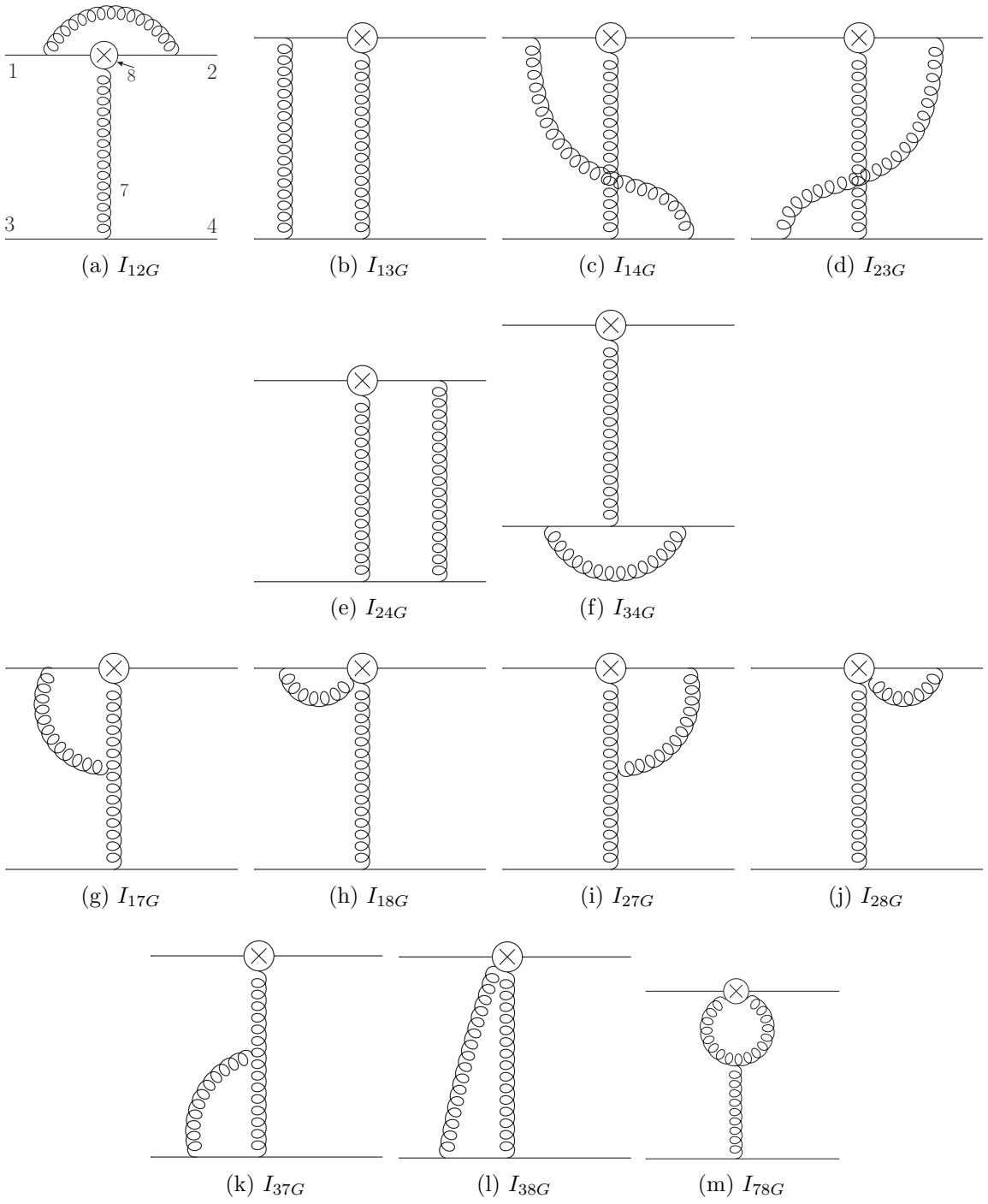

(a) I_{12G} (b) I_{13G} (c) I_{14G} (d) I_{23G}

(e) I_{24G} (f) I_{34G}

(g) I_{17G} (h) I_{18G} (i) I_{27G} (j) I_{28G}

(k) I_{37G} (l) I_{38G} (m) I_{78G}

Figure A.1: One-loop (NLO) corrections to the Q_{8G} penguins.

Appendix B

Details to Phenomenology

B.1 Factorized matrix elements

The naively factorized color singlet is given by

$$\begin{aligned} \langle \psi P | \, Q_{0V} \, | B \rangle |_{\text{fact.}} &= \langle \psi P | \, (\bar{c}c)_{V-A} (\bar{q}b)_{V-A} \, | B \rangle |_{\text{fact.}} & \text{(B.1)} \\ &= \langle \psi | \, \bar{c} \gamma_\mu (1-\gamma_5) c \, | 0 \rangle \, \langle P | \, \bar{q} \gamma^\mu (1-\gamma_5) b \, | B \rangle \, . & \text{(B.2)} \end{aligned}$$

The factorization separates the two currents and leads to a part that describes the production of the ψ and a part which describes the transition $B \to P$. These two processes can be expressed by universal hadronic quantities

$$\begin{aligned} \langle \psi(q,\epsilon) | \, \bar{c} \gamma_\mu c \, | 0 \rangle &= -i f_\psi m_\psi \epsilon^*_\mu, & \text{(B.3)} \\ \langle P(p') | \, \bar{q} \gamma_\mu b \, | B(p_B) \rangle &= \left((p_B + p')_\mu - \frac{m_B^2 - m_P^2}{q^2} q_\mu \right) F_1^{BP}(q^2) & \text{(B.4)} \\ &\quad + \frac{m_B^2 - m_P^2}{q^2} q_\mu \, F_0^{BP}(q^2). & \text{(B.5)} \end{aligned}$$

Here, ϵ_μ and f_ψ are the charmonium polarization vector and the charmonium decay constant, respectively, the parameters F_1^{BP} and F_0^{BP} are the $B \to P$ form factors. Note that the axial currents both vanish $\langle \psi(q,\epsilon) | \, \bar{c} \gamma_\mu \gamma_5 c \, | 0 \rangle = \langle P(p') | \, \bar{q} \gamma_\mu \gamma_5 b \, | B(p_B) \rangle = 0$. Since $q.\epsilon^* = 0$ the full matrix element takes a simple form

$$\langle \psi P | \, Q_{0V} \, | B \rangle = -i 2 f_\psi m_\psi \epsilon_* . p_B F_1^{BP}. \qquad \text{(B.6)}$$

Hence, the form factors F_0^{BP} are irrelevant for our considerations. In the center-of-mass system (see section 3.1.1) $\epsilon^* . p_B = -p_{\text{cm}} / m_\psi m_B$ such that matrix element simplifies even

further to

$$\langle \psi P | \, Q_{0V} \, | B \rangle = i 2 f_\psi m_B p_{\rm cm} F_1^{BP}. \tag{B.7}$$

B.2 Rescaling the Branching Ratios of B_s Decays

According to references [27, 100], the experimentally measured time-integrated branching ratio in B_s decays is not equal to what is understood as the 'theoretical' branching ratio because of the nonvanishing decay width difference in the $B_s - \bar{B}_s$ system [29]

$$y_s \equiv \frac{\Delta\Gamma_s}{2\Gamma_s} = 0.0606 \pm 0.0045. \tag{B.8}$$

They derive the relation

$$\mathrm{BR}(B_s \to f)_{\rm theo} = \left[\frac{1 - y_s^2}{1 + \mathcal{A}^f_{\Delta\Gamma}} \right] \mathrm{BR}(B_s \to f)_{\rm exp}. \tag{B.9}$$

In general we use

$$A_{\Delta\Gamma_s} = -\eta_f \cos(\phi_s) \tag{B.10}$$

because the penguin pollution has only a very small influence on $A_{\Delta\Gamma_s}$.

Appendix C

Abbreviations

BSS mechanism	Bander-Silverman-Soni mechanism [11]
CKM matrix	Cabibbo-Kobayashi-Maskawa matrix [3, 4]
e.g.	Example given
i.e.	This means *Latin: id est*
IR	Infrared
KM mechanism	Kobayashi-Maskawa mechanism [4]
LCDA	Light-cone distribution amplitude
LHS	Left-hand side
LO	Leading order
$\overline{MS}$	Modified minimal subtraction scheme
NDR	Naive dimensional regularization (scheme)
NLO	Next-to-leading order
NP	New physics
OPE	Operator-product expansion
OZI rule	Okubo-Zimmerman-Iizuka rule [64–66]
QCD	Quantum chromodynamics
QCDF	QCD factorization
RHS	Right-hand side
SM	Standard Model
UT	Unitarity triangle
UV	Ultraviolet
w.r.t	With respect to

Mathematical symbols

$=$	equal (analytically)
$=$	equal (numerically, rounded to last displayed digit)
$\equiv$	defining equation
$\approx$	approximately equal (numerically, several digits rounded)
$\simeq$	equal up to higher orders
$\sim$	scales as
.	scalar product of four-vectors
$\mathcal{B}$	branching ratio
$\lambda \sim \Lambda_{\rm QCD}$	power-counting parameter
$\lambda = 0.225$	Wolfenstein parameter
λ_f	quantity that encodes all *CP* violation
$\lambda_{pq} = V_{pq}^* V_{pb}$	combination of CKM elements
q	quark that is created at the effective vertex
q	hard momentum that creates the $\bar{c}c$ quark pair
p	coefficient of $\|B\rangle$ in the mass eigenstate $\|B_{H,L}\rangle$
q	$\pm$ coefficient of $\left\|\bar{B}\right\rangle$ in the mass eigenstate $\|B_{H,L}\rangle$
p	spectator quark in the (decaying) $\bar{B}_p$ meson

Bibliography

[1] **CMS** Collaboration, S. Chatrchyan et al., *Observation of a new boson at a mass of 125 GeV with the CMS experiment at the LHC*, *Phys. Lett.* **B716** (2012) 30–61, [arXiv:1207.7235].

[2] **ATLAS** Collaboration, G. Aad et al., *Observation of a new particle in the search for the Standard Model Higgs boson with the ATLAS detector at the LHC*, *Phys. Lett.* **B716** (2012) 1–29, [arXiv:1207.7214].

[3] N. Cabibbo, *Unitary Symmetry and Leptonic Decays*, *Phys. Rev. Lett.* **10** (1963) 531–533.

[4] M. Kobayashi and T. Maskawa, *CP Violation in the Renormalizable Theory of Weak Interaction*, *Prog. Theor. Phys.* **49** (1973) 652–657.

[5] I. I. Y. Bigi and A. I. Sanda, *Notes on the Observability of CP Violations in B Decays*, *Nucl. Phys.* **B193** (1981) 85.

[6] M. Beneke, G. Buchalla, M. Neubert, and C. T. Sachrajda, *QCD factorization for $B \to \pi\pi$ decays: Strong phases and CPviolation in the heavy quark limit*, *Phys. Rev. Lett.* **83** (1999) 1914–1917, [hep-ph/9905312].

[7] M. Beneke, G. Buchalla, M. Neubert, and C. T. Sachrajda, *QCD factorization for exclusive, nonleptonic B meson decays: General arguments and the case of heavy light final states*, *Nucl. Phys.* **B591** (2000) 313–418, [hep-ph/0006124].

[8] M. Beneke and M. Neubert, *QCD factorization for $B \to PP$ and $B \to PV$ decays*, *Nucl. Phys.* **B675** (2003) 333–415, [hep-ph/0308039].

[9] J. Chay and C. Kim, *Analysis of the QCD-improved factorization in $B \to J/\psi K$*, *ArXiv High Energy Physics - Phenomenology e-prints* (Sept., 2000) [hep-ph/000].

[10] H.-Y. Cheng and K.-C. Yang, *$B \to J/\psi$ K decays in QCD factorization*, *Phys. Rev.* **D63** (2001) 074011, [hep-ph/0011179].

[11] M. Bander, D. Silverman, and A. Soni, *CP Noninvariance in the Decays of Heavy Charged Quark Systems*, *Phys.Rev.Lett.* **43** (1979) 242.

[12] G. 't Hooft, *A Planar Diagram Theory for Strong Interactions*, *Nucl.Phys.* **B72** (1974) 461.

[13] S. Glashow, *Partial Symmetries of Weak Interactions*, *Nucl.Phys.* **22** (1961) 579–588.

[14] S. Weinberg, *A Model of Leptons*, *Phys.Rev.Lett.* **19** (1967) 1264–1266.

[15] A. Salam, *Weak and Electromagnetic Interactions*, *Conf.Proc.* **C680519** (1968) 367–377.

[16] T. Muta, *Foundations of Quantum Chromodynamics: An Introduction to Perturbative Methods in Gauge Theories, (3rd ed.)*, vol. 78 of *World scientific Lecture Notes in Physics*. World Scientific, Hackensack, N.J., 2010.

[17] G. 't Hooft, *Computation of the Quantum Effects Due to a Four-Dimensional Pseudoparticle*, *Phys. Rev.* **D14** (1976) 3432–3450. [Erratum: Phys. Rev.D18,2199(1978)].

[18] G. 't Hooft, *Symmetry Breaking Through Bell-Jackiw Anomalies*, *Phys. Rev. Lett.* **37** (1976) 8–11.

[19] C. A. Baker, D. D. Doyle, P. Geltenbort, K. Green, M. G. D. van der Grinten, P. G. Harris, P. Iaydjiev, S. N. Ivanov, D. J. R. May, J. M. Pendlebury, J. D. Richardson, D. Shiers, and K. F. Smith, *Improved experimental limit on the electric dipole moment of the neutron*, *Phys. Rev. Lett.* **97** (Sep, 2006) 131801.

[20] L. Wolfenstein, *Parametrization of the Kobayashi-Maskawa Matrix*, *Phys. Rev. Lett.* **51** (1983) 1945.

[21] A. J. Buras, M. E. Lautenbacher, and G. Ostermaier, *Waiting for the top quark mass, $K \to \pi^+ \nu\bar{\nu}$, $B_s^0 - \bar{B}_s^0$ mixing and CP asymmetries in B decays*, *Phys.Rev.* **D50** (1994) 3433–3446, [hep-ph/9403384].

[22] **CKMfitter Group** Collaboration, J. Charles et al., *CP violation and the CKM matrix: Assessing the impact of the asymmetric B factories*, *Eur.Phys.J.* **C41** (2005) 1–131, [hep-ph/0406184].

[23] **UTfit** Collaboration, M. Bona et al., *The Unitarity Triangle Fit in the Standard Model and Hadronic Parameters from Lattice QCD: A Reappraisal after the Measurements of Δm_s and $\mathcal{B}(B \to \tau\nu_\tau)$*, *JHEP* **10** (2006) 081, [hep-ph/0606167].

[24] I. I. Y. Bigi and A. I. Sanda, *CP violation*, *Camb. Monogr. Part. Phys. Nucl. Phys. Cosmol.* **9** (2000) 1–382.

[25] G. C. Branco, L. Lavoura, and J. P. Silva, *CP Violation*, *Int. Ser. Monogr. Phys.* **103** (1999) 1–536.

[26] U. Nierste, *Three Lectures on Meson Mixing and CKM phenomenology*, in *Heavy quark physics. Proceedings, Helmholtz International School, HQP08, Dubna, Russia, August 11-21, 2008*, pp. 1–38, 2009. arXiv:0904.1869.

[27] I. Dunietz, R. Fleischer, and U. Nierste, *In pursuit of new physics with B_s decays*, *Phys. Rev.* **D63** (2001) 114015, [hep-ph/0012219].

[28] **Particle Data Group** Collaboration, K. Olive et al., *Review of Particle Physics*, *Chin.Phys.* **C38** (2014) 090001.

[29] **Heavy Flavor Averaging Group (HFAG)** Collaboration, Y. Amhis et al., *Averages of b-hadron, c-hadron, and τ-lepton properties as of summer 2014*, arXiv:1412.7515.

[30] M. Ciuchini, M. Pierini, and L. Silvestrini, *The Effect of penguins in the $B_d \to J/\psi K^0$ CP asymmetry*, *Phys.Rev.Lett.* **95** (2005) 221804, [hep-ph/0507290].

[31] S. Faller, M. Jung, R. Fleischer, and T. Mannel, *The Golden Modes $B^0 \to J/\psi K_{(S,L)}$ in the Era of Precision Flavour Physics*, *Phys.Rev.* **D79** (2009) 014030, [arXiv:0809.0842].

[32] M. Ciuchini, M. Pierini, and L. Silvestrini, *Theoretical uncertainty in sin 2β: An Update*, arXiv:1102.0392.

[33] M. Jung, *Determining weak phases from $B \to J/\psi P$ decays*, *Phys.Rev.* **D86** (2012) 053008, [arXiv:1206.2050].

[34] K. De Bruyn and R. Fleischer, *A Roadmap to Control Penguin Effects in $B_d^0 \to J/\psi K_S^0$ and $B_s^0 \to J/\psi\phi$*, arXiv:1412.6834.

[35] G. Buchalla, A. J. Buras, and M. E. Lautenbacher, *Weak decays beyond leading logarithms*, *Rev.Mod.Phys.* **68** (1996) 1125–1144, [hep-ph/9512380].

[36] W. A. Bardeen, A. J. Buras, D. W. Duke, and T. Muta, *Deep Inelastic Scattering Beyond the Leading Order in Asymptotically Free Gauge Theories*, *Phys. Rev.* **D18** (1978) 3998.

[37] D. Fakirov and B. Stech, *F and D Decays*, *Nucl. Phys.* **B133** (1978) 315–326.

[38] M. Bauer and B. Stech, *Exclusive d Decays*, *Phys. Lett.* **B152** (1985) 380.

[39] M. Bauer, B. Stech, and M. Wirbel, *Exclusive Nonleptonic Decays of D, D(s), and B Mesons*, *Z. Phys.* **C34** (1987) 103.

[40] M. Neubert and B. Stech, *Nonleptonic weak decays of B mesons*, *Adv. Ser. Direct. High Energy Phys.* **15** (1998) 294–344, [hep-ph/9705292].

[41] J. D. Bjorken, *Topics in B Physics*, *Nucl. Phys. Proc. Suppl.* **11** (1989) 325–341.

[42] M. Beneke, *Conceptual aspects of QCD factorization in hadronic B decays*, *J. Phys.* **G27** (2001) 1069–1080, [hep-ph/0009328]. [,241(2000)].

[43] A. Buras, J. Gerard, and R. Ruckl, *$1/N_C$ Expansion for Exclusive and Inclusive Charm Decays*, *Nucl.Phys.* **B268** (1986) 16.

[44] A. J. Buras and L. Silvestrini, *Nonleptonic two-body B decays beyond factorization*, *Nucl. Phys.* **B569** (2000) 3–52, [hep-ph/9812392].

[45] G. Buchalla, G. Isidori, and S. J. Rey, *Corrections of order Λ_{QCD}^2/m_c^2 to inclusive rare B decays*, *Nucl. Phys.* **B511** (1998) 594–610, [hep-ph/9705253].

[46] B. Grinstein and D. Pirjol, *Exclusive rare $B \to K^{(*)} l^+ l^-$ decays at low recoil: Controlling the long-distance effects*, *Phys. Rev.* **D70** (2004) 114005, [hep-ph/0404250].

[47] M. Beylich, G. Buchalla, and T. Feldmann, *OPE and quark-hadron duality*, *Eur.Phys.J.* **C71** (2011) 1635, [arXiv:1101.5118].

[48] G. Chalons and F. Domingo, *Dimension 7 operators in the b to s transition*, *Phys. Rev.* **D89** (2014), no. 3 034004, [arXiv:1303.6515].

[49] M. Beneke, G. Buchalla, M. Neubert, and C. T. Sachrajda, *Penguins with Charm and Quark-Hadron Duality*, *Eur. Phys. J.* **C61** (2009) 439–449, [arXiv:0902.4446].

[50] E. C. Poggio, H. R. Quinn, and S. Weinberg, *Smearing the Quark Model*, *Phys. Rev.* **D13** (1976) 1958.

[51] M. Bohm, A. Denner, and H. Joos, *Gauge theories of the strong and electroweak interaction*, *Stuttgart, Germany: Teubner (2001) 784 p* (2001).

[52] L. Landau, *On analytic properties of vertex parts in quantum field theory*, *Nucl.Phys.* **13** (1959) 181–192.

[53] F. V. Tkachov, *Landau equations and asymptotic operation*, *Int.J.Mod.Phys.* **A14** (1999) 683–715, [hep-ph/9703423].

[54] T. Kinoshita, *Mass singularities of Feynman amplitudes*, *J.Math.Phys.* **3** (1962) 650–677.

[55] G. F. Sterman, *Mass Divergences in Annihilation Processes. 1. Origin and Nature of Divergences in Cut Vacuum Polarization Diagrams*, *Phys.Rev.* **D17** (1978) 2773.

[56] V. V. Sudakov, *Vertex parts at very high-energies in quantum electrodynamics*, *Sov. Phys. JETP* **3** (1956) 65–71. [Zh. Eksp. Teor. Fiz.30,87(1956)].

[57] G. Leibbrandt, *Introduction to Noncovariant Gauges*, *Rev. Mod. Phys.* **59** (1987) 1067.

[58] R. K. Ellis, W. J. Stirling, and B. R. Webber, *QCD and collider physics*, *Camb. Monogr. Part. Phys. Nucl. Phys. Cosmol.* **8** (1996) 1–435.

[59] T. D. Lee and M. Nauenberg, *Degenerate Systems and Mass Singularities*, *Phys. Rev.* **133** (1964) B1549–B1562.

[60] S. Catani, S. Dittmaier, and Z. Trocsanyi, *One loop singular behavior of QCD and SUSY QCD amplitudes with massive partons*, *Phys. Lett.* **B500** (2001) 149–160, [hep-ph/0011222].

[61] T. Becher and M. Neubert, *Infrared singularities of QCD amplitudes with massive partons*, *Phys. Rev.* **D79** (2009) 125004, [arXiv:0904.1021]. [Erratum: Phys. Rev.D80,109901(2009)].

[62] M. Beneke and S. Jager, *Spectator scattering at NLO in nonleptonic B decays: Leading penguin amplitudes*, *Nucl. Phys.* **B768** (2007) 51–84, [hep-ph/0610322].

[63] J. Bolz, P. Kroll, and G. A. Schuler, *Higher Fock states and power counting in exclusive P wave quarkonium decays*, *Eur. Phys. J.* **C2** (1998) 705–719, [hep-ph/9704378].

[64] S. Okubo, *Phi meson and unitary symmetry model*, *Phys. Lett.* **5** (1963) 165–168.

[65] G. Zweig, *An SU(3) model for strong interaction symmetry and its breaking. Version 2*, in *DEVELOPMENTS IN THE QUARK THEORY OF HADRONS. VOL. 1. 1964 - 1978* (D. Lichtenberg and S. P. Rosen, eds.), pp. 22–101. 1964.

[66] J. Iizuka, *Systematics and phenomenology of meson family*, *Prog. Theor. Phys. Suppl.* **37** (1966) 21–34.

[67] L. Bel, K. De Bruyn, R. Fleischer, M. Mulder, and N. Tuning, *Anatomy of $B \to D\overline{D}$ decays*, *JHEP* **07** (2015) 108, [arXiv:1505.01361].

[68] R. R. Horgan, Z. Liu, S. Meinel, and M. Wingate, *Lattice QCD calculation of form factors describing the rare decays $B \to K^* \ell^+ \ell^-$ and $B_s \to \phi \ell^+ \ell^-$*, arXiv:1310.3722.

[69] C. Albertus, E. Hernández, and J. Nieves, *$B \to \rho$ semileptonic decays and $|V_{ub}|$*, *Phys.Rev.* **D90** (2014), no. 1 013017, [arXiv:1406.7782].

[70] I. S. Imsong, A. Khodjamirian, T. Mannel, and D. van Dyk, *Extrapolation and unitarity bounds for the $B \to \pi$ form factor*, arXiv:1409.7816.

[71] C. Bouchard, G. P. Lepage, C. Monahan, H. Na, and J. Shigemitsu, *Rare decay $B \to K \ell^+ \ell^-$ form factors from lattice QCD*, *Phys.Rev.* **D88** (2013) 054509, [arXiv:1306.2384].

[72] C. Bouchard, G. P. Lepage, C. Monahan, H. Na, and J. Shigemitsu, *$B_s \to K \ell \nu$ form factors from lattice QCD*, *Phys.Rev.* **D90** (2014), no. 5 054506, [arXiv:1406.2279].

[73] G. Duplancic and B. Melic, *Form factors of B, Bs -¿ eta, eta' and D, Ds -¿ eta, eta' transitions from QCD light-cone sum rules*, arXiv:1508.05287.

[74] A. Bharucha, D. M. Straub, and R. Zwicky, *$B \to V \ell^+ \ell^-$ in the Standard Model from Light-Cone Sum Rules*, arXiv:1503.05534.

[75] A. J. Buras, J. Girrbach-Noe, C. Niehoff, and D. M. Straub, *$B \to K^{(*)}\nu\overline{\nu}$ decays in the Standard Model and beyond*, *JHEP* **02** (2015) 184, [arXiv:1409.4557].

[76] D. Bečirević, G. Duplančić, B. Klajn, B. Melić, and F. Sanfilippo, *Lattice QCD and QCD sum rule determination of the decay constants of η_c, J/ψ and h_c states*, *Nucl.Phys.* **B883** (2014) 306–327, [arXiv:1312.2858].

[77] G. Donald, C. Davies, R. Dowdall, E. Follana, K. Hornbostel, et al., *Precision tests of the J/ψ from full lattice QCD: mass, leptonic width and radiative decay rate to η_c*, *Phys.Rev.* **D86** (2012) 094501, [arXiv:1208.2855].

[78] M. Maior de Sousa and R. Rodrigues da Silva, *The $\rho(2S)$ and $\psi(2S)$ meson in a double pole QCD Sum Rules*, arXiv:1205.6793.

[79] A. S. Dighe, I. Dunietz, H. J. Lipkin, and J. L. Rosner, *Angular distributions and lifetime differences in $B_s \to J/\psi\phi$ decays*, *Phys.Lett.* **B369** (1996) 144–150, [hep-ph/9511363].

[80] A. S. Dighe, I. Dunietz, and R. Fleischer, *Extracting CKM phases and $B_s - \bar{B}_s$ mixing parameters from angular distributions of nonleptonic B decays*, *Eur.Phys.J.* **C6** (1999) 647–662, [hep-ph/9804253].

[81] **LHCb** Collaboration, R. Aaij et al., *Measurement of CP violation in $B^0 \to J/\psi K^0_S$ decays*, *Phys. Rev. Lett.* **115** (2015), no. 3 031601, [arXiv:1503.07089].

[82] T. Gerson, *Updated sensitivity projections for the LHCb Upgrade*, Tech. Rep. LHCb-PUB-2013-015. CERN-LHCb-PUB-2013-015, CERN, Geneva, Sep, 2013.

[83] **CMS** Collaboration, V. Khachatryan et al., *Measurement of the CP-violating weak phase ϕ_s and the decay width difference $\Delta\Gamma_s$ using the $\mathrm{B}^0_s \to \mathrm{J}/\psi\phi(1020)$ decay channel in pp collisions at $\sqrt{s} = 8$ TeV*, arXiv:1507.07527.

[84] **LHCb Collaboration** Collaboration, R. Aaij et al., *Precision measurement of CP violation in $B^0_s \to J/\psi K^+K^-$ decays*, arXiv:1411.3104.

[85] **Belle Collaboration** Collaboration, S. Lee et al., *Improved measurement of time-dependent CP violation in $B^0 \to J/\psi\pi^0$ decays*, *Phys.Rev.* **D77** (2008) 071101, [arXiv:0708.0304].

[86] **BaBar Collaboration** Collaboration, B. Aubert et al., *Evidence for CP violation in $B^0 \to J/\psi\pi^0$ decays*, *Phys.Rev.Lett.* **101** (2008) 021801, [arXiv:0804.0896].

[87] **LHCb** Collaboration, R. Aaij et al., *Measurement of CP violation parameters and polarisation fractions in $B_s^0 \to J/\psi \overline{K}^{*0}$ decays*, arXiv:1509.00400.

[88] **LHCb** Collaboration, R. Aaij et al., *Measurement of the CP-violating phase β in $B^0 \to J/\psi\pi^+\pi^-$ decays and limits on penguin effects*, *Phys. Lett.* **B742** (2015) 38–49, [arXiv:1411.1634].

[89] H. Boos, T. Mannel, and J. Reuter, *The Gold plated mode revisited:* $\sin(2\beta)$ *and $B^0 \to J/\psi K_S$ in the Standard Model*, *Phys.Rev.* **D70** (2004) 036006, [hep-ph/0403085].

[90] B. Melic, *Nonfactorizable corrections to $B \to J/\psi K$* , *Phys. Rev.* **D68** (2003) 034004, [hep-ph/0303250].

[91] J. O. Eeg, S. Fajfer, and A. Hiorth, *On the color suppressed decay modes $\bar{B}^0 \to D_s^+ D_s^-$ and $\bar{B}_s^0 \to D^+ D^-$*, *Phys. Lett.* **B570** (2003) 46–52, [hep-ph/0304112].

[92] J. O. Eeg, S. Fajfer, and A. Prapotnik, *Color suppressed contributions to the decay modes $B_{(d,s)} \to D_{(s,d)} D_{(s,d)}$, $B_{(d,s)} \to D_{(s,d)} D^*_{(s,d)}$, and $B_{(d,s)} \to D^*_{(s,d)} D^*_{(s,d)}$*, *Eur. Phys. J.* **C42** (2005) 29–36, [hep-ph/0501031].

[93] **Belle** Collaboration, M. Roehrken et al., *Measurements of Branching Fractions and Time-dependent CP Violating Asymmetries in $B^0 \to D^{(*)\pm} D^{\mp}$ Decays*, *Phys. Rev.* **D85** (2012) 091106, [arXiv:1203.6647].

[94] **BaBar** Collaboration, B. Aubert et al., *Measurements of time-dependent CP asymmetries in $B^0 \to D^{(*)} + D^{(*)}$ - decays*, *Phys. Rev.* **D79** (2009) 032002, [arXiv:0808.1866].

[95] **LHCb** Collaboration, R. Aaij et al., *Measurement of the CP-violating phase ϕ_s in $\bar{B}_s^0 \to D_s^+ D_s^-$ decays*, *Phys. Rev. Lett.* **113** (2014), no. 21 211801, [arXiv:1409.4619].

[96] Z.-z. Xing, *CP violation in $B_d \to D^+ D^-$, $D^{*+} D^-$, $D^+ D^{*}-$ and $D^{*+} D^{*}$- decays*, *Phys. Rev.* **D61** (2000) 014010, [hep-ph/9907455].

[97] R. Fleischer, *Exploring CP violation and penguin effects through $B_d^0 \to D^+D^-$ and $B_s^0 \to D_s^+D_s^-$*, *Eur. Phys. J.* **C51** (2007) 849–858, [arXiv:0705.4421].

[98] M. Jung and S. Schacht, *Standard model predictions and new physics sensitivity in $B \to DD$ decays*, *Phys.Rev.* **D91** (2015), no. 3 034027, [arXiv:1410.8396].

[99] C. W. Bauer, S. Fleming, D. Pirjol, and I. W. Stewart, *An Effective field theory for collinear and soft gluons: Heavy to light decays*, *Phys. Rev.* **D63** (2001) 114020, [hep-ph/0011336].

[100] K. De Bruyn, R. Fleischer, R. Knegjens, P. Koppenburg, M. Merk, et al., *Branching Ratio Measurements of B_s Decays*, *Phys.Rev.* **D86** (2012) 014027, [arXiv:1204.1735].